UNIVERSITY OF LIVERPOOL

The Properties of Environmentally-Friendly Sandwich Structures

Thesis submitted in accordance with the requirements of the
University of Liverpool for the degree of
Doctor of Philosophy

By
Mohd Zuhri Mohamed Yusoff
March 2015

ACKNOWLEDGEMENTS

بِسْمِ اللَّهِ الرَّحْمَٰنِ الرَّحِيمِ

First and foremost, I would like to extend my deepest praise to Allah S.W.T for giving me the strength and patience to complete this piece of work.

I wish to express my gratitude to my supervisor, Professor Wesley Cantwell, for his valuable guidance, encouragement, comments and patience throughout the course of this study. I appreciate all his contributions of time and ideas to make my PhD experience productive and stimulating. Sincere appreciation is also extended to Dr Zhongwei Guan for his feedback and motivations throughout this journey.

My sincere gratitude to all the staffs at the Department of Engineering, especially Mr. Stephen Pennington, Mr. Dave Atkinson, and Mr. Jijimon Mathew for their technical support and also Mrs Denise Stewart and Mrs Lesia Swain for their services.Also to my colleagues,including Dr Mohamad Zaki Hasan, Dr Rafidah Hasan, Dr Siti Hajar Sheikh Md Fadzullah, Dr Mohd Ruzaimi Mat Rejab, Dr Mohamed Al Tenaiji, Mrs Alia Ruzanna Aziz, Mr Amit Kumar Haldar, Mr Tawan Boonkongwathana, Mr Adil Jamil and Mr Shaharudin Shah Zaini. I have had the pleasure to work with and alongside them. My appreciation is also due to all the staffs and friends in the university that I have been associating directly or indirectly.

Special appreciation goes to my lovely parents, Mohamed Yusoff Mohd Noor and Suriah Abdul Rahman, for their support, assistance and encouragement, as well as my lovely wife, Zafirah Salim, for her love, support, understanding and patience through thick and thin in finishing this study. Also, my childrens, Zahra, Muhammad Zahran and Muhammad Zayyan for giving me the tears and joys all these years. Thanks also to the Malaysian Community who helped me directly or indirectly during my stay in Liverpool.

Finally, I would like to thank to Universiti Putra Malaysia and the Government of Malaysia for sponsoring this PhD study.

"My Lord, increase me in knowledge" [Ta-Ha, 20:114]

LIST OF PUBLICATIONS

Journals

1. Zuhri M.Y.M., Guan Z.W. and Cantwell W.J. The mechanical properties of natural fibre based honeycomb core materials, Composites: Part B, 2014; 58: 1 – 9.

Conferences

1. Zuhri M.Y.M. and Cantwell W.J. Biodegradable sandwich structures for lightweight environmentally-friendly design, SAMPE Europe 33rd International ConferenceSEICO 12, Paris, France, 2012.
2. Zuhri M.Y.M., Guan Z.W. and Cantwell W.J. Compression properties of flax fibre based honeycomb core structures, SAMPE Tech Conference and Exhibition, Wichita, USA, 2013.
3. Zuhri M.Y.M., Guan Z.W. and Cantwell W.J. The energy absorption of environmentally-friendly structures based on bamboo tubes, The 22nd Annual International Conference on Composites/Nano Engineering (ICCE-22), Malta, 2014.
4. Zuhri M.Y.M., Guan Z.W. and Cantwell W.J. Modelling structural response of flax-based composite interlocking structures, The 5th International Conference on Computational Methods (ICCM), Cambridge, UK, 2014.

ABSTRACT

This research study aims to manufacture and characterise the properties of sandwich structures based on natural fibre composites. Bamboo tubes and flax-based composite (reinforced polypropylene and polylactide) were selected as the main materials to be investigated.

Initial testing was focused on investigating the sensitivity of the tensile properties of the composites from various processing conditions and understanding the energy-absorbing characteristics of the individual bamboo tubes. Following this, bamboo honeycomb, bamboo-reinforced foam, corrugated flax-based composites, square and triangular interlocking flax-based composites and corrugated paperboard with flax-based composite skins were manufactured.The flax-based honeycomb and corrugated structures were manufactured using compression moulding techniques and subsequently bonded to skins based on the same material using an epoxy resin. These structures were tested in compression at quasi-static and dynamic rates of strain in order to determine their mechanical strength and specific energy absorption characteristics. It has been shown that the energy-absorbing capacity of the bamboo tubes tends to increase with decreasing inner diameter to the thickness (D/t) ratio. In addition, a chamfered profile was employed to successfully trigger the tubes to fail in a progressive manner. Bamboo tubing has been observed to offer excellent energy absorption characteristics and has potential for use inenergy-absorbing engineering applications. Tests on the flax-based composite structures have shown that the wall thickness and the number of unit cells have an effect on the strength and energy-absorbing capability of the core. The flax reinforcedpolypropylene (flax/PP) composite structures failed in buckling and fibre fracture, whereasthe flax reinforced polylactide (flax/PLA) systemfailed in buckling with delamination. Of the structures investigated here, the flax/PP cores offer superior mechanical properties to their flax/PLA counterparts. Further investigations on the effect of bonding flax/PP and flax/PLA skins to a corrugated paperboard have show that there is no significant difference in the properties between those two flax-based materials.

Finally, the compression response of the square and triangular honeycomb structures has been modelled using finite element (FE) techniques. The FE model succesfully predicted the strength, energy-absorbing characteristics, buckling behaviour and failure modes observed in these natural fibre based core materials.

TABLE OF CONTENTS

CHAPTER 4: MECHANICAL PROPERTIES OF NATURAL FIBRE-BASED SANDWICH STRUCTURES

LIST OF FIGURES

LIST OF TABLES

CHAPTER 1 : INTRODUCTION

1.1 Overview

By the broadest definition, a sandwich structure is defined as a structure which is formed from a core and two identifiable skins. Generally, sandwich composite structures use stiff and strong skins, while the core is a lightweight material that transfers the load from one skin to the other. The adhesive acts as a bonding agent, capable of transmitting the shear and axial loads to and from the core material. Skins are used to provide the bending and shear stiffness. Numerous studies have shown that sandwich structures are good at absorbing energy, which are also very lightweight, offer superior strength and stiffness-to-weight ratios and offer opportunities to reduce some components from the core part through design integration [1-3]. The principle behind the design of a sandwich structure is an I-beam, where the flanges can carry direct compression and tension loads, while the web carries shear loads. The flanges can be regarded as the sandwich skins and the web as the sandwich core. Interestingly, sandwich structures are also found in nature, such as in natural fibre structures (e.g. bamboo and grass), cell structures, bones and beehives.

Today, many industries use composite sandwich structures in a range of components. For example, Bayer Material Science, has developed a new sandwich structure made from continuous glass fibre mats impregnated with polycarbonate for use in the manufacture of automotive body panels [4]. In a prototype of a trunk lid, the volume between the lid was filled with a polyurethane foam, making the component very lightweight and resistant to minor damage. The aerospace industry uses sandwich structures in many applications, for example aluminium-based honeycomb panels are used as flooring material in commercial airliners. Airbus has developed a sandwich fuselage concept, called the Ventable Shear Core (VeSCo) [5]. This concept is an open channel core structure that provides good protection from impact and noise.

Due to increasing awarenessof environmental issues, environmentally-friendly compositesare attracting interest from many researchers, where natural fibresare seen as a potential replacement for glass fibres. In addition, the motivation to reduce raw material costs, reduction of weight and ecological advantages of using renewable resources have created further interest in this natural fibre. Researchers and scientists have used many terms to describe natural fibres, such as 'green', 'eco', 'sustainable' and 'environmentally-friendly', in order to promote them. As interest in natural fibres has increased, efforts to formulate and characterise them have grown rapidly, in order to suit the requirements of industries, such as the aircraft, building and appliance industries. In 2009, the Food and Agriculture Organization (FAO) of the United Nations (UN) officially declared it as the International Year of Natural Fibres. One of the aims of this strategy was to build up the efficiency and sustainability of industries that use natural fibres.

By far, the greatest use of natural fibre composites is in the automotive industry, where natural fibres have been employed in the manufacture of both interior and exterior vehicle components. Here, the idea is to reduce the overall weight of the vehicle, whilst increasing its fuel efficiency and sustainability. For example, Daimler AG and Toyota have introduced natural fibre composites into their products and planned to further increase their use in future components [6]. Similarly, Jaguar and Land Rover have reported that natural fibre components offer an excellent performance compared to many traditional parts [7]. The Centre for Research and Innovation in the Bio-Economy (CRIBE),in partnership with GreenCore,has also developed a product from wood fibre for the use in packaging and building applications, such as pallets and various containers [8].

In general, natural fibres can be divided into two categories, these being animal fibres (silk and wool) and plant fibres. Plant fibres can be classified into two groups, these being non-wood fibres (e.g. straw, bast, leaf, seed and grass) and wood fibres (e.g. soft and hard wood). Hemp, flax, jute and kenaf are examples of natural fibres that offer a techno-ecological advantage over synthetic fibres and are considered as an alternative material to glass fibre in many composite applications.

Table 1.1 lists the advantages and disadvantages associated with using natural fibres as reinforcements in composite materials [9-11]. Due to limitations in their mechanical properties, natural fibre composites have not been used in high-end technology applications, such as component parts for aerospace. Therefore, a study on natural fibre-based structures was carried out to investigate the potential of using natural fibre composites in sandwich structures.

Table 1.1.Advantages and disadvantages of natural fibres [9-11].

Advantages	Disadvantages
Relatively low cost compared to synthetic fibres.	Quality of the fibre depending on factors that influence its batch, e.g. weather.
Recyclable and biodegradable.	Swelling of fibres due to moisture absorption.
Good specific properties.	Lower strength properties.
Renewable resources and the production of natural fibres requires very little energy.	
Ease of processing without tool wear.	
Health advantages, for example, no skin irritation during fabrication compare to the glass. There is strong evidence that glass particles can cause respiratory problems.	
Good thermal, dieletric and acoustic insulating properties.	

1.2 Applications of Natural Fibre Composites

There are many industries that are exploring the use of natural fibre composites and sandwich structures. Today, many efforts to develop environmentally-friendly composite and sandwich structures, with the aim of cost reduction, weight reduction and even pollution have been undertaken. Here, the applications of natural fibre composites and sandwich structures in engineering applications are discussed.

As previously mentioned, natural fibre composites are more widely used in the automotive industry over the last two decades. Daimler AG, for example, used natural fibres, such as flax, hemp, sisal and coconut, for a number of their interior parts. Daimler reported that the use of natural fibre composites lead to a reduction in the component weight, thereby reducing the consumption of fuel, leading to an almost neutral CO_2 balance.

Table 1.2 show examples of Mercedes models that have used natural fibres in their interior parts [12,13]. Furthermore, the marine industry has also shown interest in using natural fibres in composite materials. For example, Corradi *et al.* [14] fabricated a hull from bamboo reinforced composites. Figure 1.1 shows a canoe made from a flax fibre composite [15].

The sports industry has also used natural fibres in the manufacture of many products. Samsara, an Australian company has produced a surfboard made from flax composites and reported that the surfboard performed very well and was much stronger than the earlier carbon fibre board [16]. In addition, a well-known bicycle company, Schwinn, has introduced a natural fibre composite frame based on flax and bamboo [17]. Figure 1.2 show examples of natural fibre composites used in sporting goods. There are also some other sectors that use natural fibre composites, for example in the manufacture of furniture and electrical appliances, as well as the construction industry.

Table 1.2.Examples of natural fibre composite applications in Mercedes vehicles [12,13].

Model	Types of Natural Fibre
 Mercedes A-Class	• Flax fibre – covers for the driver and front passenger seat backrests. • Cotton, wool – various soundproofing applications • Abaca fibre – underbody panelling. • Coconut fibre, natural latex – backrest cushion indrivers seat.
 Mercedes M-Class	• Bast fibre – load compartment linings • Wood –trim elements • Coconut husks – air conditioning combination filter

Figure 1.1. A canoe made from a flax reinforced composite [15].

(a) (b)

Figure 1.2. (a) Samara 'eco surfboard' and (b) Schwinn Vestige bicycle made from natural fibre composites [16,17].

1.3 Major Contribution of Thesis

Sandwich structures are well-known for being lightweight, while natural fibre composites offer many advantages that make them suitable as alternative materials for many applications. Hence, the use of natural fibre composites in a sandwich structure is expected to produce added benefits in the design of lightweight structures, leading to environmentally-friendly sandwich structures. Most studies on natural fibre composites have focused on mechanical properties, while very few studies have been undertaken on a sandwich structures based on natural fibres. The aim of this study is therefore to develop a sandwich structure based on natural fibre compositefrom several types of core structure that can be used in engineering applications. Attention will focus on determining their strength and specific energy absorption.

The objectives of this study are as follows:

a) To investigate the mechanical properties of flax-based composites and bamboo.
b) To develop a range of sandwich structures based on bamboo and a flax-based composite.
c) To determine the quasi-static and dynamic properties of natural fibre-based sandwich structures.
d) To model the properties of key sandwich structures using the finite element technique.

1.4 Thesis Outlines

The thesis is divided into six chapters, which are briefly described as follows:

- Chapter 1: A brief explanation on sandwich structures, natural fibre composites and their applications. It also includes the objectives of the research work.

- Chapter 2: A literature review on sandwich structures and natural fibre composites. The literature includes a brief explanation on manufacturing processes and the mechanical properties of periodic structures as well as natural fibre composites from the relevant work in the past and present.

- Chapter 3: The experimental procedure followed in this study, including the fabrication and testing methods. This chapter gives details of the specimen preparation and their sizes, techniques to fabricate the structures and the equipment used for testing.

- Chapter 4: Discussion of the mechanical properties of the skins and the core materials, as well as the properties of the resulting natural fibre-based sandwich structures. The mechanical performance focuses on the mechanical strength and specific energy absorption of sandwich structures based on bamboo cores and flax-based composite skins.

- Chapter 5: This chapter discusses the finite element modelling approaches for modelling the interlocking core structure. Here, the findings are compared with the corresponding experimental results.

- Chapter 6: This chapter summarises the key findings in the research work and gives recommendations for future work on sandwich structures based on natural fibre composites.

CHAPTER 2 : LITERATURE REVIEW

As discussed in the introduction, the use of sandwich structures in engineering applications is very broad. There are many advantages that can be derived from sandwich structures,which include low density, high strength, high stiffness, high energy absorption, etc. With careful design, these qualities can be combined to create multifunctional components. Moreover, the utilisation of natural fibrecomposites in most engineering designs is also undebatable. Natural fibres have their own value-added and are seen as a potential replacement for synthetic fibres.

This literature review will focus on the manufacturing process of sandwich cores and discuss periodic core designs. Furthermore, the mechanical performance of corrugated and honeycomb cores under quasi-static and dynamic compression loading will be discussed. In addition, relevant studies on natural fibre-based sandwich structures will be reviewed. Finite element analysis studies on the honeycomb structures, in particular, arealso discussed.

2.1 Sandwich Cores

There are several types of sandwich cores being studied in order to develop a lightweight structure that is strong and stiff. This research includes balsa wood, polymeric foam and honeycomb cores, and recently the investigation has been broadened to find the ideal lightweight cellular core candidate for use in sandwich structures. With careful design of the cellular core topology, one can maximise the strength properties and lower the density. Ashby [18] identified three dominant factors that influence core properties, i.e. (1) the properties of the parent material, (2) the topology (connectivity) and shape, as well as (3) the relative density (e.g. edge length, cell wall thickness).

Cellular materials can fall into two categories, these being stochastic and periodic cells. One of the common stochastic materials widely used is foam (either open or closed cells), which is based on a random microstructure [19]. Conversely, the periodic structures built from repeated unit cells in an array, which can be classified into three types, namely honeycomb structures, prismatic topologies and lattice truss structures [20]. Figure 2.1 shows examples of stochastic and periodic cells of the cellular materials.

2.1.1 Cellular Foams

Several techniques can be used for foaming different types of solids. Polymer foams are foamed through various phases, these being bubble nucleation, expansion and solidification [21]. Meanwhile, metal foams which consist of a solid metal, are often made from aluminium filled with gas pores [22]. In cellular foams, the pores inside the foam can be either open-cell or closed-cell. The benefit from cellular materials is their ease of manufacture for varying the densities with only a few percent (~2-10%) of the density of the base material [23].

The manufacturing process of cellular foams has been extensively studied and well documented in many research papers and books [19,21-27]. It is known that the density of polymer foams is lower than metal foams. However, they can both sustain large compressive strains, which makes them suitable for use in energy-absorbing applications.

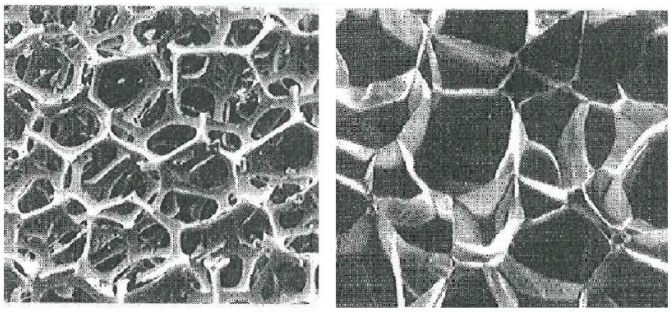

(a) foam with open cells (left) and closed cells (right),

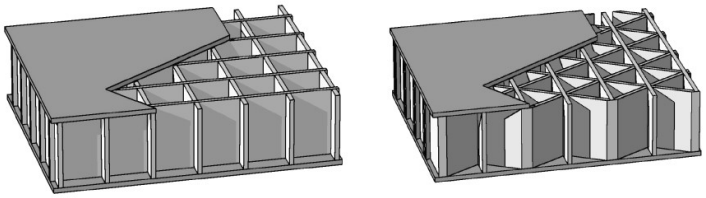

(b) honeycomb structures of square (left) and triangular (right),

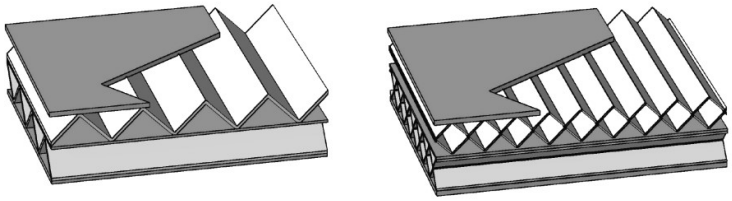

(c) prismatic topologies of triangular (left) and diamond (right),

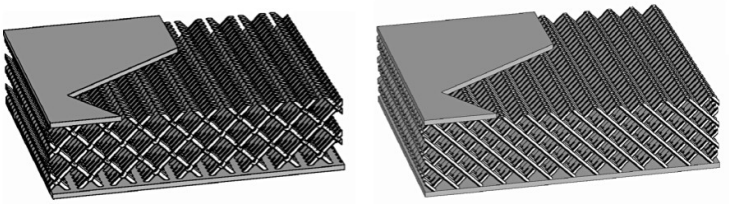

(d) lattice truss structures of diamond textile (left) and diamond collinear (right)

Figure 2.1. Examples of the topologies of cellular materials [18,20].

2.1.2 Two-dimensional Cores

There are two categories of two-dimensional periodic core, these being prismatic and honeycomb cores. Basically, a prismatic core is part of the honeycomb family, in which the cores are rotated 90° about their horizontal axis. It is formed with an open channel in one direction and a closed-cell structure in the second orthogonal direction. This prismatic topology is good for enabling cross-flow heat exchange. On the other hand, honeycombs are made from plates or sheets that form the edges of unit cells. They can be arranged in various shapes, such as hexagonal, square, triangular, circular or other related shapes. Honeycombs have closed-cell pores and thus, they are suitable for thermal protection and to provide efficient load supports.

2.1.2.1 Corrugated Core

Recently, several innovative techniques have been used to manufacture corrugated core structures. Rubino *et al*. [28] manufactured a stainless steel corrugated core with inclined struts at ±60° using computer-numerical-control (CNC) folding. They were then laser-welded to identical face sheets. However, there are limitations to using CNC folding and laser welding technology. This technology is relevant for use on metal systems because it offers good ductility. On the other hand, compression moulding is an alternative method for manufacturing polymer-based composite corrugations, as shown in Figure 2.2. The procedure is started by placing prepreg material between male and female moulds, and then heating to the recommended pressure, temperature and for the required processing time [29-31].

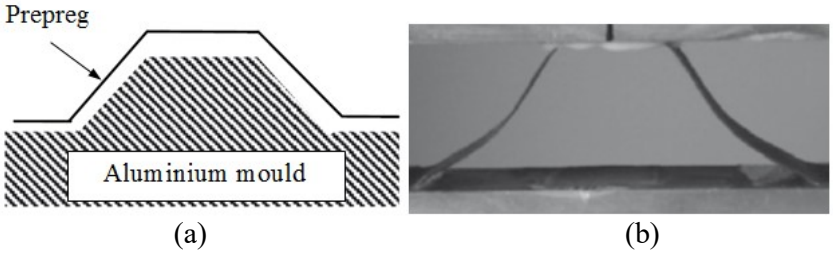

Figure 2.2. (a) Manufacturing route for a composite corrugated core and (b) a sample of a carbon fibre corrugation with an angle of 45° [30].

2.1.2.2 Honeycomb Core

A metal honeycomb core structure can be manufactured using a similar method as in the previously-discussed corrugated core, namely bending and brazing techniques [20]. Here, the honeycomb core is manufactured by stacking one corrugation of metal sheet in another corrugation. The corrugated layers can be either welded or adhesively-bonded. Dharmasena *et al*. [32,33] used a slotting approach, where the metal core was assembled by slip fitting the metal strips to form a square and triangular grid pattern, as seen in Figure 2.3. In principle, this slotting method is well suited to materials that have less ductile or brittle properties, such as composites or ceramic honeycombs. For example, Russel *et al*. [34] successfully manufactured a composite square honeycomb using this slotting technique and adhesively bonding the parts using a low viscosity epoxy resin.

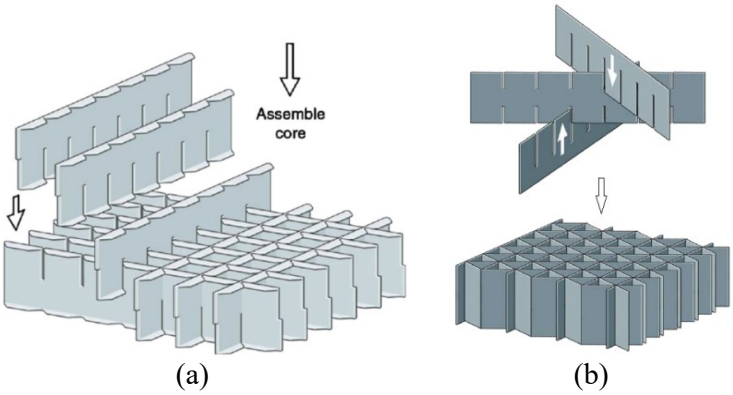

Figure 2.3. Illustration of the slotting method for assembling the (a) square and (b) triangular core [32,33].

2.2 Mechanical Properties of Sandwich Core Structures

This section discusses the mechanical performance of the corrugated and honeycomb core designs tested under static and dynamic compression loading. The mechanical properties and failure modes of sandwichcore structures can be examined under compression loading. This method is generally applied to structures with novel cores, in order to assess their load-carrying capability and energy-absorbing characteristics [35].

2.2.1 Foam

Polymeric foams have been used widely in industry and domestic applications due to their high energy absorption capability and thermal insulation. The combination of good mechanical properties as well the low density makes the rigid polymer foams suitable to be used as structural materials. Their mechanical properties depend on the cell geometric characteristics (i.e. cell wall thickness, shape and size distributions) and intrinsic properties of the polymer in the cell wall [47].

Ouellet *et al*. [48] investigated the compression response of polymeric foams underquasi-static, medium and high strain rate conditions. Expanded polystyrene (EPS), high-density polyethylene (HDPE) and polyurethane (PU) has been measured at strain rates ranging from 0.0087 to 2500 s^{-1}. This showed that the EPS and HDPE will increase their crush stress plateaus butdecrease the strain to densification, with increasing strain rate. The PU material was observed to exhibitlarge scale fractures and ejection of material at intermediate rates, leading to a reduction inthe crush plateau strength compared to the low rate tests.

A range of epoxy-based polymeric structural foams with density range from 0.83 to 1.46 g/cm^3 was tested by Subhash *et al*. [49]. They observed that under the quasi-static loading, the low-density foams failed by the early collapse of large porous cells, whereas the high-density exhibited more uniform deformation and resulted ina ductile-like fracture mode.

Saha *et al*. [122] tested cross-linked poly-vinyl chloride (PVC) and polyurethane (PU) under quasi-static loading usinga servo-hydraulic material testing system at strain ratesof 0.001, 0.01, 0.1 s^{-1}. The study included the effect of foam density and microstructure of the foam. PVC foams with three densities and two microstructures, and PU foams with two densities were considered. They have concluded that the strain rate, density, microstructure and foam material play an important role in the peak stress and energy-absorbing capability. The properties of PVC foams showed the superior performance than the PU foams, over the range of strain rate studied, largely due to their difference in the cell architecture and solid material.

Lim *et al*. [118] investigated the compressive behaviour of linear and cross-linked poly-vinyl chloride foams. The foam densities used are between 55.3 and 1026.7 kg/m^3 tested with a cross-head movement rate of 5 mm/min. It is shown that the elastic collapse for cross-linked PVC (densities from 55.3 to 141.5 kg/m^3) occurred at a similar level of deformation when the bulk PVC material (density 1026.7 kg/m^3) started to strain-harden. It is suggested that this was due to the loss of stiffness as the material yields to thereon initiate a massive onset of cell wall buckling.

A strain-rate and temperature dependence on poly-vinyl chloride foam was carried out by Kendal and Siviour [119]. The foam was investigated under three different amounts of plasticizer (referredas PVC, PPVC and sPPVC)at different strain-rates ranging from 0.001 to 5000 s^{-1} and temperatures from –115 °C to 80 °C.They observed that each material was strongly dependent on the strain rate, based on the change in the yield stress with increasing strain rate. *Figure* 2.4 shows the stress – strain behaviour tested at room temperature for the PVC foam sample. In addition, the effect of the glass transition of the PVC was clearly seen at a temperature of 80 °C. The foam exhibited a more rubbery response when the temperature reached 100°C. In contrast, the PPVC showed the glass transition effect at approximately 50 °C, whereas the sPPVC was seen at approximately –40 °C after transitioning from a more leathery response.

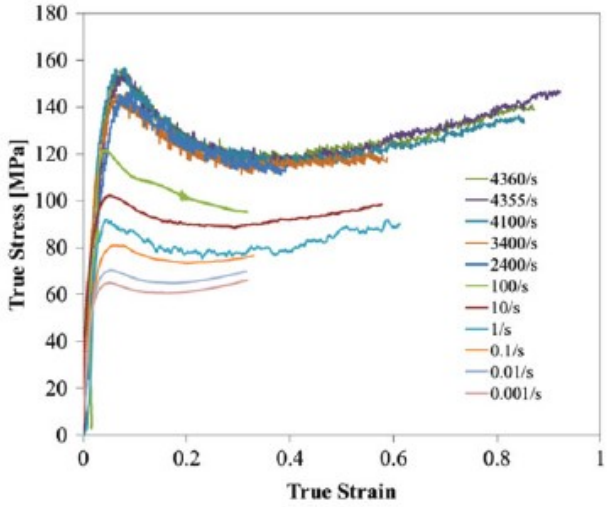

Figure 2.4. Stress – strain behaviour of PVC foam in uniaxial compression tested at room temperature over a range of strain rates [119].

Tagarielli *et al*. [120] studied the dynamic response of sandwich beams based on PVC and a balsa wood core. The densities of foams used in the study are 100 and 250 kg/m^3, and the density of balsa is 90 kg/m^3. Glass–vinylester composite was used as the face-sheets. A 28.5 mm diameter of metal foam projectile was fired from a 4.5 m long gas gun at velocity ranged from 50 to 350 m/s. The PVC core failed in cracking mode, while the face-sheets exhibited a tensile failure. In contrast, the balsa wood observed a delamination of the face-sheets from the core. They concluded that low strength PVC foam (density = 100 kg/m^3) has out-perform the high strength PVC foam (density = 250 kg/m^3) due to the higher thickness of the lower strength foam. Under a low impulse, the balsa wood out-performed the PVC foam. As the impulse increased, the balsa exhibited the shear failure and resulted to a low dynamic strength.

Vaidya *et al*. [121] conducted ballistic impact testing on sandwich panels based on balsa, PVC foam and polyurethane E-glass reinforced web core (that the author refers to as Tycor). The velocity to strike all specimens was approximately 2900 m/s. Among the three cores, the Tycorwas found to absorb the highest kinetic energy, about 1150 J, compared to the PVC and balsa core (both absorbed about the same energy, ~100 – 200 J). The post-impact view of the samples showed that the projectile had penetrated the panel thickness, tearing and delaminating the skins.

2.2.2 Corrugated Core Structure

Prismatic cores have gained much interest from the marine industry for two reasons, i.e. (1) the manufacturing process for large length scales is straightforward via a welding route and (2) the high longitudinal stretching and shear strength of the cores [36].

Côté*et al.* [36] studied the compressive responses of a metallic corrugated core. The core was manufactured from 304 stainless steel, and tested in out-of-plane compression at three different relative densities ($\bar{\rho}$ = 0.036, 0.05 and 0.1). The results indicate that the peak load was governed by buckling of the constituent struts, and the ensuing softening was associated with the post-buckling response.

Yan-Chang *et al*. [37] examined the crush behaviour of four types of corrugated core, these being V, U, X and Y shapes. In their report, cores with shapes of V, U and X experienced buckling deformation under lateral load, whereas the Y-shaped structure deformed in a bending mode along the corrugated line. This can be seen in Figure 2.5. Of these four shapes of corrugated core, the V-shaped structure exhibited a greater crushing performance and energy-absorption characteristics. The specific energy absorption of the V-shape structure measured 3.53 kJ/kg, approximately 77% higher than the Y-shape. The poor crushing performance of the Y-shape was attributed to the bending formation mode.

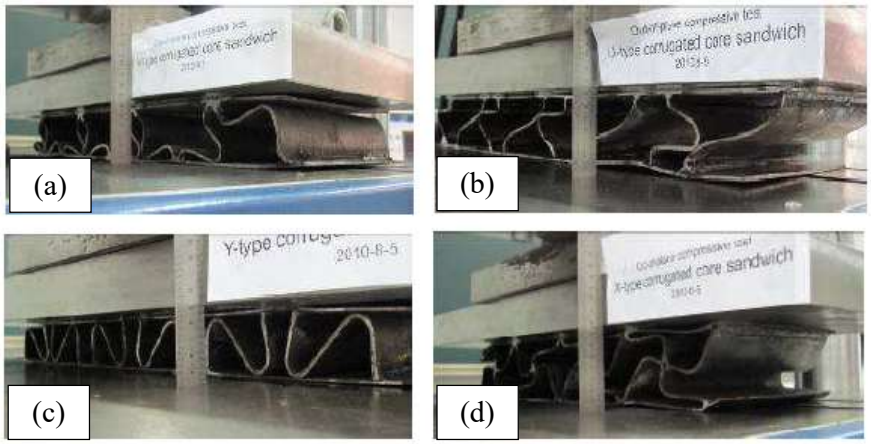

Figure 2.5. Comparison of deformation mode for corrugated core with (a) V-shape, (b) U-shape, (c) Y-shape, and (d) X-shape [37].

An experimental and theoretical investigation on composite corrugations was conducted by Kazemahvazi *et al*. [30,38]. All of the corrugations were manufactured from unidirectional carbon fibre laminate with the fibre direction along the corrugation. Compression tests were carried out on cores with two different angles, these being 45° and 70°, with a single unit cell of the same cell wall thickness. They observed similar failure mechanisms in both angles. The core struts tended to fail through a combination of splitting, buckling and compressive failure. Figure 2.6 compares the compression response of the corrugated core at different angles. The peak load for a core with an angle of 70° is higher than that with 45°, for the same cell wall thickness. The analytical model over-estimated the failure load by approximately 20% error, which is likely associated with the initial imperfections suggested by authors.

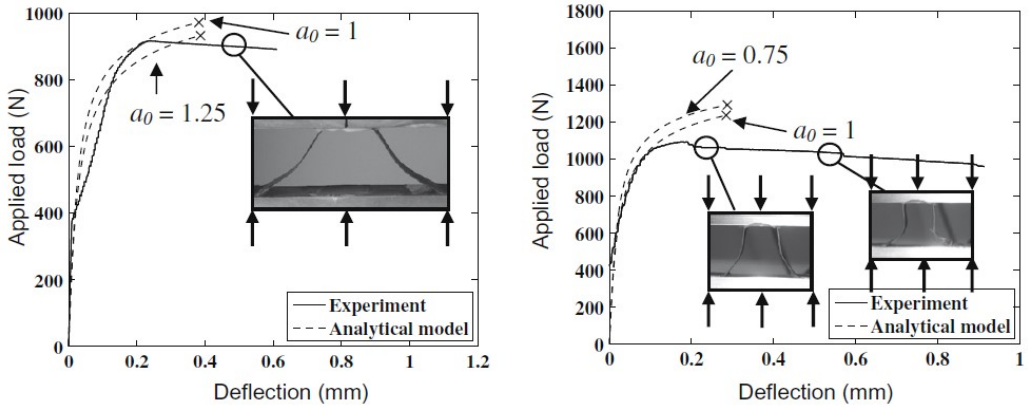

Figure 2.6. The compression response of the monolithic corrugated core with one single unit cell at (a) 45° (P_{max} ≈ 0.9 kN) and (b) 70° (P_{max} ≈ 1.05 kN) [30].

An attempt to improve the bending strength and energy-absorbing capability of the corrugated core structures was made by Zhang *et al*. [39]. Here, composite materials (glass and carbon fibre) were used to fabricate the corrugated core structures. They reported that the specific bending strength increased as the corrugation angle and core thickness increased. In contrast, as the bond length was increased, the specific bending strength decreased. They also compared the energy-absorbing capability of the glass, carbon and a hybrid of glass/carbon fibre, all with and without foam insertions. Figure 2.7 indicates that a hybrid composite with a foam insertion demonstrated the highest crush force efficiency compared to other designs.

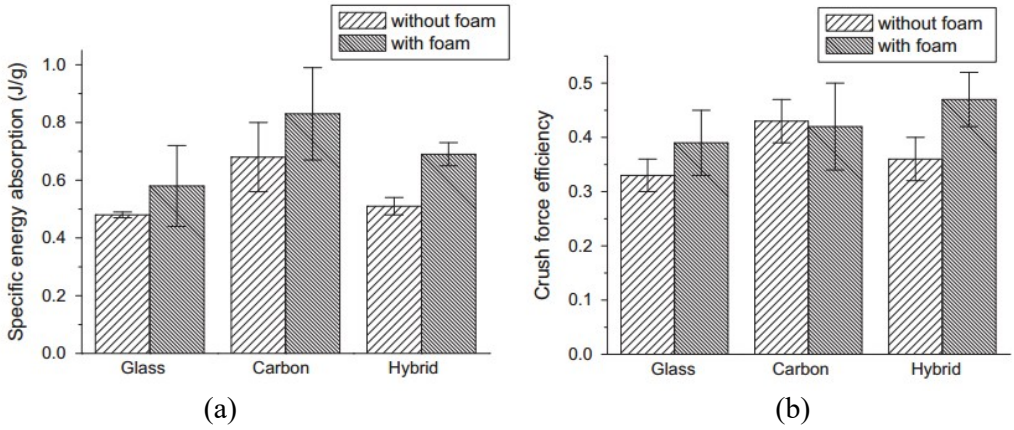

Figure 2.7. Comparison of (a) specific energy absorption and (b) crush force efficiency of composite corrugated core [39].

Kazemahvazi *et al*. [51] investigated a monolithic corrugated structure made from carbon fibre under quasi-static and dynamic loading. The monolithic configuration was based on four different densities, between 35 and 210 kg/m^3. The quasi-static tests showed that failure in the lower density corrugation was governed by elastic buckling of the strut, while the higher density corrugation failed in a combination of delamination and fibre micro-buckling. They observed that a corrugated core with a low relative density shows significant dynamic strengtheningby up to 12 times relative to its quasi-static counterpart. This is associated with an inertial stabilisation of the core members [111]. Small inertial stabilisation was observed in higher relative density cores during dynamic loading.

Further investigations were undertaken on the dynamic compressive response of a composite corrugated core made from an E-glass composite [52]. Two different corrugations were examined, i.e. (1) an unfilled core and (2) a core filled with a polyvinyl chloride (PVC) foam. The core and skins were attached using a stitching method and then the whole assembly structure was infused with an epoxy resin. Under quasi-static loading, the unfilled core collapsed by micro-buckling, due to the stubby struts. There was a minor effect associated with the PVC foam for the filled core, where the foam stabilising the post-peak strut failure response. Under dynamic loading, deformation of the structures was reasonably uniform through the core

thickness. They suggested that at higher impact velocities, about 150 m/s, the localised deformation occurs near the impacted face. This is due to the fact that the specimens were not in axial equilibrium and also due to shock effects. Figure 2.8 indicates that the foam has a small effect on the dynamic properties of the corrugated core. A linear relationship between the peak stress and strain-rate up to 4000 s^{-1} was observed due to the strain-rate sensitivity of the composite matrix.

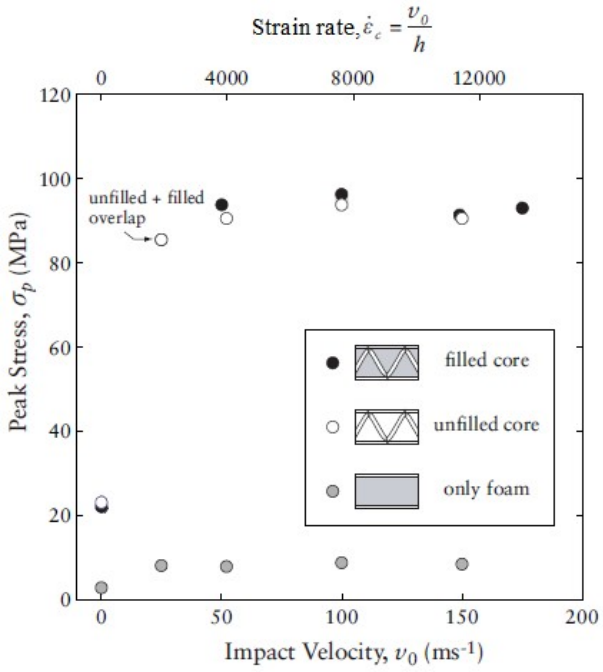

Figure 2.8. The peak stresses for the unfilled and filled core as function of impact velocity and nominal strain rate [52].

Wadley *et al*. [115] studied the impact response of corrugated core sandwich panels made from aluminum. The impact tests were conducted using a 12.7 mm diameter hardened steel projectile and a high speed camera (for the velocity measurement). They noted that the precise location of impact influenced the interaction of the structure with the projectile. Low momentum impacts, near the apex, resulted in penetration of the face sheet and the projectile was deflected by the inclined webs. However, as the impact velocity was increased, the web offered insufficient resistance to deflect the projectile. Conversely, impacts mid-way between the apex

resulted in projectile impact on apex webs on the opposite side. Here, the projectile was not deflected, since the lateral deflection forces exerted by the inclined webs is almost balanced.

2.2.3 Honeycomb Core Structure

Recent research suggests that a lightweight sandwich structure with a periodic truss (e.g. honeycomb core) offers a highly efficient load-supporting system. For example, the square or triangular honeycomb core offers a high in-plane stretch strength. The hexagonal core structure is most commonly used in honeycomb sandwich panels and is well-documented in many reports [40-43]. Those reports identified a number of failure modes in the honeycomb core structures; (1) face yielding, (2) intracell buckling, (3) face wrinkling, (4) core shear and (5) indentation.

Côté*et al*. [44] observed that the square honeycomb core exhibits axial-torsional buckling of the cells. During this mode, the cell wall section rotates about the transverse axis, while the vertical nodal axis remains straight. Figure 2.9 shows the axial torsional buckling mode for the unbonded square honeycomb core made from stainless steel. The authors stated that the compressive response of the core with a relative density of 0.20 is strongly affected by the presence of the bonded skins than the core with relative densities of 0.03 and 0.10. The steel square honeycomb was compared to the aluminium hexagonal honeycomb. The authors revealed that the hexagonal honeycomb exhibits a lower peak stress and more rapid softening beyond the peak load than the square core counterpart.

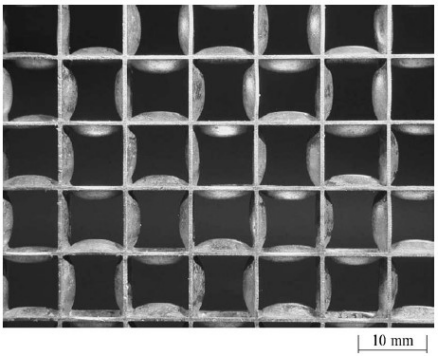

Figure 2.9. Plan view of the unbonded square honeycomb core structure compressed to a strain of approximately 0.1 [44].

Previous research on metallic sandwich structures by Dharmasena *et al*. [33] has shown that a honeycomb core experiences a higher peak strength than a truss or corrugated core. They also observed that under quasi-static loading, the square core achieved a peak strength approximately 27% higher than the triangular core honeycomb, as seen in Figure 2.10.

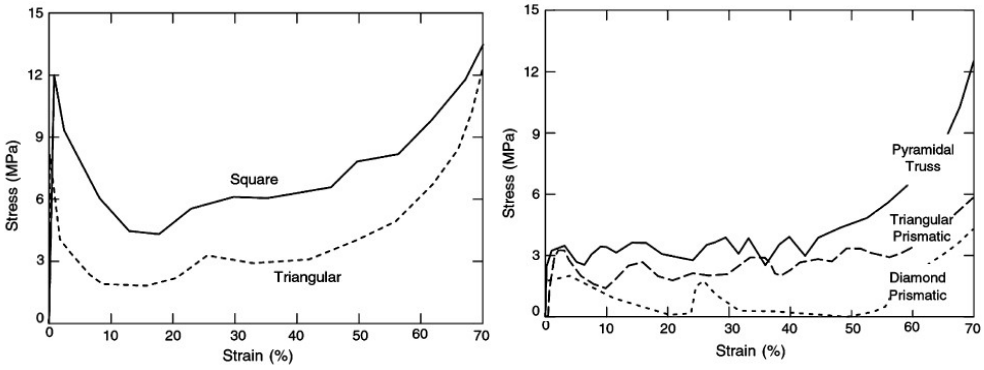

(a) honeycomb, (b) trusses, prismatics

Figure 2.10. The stress-strain responses of the metallic sandwich structures [33].

Chen *et al*. [45] compared the compressive properties of a polyurethane (PU) foam core, a glass honeycomb core preform and a carbon honeycomb core preform. The honeycomb preform was filled with PU foam in the preform gap. They found that the properties of the honeycomb preform composites were higher compared to the traditional PU foam core. In addition, the carbon honeycomb has the highest values of compressive strength, followed by the glass honeycomb.

The energy-absorbing characteristics of hierarchical woven lattice composites were evaluated by Zheng *et al*. [46]. The square interlocking structures were composed of a woven lattice as the sandwich cell walls. They concluded that the sandwich cell walls successfully restricted rib buckling. As a result, the structure had a high compressive strength and stable plateau region, thereby enhancing the specific energy absorption of the cellular material. Furthermore, even though the hierarchical lattices have lower relative densities, they offers higher densification strains. Therefore, their energy absorption capability is also improved.

Numerous studies on determining the dynamic properties of honeycomb core structures have been undertaken by previous researchers [32,53-56]. Li and Muthyala [54] investigated the impact properties of hybrid core sandwich structures. The hybrid cores were manufactured by weaving glass fibres to form a square grid, which was then filled with syntactic foam in the cells. Three different locations were studied (the cell, rib and node) with different sizes of cell area (referred to as Groups 2 – 4) and compared with the laminated composite (Group 1), as seen in Figure 2.11. The cell size and impact location were observed to have an effect on the impact response. Smaller cells offered a higher initiation energy, a higher maximum force and lower propagation energy. Furthermore, the lowest initiation energy and highest propagation energy were noted to be in the mid-cell region (bay area). The authors suggested that the node has the highest strength and stiffness as well highest capacity to transfer energy elastically. This is due to the fact that the node has the highest fibre volume fraction relative to the cell area that has no fibre reinforcement.

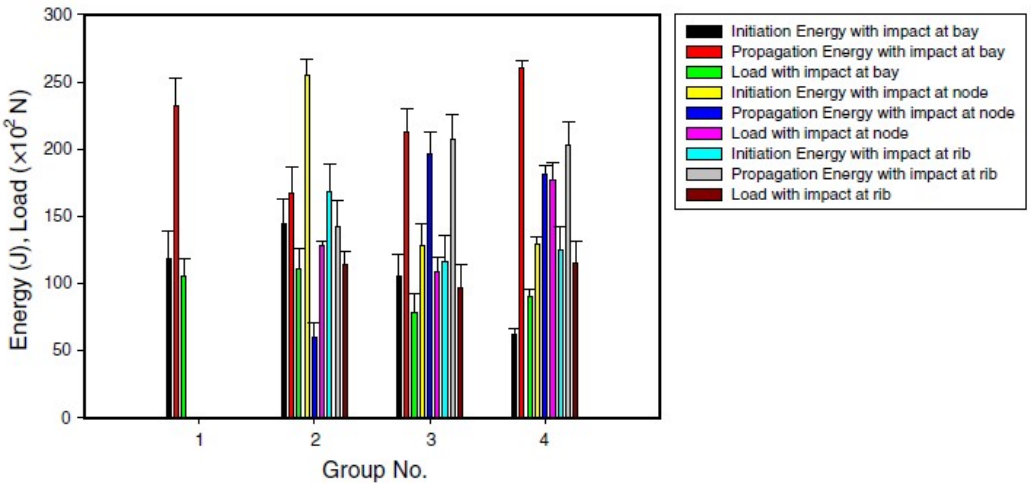

Figure 2.11. The impact properties of the hybrid core structures with different cell size and the laminated composite [54].

Park *et al*. [55] tested a carbon fibre composite honeycomb under quasi-static and dynamic compression loading. Quasi-static tests were undertaken on end-loaded specimens between the lubricated platens of a screw-driven test machine. Dynamic tests were performed using a Kolsky bar and the experimental set-up was similar to that conducted by Radford *et al*. [50]. Relative to quasi-static rates, an increase in peak stress of between 5% and 45% was observed at intermediate rates of 1,400 – 2,800 s^{-1}. The peak stress was attributed to micro-buckling at the slot root. At higher strain rates (8,400 – 16,800 s^{-1}), the increase in the peak load was more pronounced, where increases of between 43% and 67% were observed. Here, the results were associated with elastic wave propagation and inertial forces.

The dynamic axial compression behaviour of circular honeycomb was examined by D'Mello *et al*. [116]. The 3-cell and 7-cell circular cell cores were evaluated using two loading methods, these being a wave loading device method (WLD) and direct impact method (DIM) at impact velocities of approximately 12 ms^{-1} and 5 ms^{-1}, respectively. The peak loads observed in WLD tests were higher than those measured in DIM tests. This is due to the fact that the deceleration force upon impact increases as the impact velocity is increased. The circular honeycomb core failed progressively in a concertina-diamond fold mode, similar to that reported in previous work [117].

2.3 Natural Fibre Composite Systems

Increasing environmental concerns have encouraged researchers to develop a range of recyclable materials based on natural fibres, such as flax, hemp, kenaf, jute, bamboo, oil palm, coconut and many more. Fundamental research on natural fibres has intensified only in recent years, due to increasing demands for greater environmental protection [57-61]. Many researchers have shown that composites based on natural fibres can, if correctly designed, offer comparable properties to those based on conventional fibres, such as glass fibre.

For example, Bledzki and Gassan [62] reviewed the potential use of composites reinforced with cellulose-based fibres. In their article, very few natural fibre composites offered mechanical properties that are comparable to glass fibre composites. Moreover, some natural fibres are already being used in industry, such as the automotive and furniture industries. They also stated that the most popular fibres are jute, flax and coir.

Merta and Tschegg [63] reported that the fracture energy of a hemp fibre reinforced concrete was increased up to 70% that of a unreinforced concrete. They believed the increase in the fracture energy was due to the high tensile strength offered by the fibre, as well as the fine surface profile of the fibre that allows good bonding to the matrix. In contrast, straw and elephant grass-reinforced concrete showed a moderate increase in fracture energy of about 2% and 5%, respectively.

Currently, many studies on natural fibre composites are conducted on laminate and tubular structures, but fewer on periodic structures. The mechanical performance studies of these types of structure are discussed in Sections 2.3.1 to 2.3.3.

2.3.1 Sandwich Laminates

Sui *et al*. [64,65] investigated the mechanical behaviour of a bamboo/aluminium laminate. Buckling and delamination of the outer aluminium layers were observed as being the common failure modes when loaded in compression and bending. Later, Zhang *et al*. [66] extended the study by investigating the static indentation behaviour of a bamboo/aluminium laminate. They observed that laminates with a fully-supported boundary condition displayed a much higher maximum force than those supported on an open test window. Failure in the cross-ply bamboo laminate was dominated by interlaminar fracture, whereas the unidirectional bamboo laminate failed by multiple delaminations.

Vasumathi and Murali [67] investigated fibre metal laminates (FML) based on carbon and jute fibres. The laminates were fabricated using a hand lay-up technique, followed by curing at room temperature and compression for ten minutes in a compression moulding machine. They found that the carbon-jute reinforced aluminium laminate and carbon-jute reinforced magnesium laminate offered a superior impact resistance.

Three different stacking sequences of hybrid composite laminate were studied by Petrucci *et al*. [68]. The hybrid composite laminate consisted of glass mat and natural fibres (flax, basalt and hemp). The results show that hybrid laminates based on glass, flax and basalt offer a superior tensile strength compared to glass/hemp/basalt laminate and flax/hemp/basalt laminates, improved by 19% and 32%, respectively.

Verma *et al*. [69] conducted a study on the mechanical properties of bamboo laminae and laminated bamboo epoxy composite (LBCs). The laminae and LBCs were compared with wood and wood-based composites. They found that the average strength for the bamboo laminae was greater than the softwoods and was comparable with hardwood. Furthermore, the LBC results indicate that it can be a potential replacement for wood and wood-based composites for structural purposes.

Hoto *et al*. [83] developed sandwich composites from natural fibres and a cork agglomerate core. The sandwich composite was prepared with face sheets made of flax and basalt fibres. They found that the properties of the face sheets greatly affect the failure mechanisms, with the energy absorption showing a significant increase. The authors also argued that natural fibres in a bio-based matrix offer great potential for use in a range of industrial applications.

Dweib *et al*. [84] developed a range of structural beams made from a plant oil based resin and natural fibres (comprising of flax, cellulose, pulp, recycled paper and chicken feathers) using vacuum assisted resin transfer moulding (VARTM) technology. Theflexural rigidity and strength of the composite beams were nearly equal to or exceededthat of wood beams. Thus, the authors suggested that natural composite beams offer potential for use in wood-based structural applications.

An attempt to produce an environmentally-friendly core panel from bamboo skin waste was carried out by Nordin *et al*. [90]. Comparisons were made between glued-laminated bamboo strips [91] and bamboo parallel strip lumber [92]. The sandwich panel was found to offer the lowest bending strength, but, the authors concluded that the full utilisation of bamboo waste could offer better properties in the near future.

2.3.2 Tubular Structures

Meredith *et al*. [70] developed conical structures based on hemp, flax and jute fibres. The structures were tested under the static and dynamic loading. They found that the specific energy absorption (SEA) of the hemp structure was comparable to that measured on carbon fibre, whereas the SEA for flax was higher than a jute cone. The fibre volume fraction (Vf) was found to influence the SEA of the structure, as high Vfresulted in high SEA values.

A further investigation of the energy-absorbing characteristics of flax fibre tubes was undertaken by Yan and Chouw*et al*. [71]. Three length-to-diameter ratios (*L/D*), i.e. 1, 1.5 and 2, fabricated from different layers and length, were examined. The composite tube with large lengths and numbers of plies were found to absorb agreater

energy. In contrast, composite tube consisting of a large number of plies, with a shorter length, offer a greater crush force efficiency.

Węcławski *et al*. [72] studied the compressive behaviour in the elastic region and post-collapse behaviour of natural fibre composite (NFC) tubes based on hemp yarns. The tubes were manufactured by pultrusion, pullwinding and filament winding techniques. The NFC tubes were manufactured with various fibre orientations, ranging from 10° to 90°. The NFC tube, with an angle of 11.1°, offered the higher values of strength and modulus than the other angles. Four principal fracture modes were observed in their study, these being micro-buckling, diamond shape buckling, concertina buckling and progressive crushing, which are closely related to the geometries of the tube architectures.

Bamboo was one of the natural tubular structures that also offered good mechanical properties. Bamboo is a composite material reinforced axially by fibres,referred to as bundle sheath [73]. Amada *et al*. [73] observed that the strength of bamboo bundle sheaths is about 12 times higher than the bamboo matrix. They also suggest that this bamboo tube structure can resist environmental loads (e.g. wind), where the maximum surface stress are constant along the entire bamboo length. A large number of works have been carried out to investigate the mechanical properties of natural bamboo tubes. Previous work identified that the properties of bamboo tubes aredependant on various effects, such as the species of bamboo, the height of the culm (from top to bottom), the age of the tree (in years), and the moisture content [74-78].

Lakkad and Patel [108] tested a bamboo tube with an outside diameter of 55 mm and a wall thickness of 8 mm. The specific strength of the bamboo showed higher values compared to a mild steel, a glass reinforced polymer and a polyester resin. Thus, the authors recommended that bamboo can be considered as a structural material. However, due to its environmental sensitivity that can degrade the mechanical properties, suitable coating or treatment should be applied to avoid such effects.

Tan *et al*. [79] proved that the outside surface of a bamboo tube has a higher fibre density, while the inside surface has a lower fibre density. Therefore, the outside

regions exhibit lower levels of crack tip shielding, whereas the inside regions resulted in higher levels of crack tip shielding.

Previous work on the mechanical performance of the nodal regions in bamboo shows a lower strength than the internodal region [104,105]. Later, Jiang *et al*. [77] examined the effect of nodes and internodes in bamboo tubes on their mechanical performance. The radial-circumference strength of the node was about 2.38 times greater than that of the internode. They proposed the nodes in bamboo to have a positive effect on the transverse strength and stability.

2.3.3 The Performance of Natural Fibre Periodic Cellular Structures

Recently, lightweight sandwich structures based on natural fibre have started to attract interest from various researchers [80-82]. The mechanical properties of natural fibre-based cellular structure are discussed below.

The mechanical properties of hexagonal and sinusoidal core structures based on sisal reinforced polypropylene (PP) composite were investigated by Rao *et al.* [106]. The specimens were tested under the flatwise compression loading. Comparisons were made between the unreinforced PP, hexagonal sisal-PP, sinusoidal sisal-PP and hexagonal wood-PP structures. They observed that the specific compressive strength of both hexagonal and sinusoidal sisal-PP cores exhibited higher values than the unreinforced PP and hexagonal wood-PP cores. They also reported that sisal-PP cores couldbe compressed to over 80% of their initial height. It was suggested that sisal-PP composite cores are suited for use in the packaging application.

Rao *et al*., [85] tested a honeycomb core based on a sisal-polypropylene (PP) composite. Compression tests at a crosshead displacement rate of 0.5 mm/min were carried out to investigate the collapse behaviour and the failure mechanisms. Axial failure was dominated by buckling of the cell walls and subsequently material fracture. The sisal-PP cores were compared with pure PP cores by normalising the properties with respect to density. It was found that the specific strength of the sisal-PP honeycomb cores were almost twice those of the PP honeycomb cores. The sisal-PP core was observed to exhibit higher energy absorption values than the PP cores,

as shown in Table 2.1. The sisal reinforcement increased the elastic modulus, resulting in a greater buckling resistance in the cell walls. The authors suggested the increase in energy absorption was due to geometrical parameters, as well the reinforcing effect. Moreover, as the ratio of cell wall thickness to length (*t/l*) increased, the energy absorption capability in the elastic region also increased.

Table 2.1. Summary of the energy absorption capability of PPcores and sisal-PP cores [85].

Honeycomb CoreMaterial (core height in mm)	Density (kg/m^3)	Volume (m^3)	Energy absorbed per unit volume (MJ/m^3)
Polypropylene (25)	49	7.6 x 10^{-5}	0.44
Sisal-PP (25)	151	7.6 x 10^{-5}	1.9
Sisal-PP (50)	151	15 x 10^{-5}	1.5

Rao *et al*. [86,87] argued that natural fibre reinforcement of the cell walls could significantly enhance the load-carrying capacity and the energy-absorbing capability of fibre reinforced honeycomb cores. Figure 2.12 shows a sisal-PP composite core during compression testing.

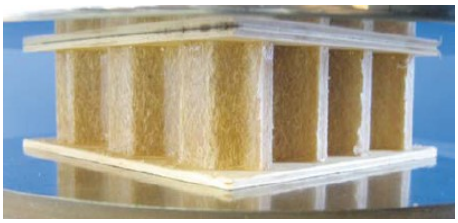

Figure 2.12. Photograph of a sisal-PP honeycomb core structures [86].

More recently, a honeycomb core made of jute fibre/vinylester (jute/VE) composite was proposed by Stocchi *et al*. [82]. The jute/VE core was observed to fail in a progressive damage mode, due to fibre pull-out and fibre fracture. This failure behaviour was affected by the large wall thickness relative to the cell size, that restricted buckling, as well as the heterogeneities in the composite material. They compared this natural fibre honeycomb core with commercially-available honeycomb cores, as seen in Figure 2.13. Clearly, the performance of jute/VE core is comparable to that of the commercially available products. Furthermore, the specific compressive strength for 10 mm cell of jute/VE core shows the superior performance than the other cores.

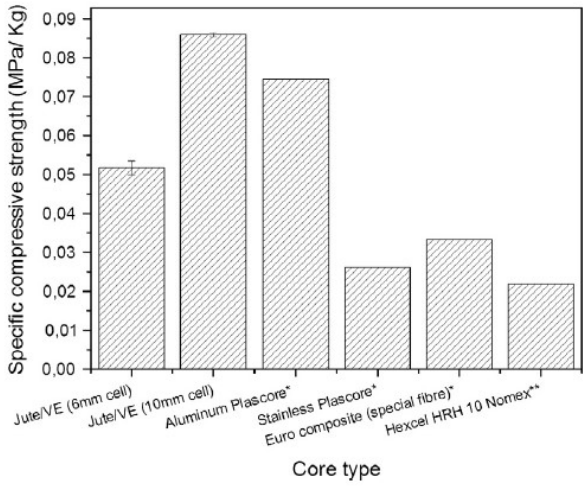

Figure 2.13. Comparison of specific compressive strength between Jute/VE honeycomb and those of the commercially available cores [82].

A comparison of the in-plane compressive properties of corrugated corestructures made of manicaria/polylactide and plain polylactide was undertaken by Porras and Maranon [88]. Specimens with sizes of 50 x 50 x 11 mm were tested at a crosshead speed of 0.5 mm/min. The mechanical properties of the corrugated core based on manicaria/polylactide increased to more than twice those of the plain polylactide. The manicaria-based corrugated structure was observed to fail due to the formation of plastic hinges when the critical stress was reached.

Yang and Fei [89] tested bamboo-wood corrugated cores with a cubic size of 100 x 100 mm. The influence of pressure, temperature and time were examined, as those play a dominant role in the mechanical performance of natural fibre composites. This has also been confirmed by Ho *et al*. [107]. The strength properties of the bamboo-wood corrugated core increase with increasing pressure. However, temperature and time have a less significant effect on their strength properties. They observed that this natural fibre corrugated core structure offers a superior strength to that of commercial non-structural products.

Petrone *et al*. [93] compared unidirectional and short random flax fibre/polyethylene (PE) honeycomb structures under dynamic loading conditions. All of the specimens were tested using a drop-weight impact tester with a 165 mm diameter flat striker [64] and a mass of 16.46 kg. The study was carried out to investigate the effect of core height and the presence of face sheets. The unidirectional flax/PE cores offered a superior impact response with a large elastic region and a higher peak load than the short random flax/PE cores. The cores with face sheets proved to improve the energy-absorbing capacity, due to the presence of bending and stretching in the face sheets. Nonetheless, the influence of the face sheets was less pronounced for larger core heights, where the energy was predominantly absorbed by the core. Figure 2.14 shows images of the flax/PE honeycomb core subjected to a 90 J impact loading.

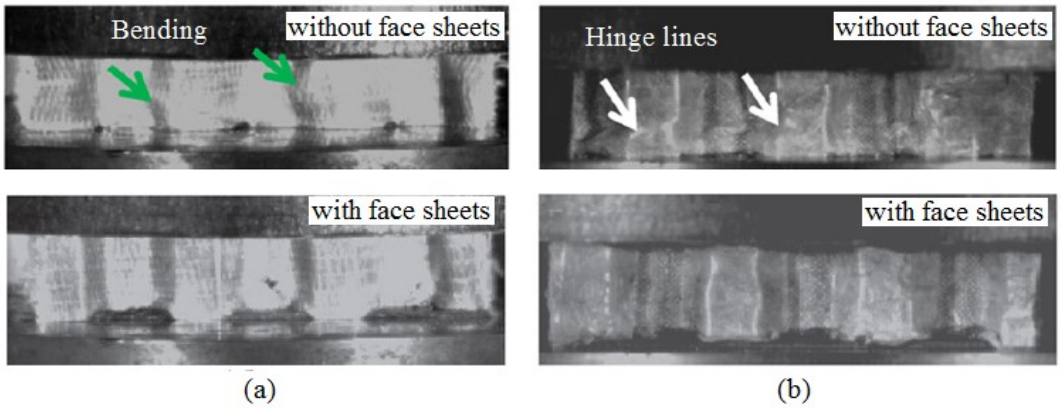

Figure 2.14. Photograph during the low velocity impact tests at the speed of 1.5 ms for (a) unidirectional flax/PE core without and with face sheets, and (b) short random flax/PE without and with face sheets [93].

2.4 Numerical Analysis of Sandwich Structures

In general, dealing with a large number of experimental works on sandwich structures will involve long periods and sometimes can be very expensive. Finite element (FE) simulations, if adequately formulated and accurately realised, help to greatly reduce the number of laboratory tests required to characterise the response of a sandwich structure subjected to various loading conditions [96]. FE analyses can offer detailed structural stress distributions and highlight the internal structural deformation, where it is difficult to visualise experimentally.

Côté *et al*. [97] developed FE models to analyse the response of hierarchical square honeycomb structures under the static compressive loading. The cell walls of the honeycomb core comprised of a polymethacrylimide (PMI) foam sandwiched between woven glass/epoxy composite faces. Simulations were performed using Abaqus and modelled using linear three-dimensional brick elements (C3D8R) with reduced integration points. The model consists of four brick elements through the thickness of each composite cell wall. Five to ten elements through the depth of the foam core were chosen to avoid excessive distortion. Antiperiodic boundary conditions were applied to the outer plate edges of the cruciform section to develop torsional-axial buckling and face wrinkling mode. The PMI foam was set as an isotropic elastic-ideally plastic solid, and the post-yield behaviour using a crushable foam formulation. The glass composite was modelled as an orthotropic elastic-ideally plastic solid to mimic plastic microbuckling. The predictions of the FE models were compared to corresponding experimental and analytical results. Under the elastic buckling analysis, the predicted first eigenvalues were in good agreement with the lowest collapse load predicted analytically. Initial geometric imperfections, in the shape of the first elastic eigenmode, were introduced into the sandwich plates. The imperfection factor ,ζ , was set in the range of 0-1.7%. The authors identified that the peak stress is sensitive to the magnitude of the initial imperfection. Here, an imperfection factor of ζ = 0.3% was found to produce the qualitative shape of the measured collapse response.

Russell *et al*. [98] analysed the three-point bending response of carbon fibre sandwich beams with square honeycomb cores using Abaqus/Explicit. They assumed perfect bonding between the honeycomb core and face sheets. The composite sandwich beams were meshed with square elements of 1.2 mm size in the face sheets and 0.7 mm in the core. The authors applied an element removal option from Abaqus, where the element would be removed once it reached the value of unity and could not resist any further stress. Comparisons between the FE calculations and the experimental results showed good agreement in the measured peak load, and accurately captured the deformation and failure modes.

Burlayenko *et al*. [99] predicted the elastic properties of foam-filled honeycomb core structures using a combination of shell and solid elements for the honeycomb cell walls and core foam, respectively. Three types of boundary condition were examined in order to find the appropriate engineering constants. It was suggested that the foam-filled core exhibited a uniform stress distribution through the core thickness than the core without the foam. They found that the influence of polyvinyl chloride (PVC) H200 foam filling increased the out-of-plane transverse Young's modulus and shear moduli by 15% and 24%, respectively.

Wang and McDowell [100] studied the effects of defects on the in-plane properties of square and triangular cell metal honeycombs using the Abaqus software package. The defects were introduced by removing the cell walls at random locations. The properties of triangular cell reduced more gradually than the square cell, whilst maintaining the residual stiffness and strength.

The level of stress concentration at the slot-ends of the square honeycomb core was analysed by Park *et al*. [55]. The investigation was carried out to estimate the onset of damage in the composite. The finite element analysis shows that the local stress concentration generates fibre micro-buckling from the root of the slot, which was confirmed by using the optical microscopy.

Chen *et al*. [101] investigated the dynamic crushing characteristics of square honeycomb thin rubber wall. The honeycombs were meshed by eight node brick elements with reduced intergration (C3D8R), with five elements through the web thickness and forty through the wall height. In order to avoid any penetration between the solids, a general contact condition was used between the web and rigid plate, as well as the web itself. They studied the geometric imperfections and the effect velocity on the crush behaviour. Details of imperfection sensitivity were reported in previous studies [109,110]. A series of geometric imperfections were obtained by performing a quasi-static buckling eigenvalue analysis with Abaqus/Standard. The change of the geometry shape was transported from one code to the other, since the model is in the same meshing elements. Three different imperfection shapes were created, as seen in Figure 2.15, representing the first, fifth and tenth eigenvalues. They suggested an initial imperfection shape can influence the dynamic deformation shape of the core. Due to unknown real imperfections, the imperfection of first, fifth and tenth modes were used with the scale factor of ζ = 1/10. An analysis of different impact velocities was undertaken at 1, 10, 25 and 50 m/s (strain-rate = 20, 200, 500 and 10,001 s^{-1}) using the same imperfection scale factor. The results proved that the influence strain-rate on the buckling behaviour is very prominent. At a low strain rate, they observed a global buckling mode with a long wavelength, and as the strain-rate was increased, the local mode became smaller with shorter wavelengths. Thus, the crushing velocity was found to be the dominant factor controlling the crush behaviour of the core. The authors also identified that both inertial resistance and strain hardening increase the stress plateau, whereas inertial buckling stabilisation delays the buckling moment of the core.

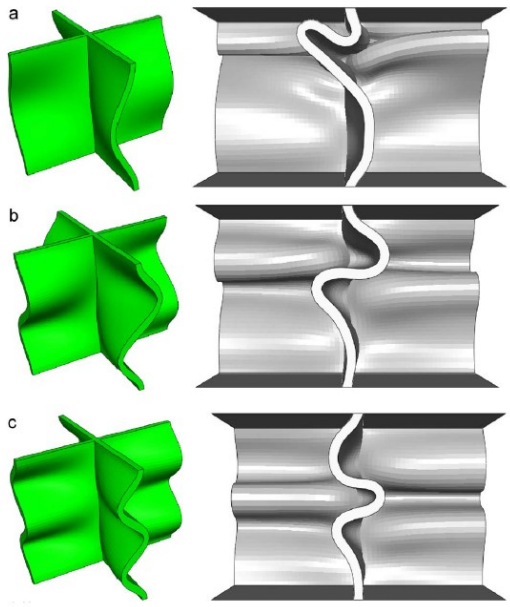

Figure 2.15. The first, fifth and tenth modes of the core and the corresponding crush deformation shape of the core (velocity constant at 25 m/s) [101].

Vaziri *et al*. [102] developed square and folded core model structures using Abaqus/CAE software. All of the components (face sheets, core webs and polymeric foams) were modelled using eight-node brick elements with reduced integration (C3D8R). A classical flow theory, based on the von-Mises yield surface and isotropic hardening, was employed in the computations. The models were performed under quasi-static and dynamic loading conditions, using explicit time integration (Abaqus/Explicit). This was due to the complexity of the geometry and variations in the material behaviour, as well as the convergence difficulties when using the implicit version (Abaqus/Standard).

Numerical investigations on the structural response of natural fibre sandwich structures are limited. Rao *et al*. [103] conducted a linear elastic finite element analysis on a hollow core sandwich structure manufactured from a sisal fibre composite. They found that the mid-span deflections predicted by the FE analysis were in good agreement with the experimental results. In addition, the specific shear strength of the core was more than double that associated with an unreinforced polypropylene core.

Rao *et al*. [87] used numerical modelling techniques to characterise the energy absorption capabilities of recyclable sandwich panels made from sawdust polypropylene (PP) composites. The FE analysis included a convergence study on the unit cell model, with various numbers of elements through the thickness of the core. The FE results reveal that the energy-absorbing capability of PP honeycombs (unreinforced and reinforced) increased constantly with increasing thickness (t) to length (l) ratio of the cell walls.

2.5 Interim Conclusions

Chapter 2 has presented a review of relevant studies from past and current research work on sandwich structures subjected to quasi-static and dynamic compression loading. The review includes a brief explanation of the classification of cellular materials, such as foams and periodic cores. Here, a review of the mechanical response of related core structures under the quasi-static and dynamic loading is presented. Based on the literature, a periodic core structure using composite material offered good mechanical properties to be used as energy-absorbing engineering applications. Failure mode of the periodic structure aremainly associated with buckling, delamination and compressive failure. A number of factors on their static and dynamic properties have been observed such as the material effect, cell wall thickness, angle of corrugation, relative density, strain-rate, inertial stabilisation as well the skins effect. Finally, procedures and techniques for modelling the response of honeycomb sandwich structures using commercially-available FE codes have been reviewed.The use of imperfection in a model can help to accurately predict the structural response to be compared to experimental work.

To date, natural fibre composite structures studied by previous workers have been in the form of sandwich laminates and tubular structures. Most of the structures offer a very good mechanical performance suited for future engineering applications. There is also an interest to use natural fibre as face sheets bonded to commercial cores, such as honeycomb, foam, etc. [94,95,112-114]. However, there are few studies on natural fibre composites designed in the form of periodic cellular cores, e.g. with honeycomb and prismatic topologies.

CHAPTER 3 : EXPERIMENTAL PROCEDURE

3.1 Design and Fabrication of Sandwich Core Structures

Five types of sandwich structures were fabricated and tested in this study, these being bamboo honeycomb, foam reinforced bamboo tubes, corrugated, interlocking and corrugated paperboard. The corrugated, interlocking and corrugated paperboard structures were manufactured using the compression moulding method (Meyer hot press), as well the flax-based composite panels. Two types of mould were used to prepare the composite specimens, a flat mould and a corrugated mould. The moulds were covered with a Teflon film in order to avoid the material sticking to the mould during the compression moulding process. This self-adhesive is a non-stick, heat resistant material and the thickness is 0.08 mm. It is supplied by Techbelt®, United Kingdom. The Araldite 420 A/B structural adhesive used to bond the core to the two skins was supplied by Huntsman Advanced Materials GmbH. The recommended ratio for mixing the epoxy resin and hardener is 100:40.

3.1.1 Fabrication of the Skins

Biotex flax/polypropylene (hereafter known as flax/PP) and Biotex flax/polylactide (flax/PLA), supplied by Composite Evolution, Chesterfield, United Kingdom, were used as the skins and as a core for the corrugated and interlocking structures. The flax-based woven mats were supplied in the form of fabric roll. The materials were heated between 170°C to 200°C under a pressure of 1.5 bar. The fibre volume fraction of the flax-based composite materials was 0.4.

Here, flax-based composite panels, with a size of 200 x 200 mm, were prepared by stacking three plies of woven flax/PP and flax/PLA in 0°/90° fibre orientations as shown in Figure 3.1. The flax-based composite material was then placed in the mould. Next, the mould was placed in a Meyer hot press and heated to the required temperature under a pressure of 1.5 bar for approximately one hour. Finally, the pressure was released after the panel had cooled to room temperature.

A thermocouple was inserted in the mould to monitor the temperature during the heating process.Figure 3.2and Figure 3.3show the Meyer hot press machine and the flax/PP composite panel.

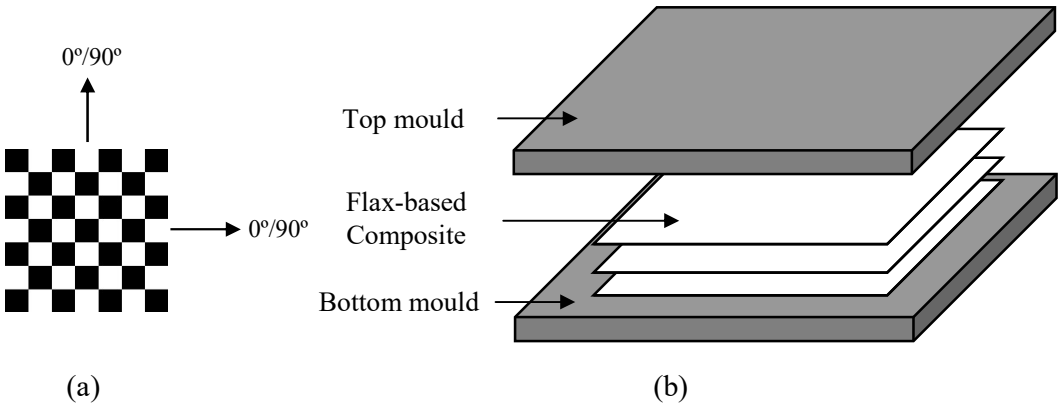

Figure 3.1.(a) Schematic of the stacking orientations of the flax-based composite and (b) the preparation for the composite panel.

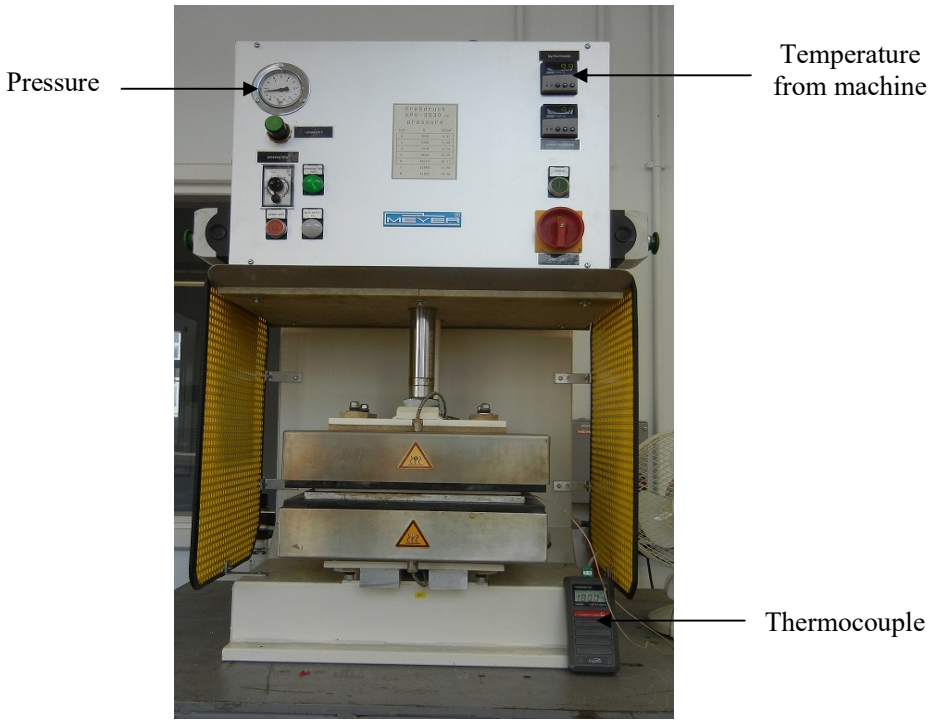

Figure 3.2. Photograph of the Meyer hot press machine.

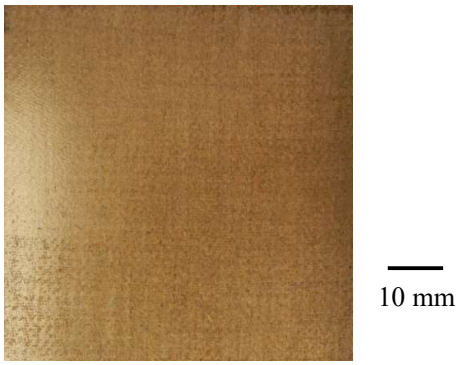

Figure 3.3.Top view of flax/PP composite panel following manufacture at the temperature of 190°C.

3.1.2 Bamboo–based Core Structures

Figure 3.4 shows the bamboo tubes with small and large diameters used in this study. The bamboo tubes wassupplied by Gardman, United Kingdom. This bamboo is used as an attractive edging in gardens [123].The bamboo had a light brown colour. The outer diameters (D_{out}) of the small bamboo tubes ranged from 6 to 15 mm and the large diameter tubes from 22 to 25 mm. Prior to testing, tubes of length 20 mm were cut from the internode regions of the bamboo canes and weighed. The tubes were then ground at both ends to ensure that the two surfaces were parallel, thereby minimizing the level of friction between the tube surfaces and the platens of the test machine.The physical properties of both small and large diameter of bamboo tubes are given in Table 3.1.

Figure 3.4.Photograph of (a) a small diameter and (b) a large diameter of bamboo tube.

Table 3.1.Physical properties of the small and large bamboo tubes.

	Mass (g)	Density (kg/m^3)	D_{out} (mm)	D_{in}/t ratio
Small	0.5 – 2.6	780 – 1140	6 – 15	1 – 4
Large	3.7 – 6.2	850 – 960	22 – 25	3 – 6

3.1.2.1 Bamboo Honeycomb

The bamboo honeycomb cores were manufactured from 20 mm long bamboo tubes. The cores were produced by bonding large numbers of bamboo tubes together using a two part epoxy resin to the flax-based composite skins, as shown in Figure 3.5. The curing time for the epoxy resin was approximately 24 hours at room temperature. The bamboo honeycomb structures were subsequently cut into 40 x 40 mm squares in preparation for mechanical testing.Here, the bamboo was placed in random positionsand due to variabilitiesof the outside diameter in nature, it is difficult to control gaps between the tubes. Therefore, the core structure was controlled through the pre-defined specimen size, regardless the number of tubes used. These procedures were applied to both the large and small diameter bamboo tubes with both flax/PP and flax/PLA skins. Figure 3.6 shows a photograph of the large bamboo honeycomb structure with flax/PP skins.

Figure 3.5.Top view showingthe arrangement of (a) small and (b) large bamboo cores.

Figure 3.6.Large diameter bamboo honeycomb with flax/PP skins.

3.1.2.2 Bamboo Tube-reinforced Foam

Bamboo tube-reinforced foam samples were designed by embedding 20 mm long bamboo tubes in four different densities of crosslinked foam with 20 mm thickness. Tubes with outer diameters of approximately 24 mm were selected for this structure. Here, expanded polystyrene (EPS70) was chosen as a lower density core material. The polystyrene foam is flammable and is a good thermal insulator. It is white in colour. It is used as a building insulation material. Three different types of thermoplastic crosslinked PVC (C70) foam were supplied by Alcan Ltd., these being C70.55, C70.75 and C70.130. The foams are yellow (C70.55), light green (C70.75) and dark green (C70.130) in colour.

These cross-linked PVC foamsare a unique closed cell foam which offers high stiffness and strength to weight ratios and also a high impact strength. A foam thickness of 20 mm was used in the study and samples were cut into square blocks with dimensions of 50 x 50 mm. Table 3.2 gives the mechanical properties of the polystyrene and crosslinked PVC foams, as given by the supplier [124,132].

Initially, the bamboo was chamfered at one end prior to being embedded into the foam. A hole was introduced into the centre of the foam for insertion of a bamboo tube of similar size. The bamboo was placed with the chamfered profile facing upwards. Figure 3.7 shows the large diameter bamboo tube embedded in foam.

Table 3.2.Mechanical properties of the polystyrene and crosslinked PVC (C70) foams [124,132].

	EPS70 (P1)	C70.55	C70.75	C70.130
Density (kg/m^3)	15	60	80	130
Compression strength (MPa)	0.08	0.90	1.45	3.0
Compression modulus (MPa)	-	69	104	170
Bending strength (MPa)	0.12	-	-	-
Shear strength (MPa)	-	0.85	1.20	2.40
Shear modulus (MPa)	-	22	30	54
Thermal conductivity (W/mK)	0.038	-	-	-

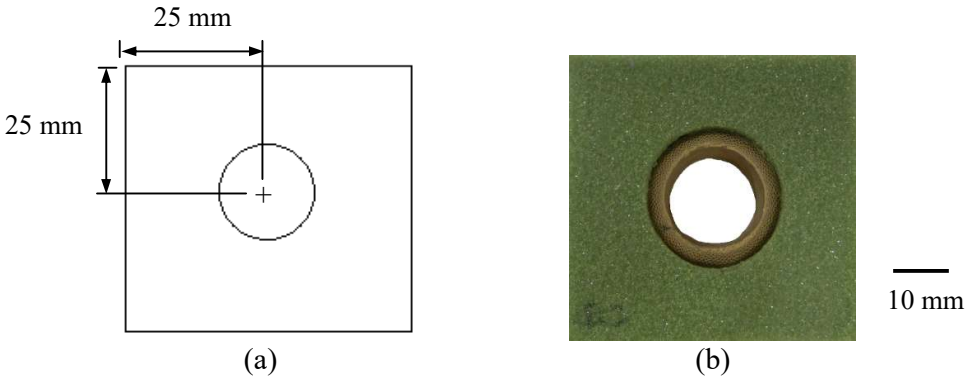

Figure 3.7.(a) Schematic geometry and (b) top view of a foam (C70.55) sample reinforced with a large diameter bamboo tube.

3.1.3 Flax-based Core Structures

3.1.3.1 Corrugated Structures

A corrugated mould made from mild steel with dimensions of 210 x 240 mm was used to manufacture the corrugated core structure. The mould had a nominal height of 10 mm and a length of 20 mm from peak-to-peak with an angle of 45°. This can be seen in Figure 3.8. This type of core was based on the triangular profile shown in Figure 3.9, where, h_t and h_b are the top and bottom skins thicknesses, respectively; h_c is the core height; t is the wall thickness;W is the width; L_1 and L_2 are the core length and strut member length, respectively. As the core was predetermined by the mould design, the value for L_1 was set to 20 mm while the angle α and β is 45º and 90º, respectively.

Thecorrugated core was manufactured from a total of four plies of thin PP film and four plies of flax/PP. The stacking sequence was one ply of PP film at the top and bottom, followed by two plies of flax/PP between the film. Initially, a pressure of 6 bar was applied for approximately 10 minutes, to allow the materials to form into the required shape. Subsequently, the pressure was reduced to 1.5 bar, and the heating process continuedfor one hour at a temperature of 190°C.Next, the corrugated flax composite core was bonded to the top and bottom skins using an epoxy resin. The skins were made from the same material as the core. Then, the corrugated flax composite core was cut into rectangular blocks with a 25 mm width and three different lengths, these being associated with two, three and five cells.Figure 3.10 shows a sample of flax/PP corrugated structure based on three cells.A similar method wasused for the flax/PLA composite and a thin PLA film at a temperature of 180°C.

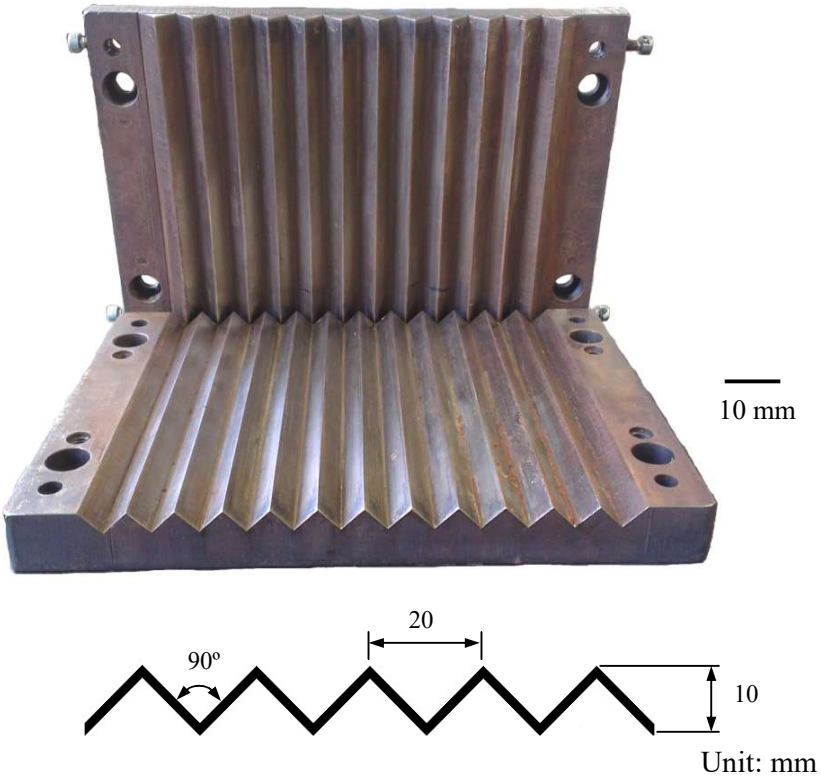

Figure 3.8. Mould used for making the corrugated core.

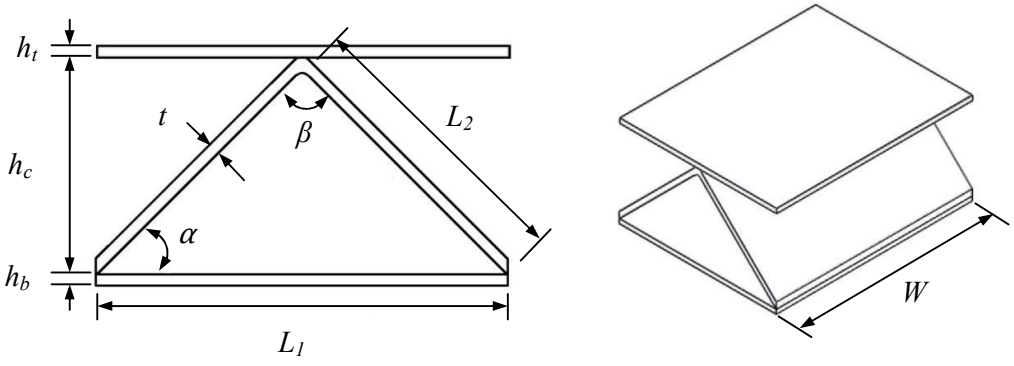

Figure 3.9.Schematic geometry of one unit cell of the corrugated core structure.

Figure 3.10.Flax/PP corrugated structure with three unit cells.

3.1.3.2 Interlocking Structures

Two types of interlocking core structure were manufactured in this study, these being square and triangular core. Initially, composite panels based on flax/PP and flax/PLA were manufactured using a hot press machine. Here, the manufacturing processes of the skins and core of the flax-based composite were the same as those skins for the bamboo honeycomb structures. The flax-based composite was manufactured under a pressure of 1.5 bar for one hour at temperature of 190°C (for flax/PP) and 180°C (for flax/PLA). Then, the composite panel was cut into rectangular strips using a bench saw. A total of six strips were used to fabricate the square interlocking and seven strips for the triangular core; four strips with the shape (a), two strips with shape (b) and one strip with shape (c), as shown in Table 3.3.

A simple slotting technique was used to make both the square and triangular structures; t = thickness, h_c = height of the core and L = length between the two strips, as shown inFigure 3.11. The core was then bonded to two skins, using an epoxy resin. The specimen sizes for the square and triangular interlocking core structuresare 70x70 mm and 70 x 60 mm, respectively. Figure 3.12 shows photographs of the square and triangular interlocking cores. Three different thicknesses of flax/PP and flax/PLA composite were prepared from two, three and five plies of material.

Table 3.3.Dimension of the strips for the square and triangular interlocking cores.

Type of interlocking core	Dimension
Square	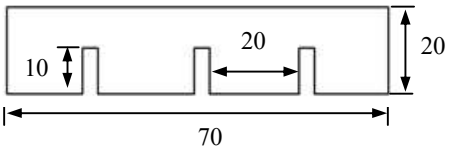 Unit: mm
Triangular	(a) 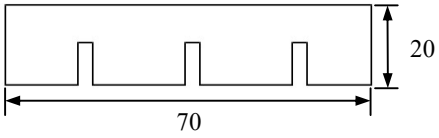 (b) 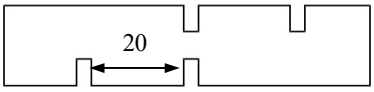 (c) 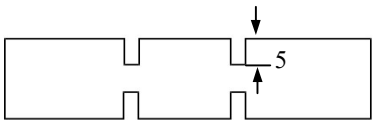 Unit: mm

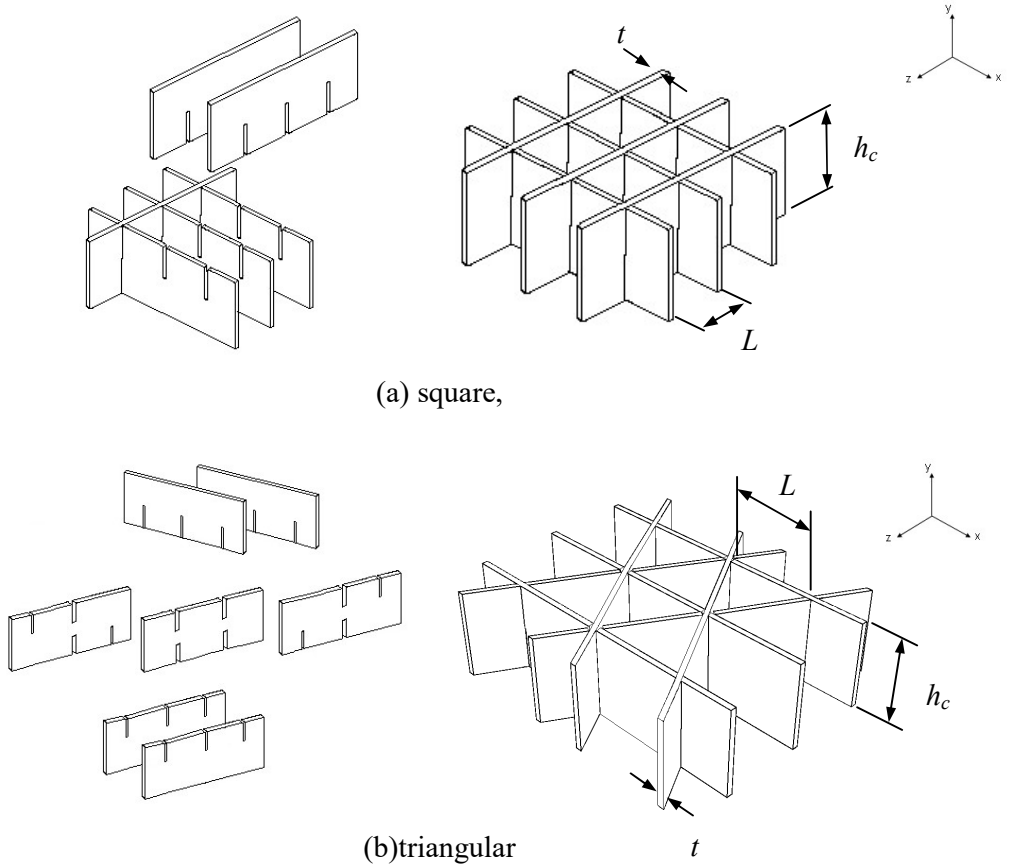

Figure 3.11.Slotting technique for the interlocking core structures.

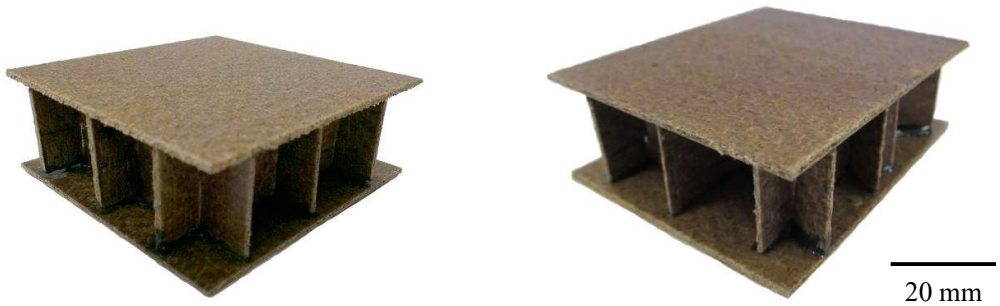

Figure 3.12.Final structurefor (a) a square and (b) a triangular interlocking core made from three plies of flax/PP.

3.1.4 Corrugated Paperboard Structures

Further investigation was carried out with flax-based composites to develop biodegradable sandwich structures using commercial corrugated paperboard. The corrugated paperboard panel was supplied by Xanita Ltd., South Africa. This core panel was brown in colour with a thickness of 20 mm and density of 80 kg/m^3 [125], as shown in Figure 3.13. It was produced from 100% recycled paper-waste, which is a recyclable and an eco-friendly material. It offers a high strength to weight ratio, high flexural strength and is also good for sound absorption.

A total of sixteen plies of thin PP film and two plies of flax/PP were prepared for the top and bottom skins. Here, a total of four plies of PP film were placed above one ply of flax/PP and four plies underneath it, as shown in Figure 3.14. The PP film was used to make a good bond between the flax/PP and core. Thus, those numbers of plies has been selected as the aim is to investigate the capability of using the flax-based composite to the corrugated paperboard structures. The materials were then heated using a Meyer hot press to a temperature of 180°C for one hour under a pressure of 1.5 bar. The flax/PLA skins were manufactured using the same procedure to those with flax/PP skins. Finally, the corrugated paperboard sandwich structure was cut into a square size of 50 x 50 mm, in preparation for subsequent mechanical testing, as shown in Figure 3.15.

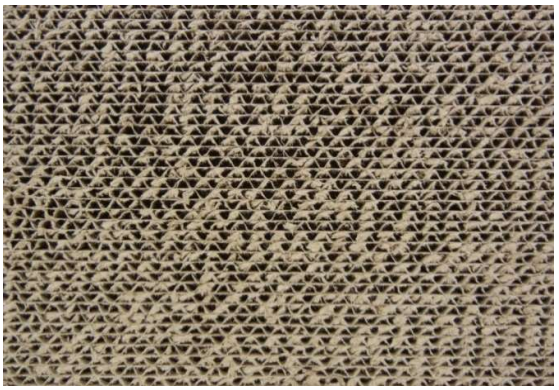

Figure 3.13.Corrugated paperboard core.

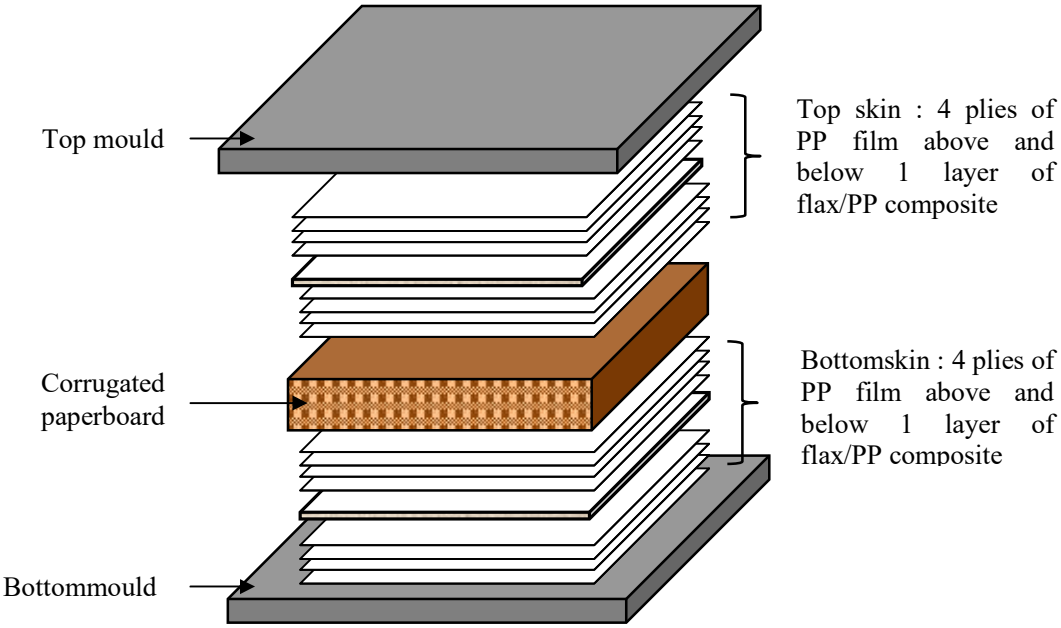

Figure 3.14.Stacking sequence for the corrugated paperboard with flax/PP skins.

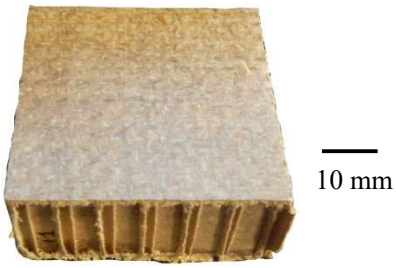

Figure 3.15. Flax/PP corrugated paperboard.

3.1.5 Stacking Sequences of the Material

A summary of stacking sequence for all of the sandwich structure cores manufactured in this study is given in Table 3.4 and Table 3.5. The difference in thicknesses was due to the compression moulding process. However, each structure was compared to the flax/PP and flax/PLA composites, except for the bamboo reinforced foam, which was compared to the differences of densities. Therefore, each structure was using the same number ofply of the flax-based composite. A total of five different materials were studied in this work, these being bamboo tube, flax/PP, flax/PLA, foam (polystyrene, C70.55, C70.75 and C70.130) and corrugated paperboard.

Table 3.4.Summary of the stacking sequences and thicknesses for the bamboo-based core structures.

Type of Structure	Constituents Materials	Stacking sequences	Nominal Thickness (mm)
Bamboo Honeycomb	6 plies flax/PP + Bamboo	FPP(x3)/Bamboo/ FPP(x3)	23
	6 plies flax/PLA + Bamboo	FPLA(x3)/Bamboo/ FPLA(x3)	22.6
Foams reinforced bamboo	Bamboo + Polystyrene (PS)	-	20
	Bamboo + C70.55 (C55)	-	20
	Bamboo + C70.75 (C75)	-	20
	Bamboo + C70.130 (C130)	-	20

Table 3.5. Summary of the stacking sequences and thicknesses for the flax-based composite and paperboard core structures.

Type of Structure	Constituents	Stacking sequence	Nominal Thickness (mm)
Corrugated	2 plies flax/PP (FPP) + 2 plies PP film (PP)	PP/FPP(x2)/PP	1.1
	2 plies flax/PLA (FPLA)+2 plies PLA film (PLA)	PP/FPLA(x2)/PP	0.95
Interlocking	3 plies flax/PP	FPP/FPP/FPP	1.5
	3 plies flax/PLA	FPLA/FPLA/FPLA	1.3
Paperboard	16 plies PP film + 2 flax/PP + Corrugated Paperboard (CP)	PP (x4)/FPP/PP (x4)/CP/PP (x4)/FPP/PP (x4)	21
	16 plies PLA film + 2 flax/PLA + Corrugated Paperboad (CP)	PLA(x4)/FPLA/PLA(x4)/CP/PLA (x4)/FPLA/PLA(x4)	21

3.2 Mechanical Properties of Materials

The initial focus of this study was to determine the mechanical response of the materials. Here, tensile tests were undertaken on the flax-based composite, and compression tests were conducted on the bamboo tubes. Here,the tensile and compression tests were conducted on an Instron 4204 and 4505 testing machine, respectively. The output from both tests was in the form of a load against displacement curve.

3.2.1 Tensile Testing

Composite panelsbased onthe flax-based composites (flax/PP and flax/PLA), with a 0°/90° fibre orientation, were prepared for tensile testing. Straight-edged rectangular specimens were fabricated since other researchers [126,127] have used this type to successfully avoid the need to machine potentially complex dog-bone geometries. The test specimens were cut from the flax-based composite panels into a size of 190 x 20 mm (Length, L x Width, W) using a bench saw. The average thicknesses (t) of the flax/PP and flax/PLA composites were approximately 1.5 and 1.3 mm, respectively. Tensile tests were conducted with a 5kN load cell at a crosshead displacement rate of 1 mm/min. An extensometer was placed onto the specimen. The initial gauge length (L_g) was 50 mm. The tests were carried out at least three times in order to obtain reliable data. Schematic drawings of the test specimen and thetensile test set-up are shown in Figure 3.16and Figure 3.17. The tensile strength was calculated using Equation 3.1:

$$\sigma = \frac{P}{A} \tag{3.1}$$

where$P$= load (N) and A = cross-sectional area of the specimen (m^2).

The Young's modulus (E) and strain (ε) were calculated using:

$$E = \frac{\sigma}{\varepsilon} \tag{3.2}$$

$$\varepsilon = \frac{\delta L}{L_g} \tag{3.3}$$

whereσ = strength (MPa), δL = elongation length (mm) and L_g = gauge length (mm).

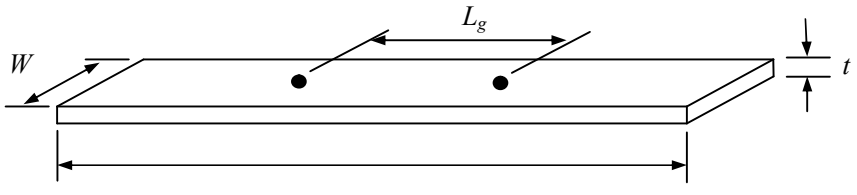

Figure 3.16.Schematic of the tensile test specimengeometry.

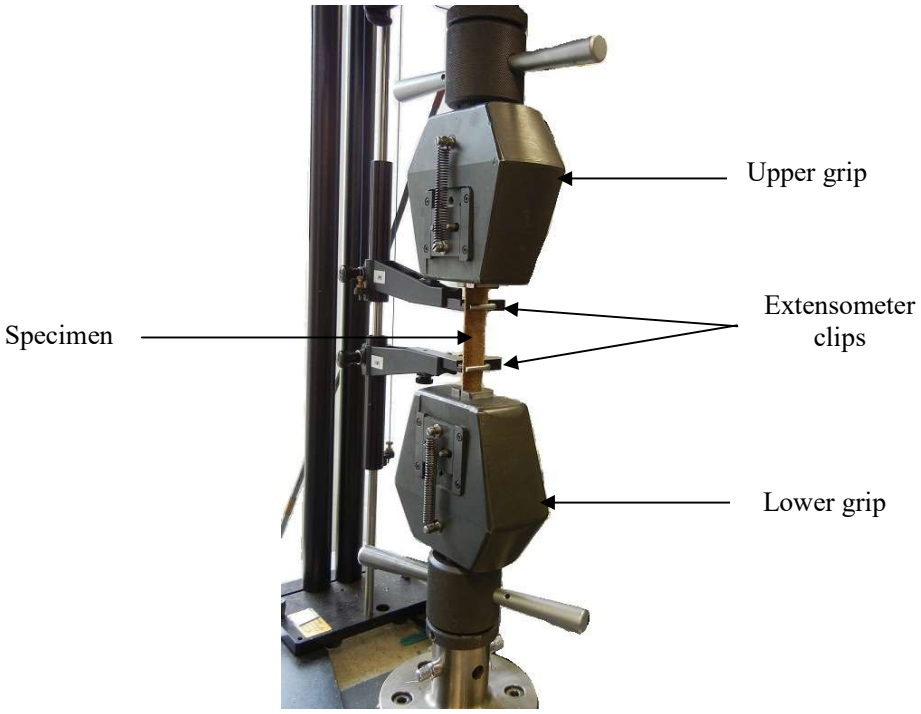

Figure 3.17. Tensile test set–up.

3.2.2 Compression Testing

Compression tests were conducted on bamboo tubes with a length of 20 mm,cutusing a band saw. An Instron testing machine with a 50 kNload cell was used at the crosshead displacement rate of 1 mm/min to determine the compression strength. The tests were undertaken in uniaxial compression in the fibre direction, similar tothose conducted by Chung and Yu [128]. Two different sizes of bamboo tubeswere tested, these being small and large diameter tubes. The specimen was placed between the two circular platens, as shown in Figure 3.18. The bamboo tubes are shown in Figure 3.4. Compression tests were also undertaken on polymerfoam block of size 50 x 50 x 20 mm.Here,the specimenswere loaded at a crosshead displacement rate of 1 mm/min.

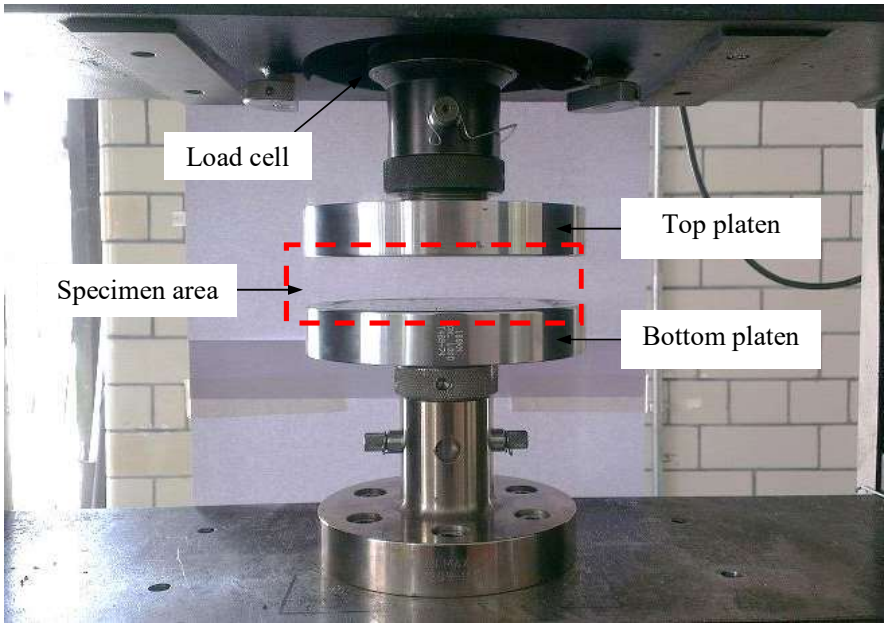

Figure 3.18.Photograph of the Instron machine used for the compression tests.

3.3 Mechanical Properties of Natural Fibre-based Sandwich Structures

In this study, different types of core structure have been manufactured and tested, these being bamboo honeycomb, bamboo reinforced foam, corrugated paperboard, corrugated and interlocking (square and triangular core) structures. A series of static compression and low-velocity impact tests were conducted to evaluate the mechanical properties of the natural fibre-based sandwich structures under static and dynamic loading conditions. The structures were then photographed in order to elucidate the prevailing failure mechanisms. Here, at least three tests were carried out on each structure.

3.3.1 Quasi – Static Testing

Quasi-static compression tests were conducted using an Instron 4505 universal testing machine at a crosshead displacement rate of 1 mm/min. Here, the specimen was placed between the two circular platens and a load was applied to the specimen until the structures had been fully crushed.The output from these tests was in the form of load against displacement traces. Following this, the compression stress-strain curves were plotted to determine the compressionstrength and modulus of the sandwich structures. The compression modulus was obtained from the initial slope of the stress-strain curve as shown in Figure 3.19. Again, Equations 3.1 to 3.3 were used to obtain the compression properties of the sandwich structures.

The energy-absorbed by the sandwich structures was calculated from the area under the load-displacement traces,using the trapezoidal rule [129]. The specific strength of the structure was calculated using Equation 3.1 and divided by the density (kg/m^3),while the specific energy absorbing was determined by dividing the energy by the mass (kg).

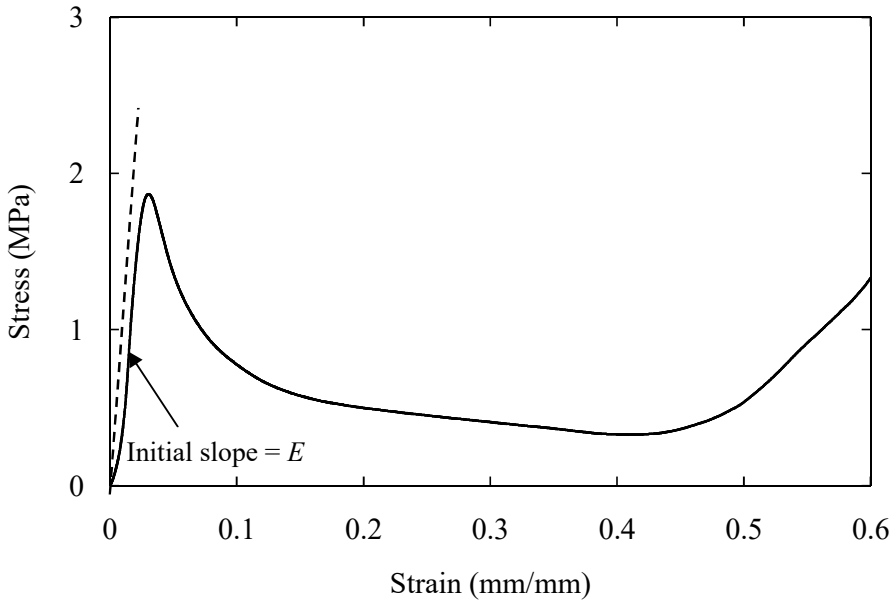

Figure 3.19.Determination of the Young's modulus from the stress-strain curve (exampleis taken from a test on square interlocking structure).

3.3.2 Dynamic Testing

Figure 3.20 shows the experimental set-up for the low-velocity impact tests on the sandwich structures using a drop-weight impact rig. The impact test relies on the free falling of a known mass from a given height in order to supply the energy required to deform the specimen. A range of masses and heights were used to produce the desired kinetic energy of the impactor. Here, a mass (M) of up to 30 kg was dropped from a height (H) of up to 1.5 meters to load the samples. In this study, the energy required for each structure was obtained based onthe energy absorption data obtained from the static compression tests. Table 3.6 summarises the energy to crush the specimens. A flat rectangular impactor was used to strike the specimens. The impactor was guided by two parallel columns to ensure that the impactor struck the specimen centrally. Frictionless contact was assumed between the two rails and the impactor. The specimen was progressively crushed from the top to the bottom once the impactor made contact with the top surface.

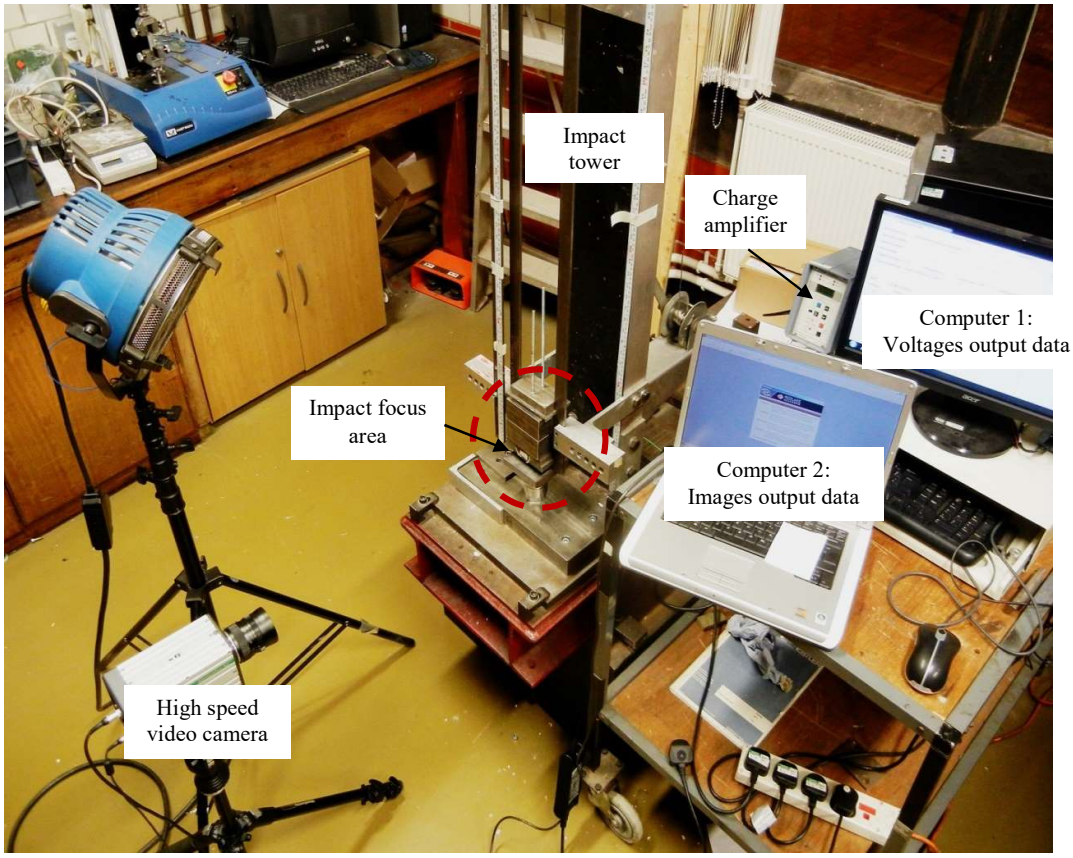

Figure 3.20.The test set-up for thelow-velocity impact tests.

The impactor load signal was obtained from the piezoelectric load cell (Kistler type 9363A) with a maximum capacity of 120 kN, and was positioned under the steel support. An insulated coaxial cable was used to connect the amplifier (Kitsler type 5011B) and the load cell. Here, the voltage was filtered using the charge amplifier, before being converted to a digital signal and recorded using the computer. The output was in the form of force (N) – time (t) traces. Details of the load-cell and amplifier are given in Table 3.7 and Table 3.8, respectively [130,131]. Figure 3.21 shows a close-up view of the test set-up used for dynamic testing.

Table 3.6.Impact energies used during the low-velocity impact tests on the different structures.

Type of structure	Materials	Impact energy (J)
Bamboo honeycomb (small and large diameter)	Flax/PP	322
	Flax/PLA	322
Foams reinforced bamboo	Foam Polystyrene	155
	Foam C70.55	273
	Foam C70.75	273
	Foam C70.130	355
Corrugated	Flax/PP	12
	Flax/PLA	4
Interlocking	Flax/PP	70
	Flax/PLA	50
Corrugated paperboard	Flax/PP	54
	Flax/PLA	54

Table 3.7.Details of the piezoelectric load cell (Kistler type 9363A) [130].

	Unit	Value
Measuring range	kN	0 – 120
Sensitivity	pC/N	– 3.8
Natural frequency	kHz	>35
Weight (without cable)	g	800

Table 3.8. Details of the Kistler amplifier type 5011B [131].

	Unit	Value
Measuring range for 10 V FS	pC	± 10 – ± 999 000
Sensor sensitivity (M.U. = mechanical units)	pC/M.U.	± 0.01 – ± 9 990
Frequency range (-3db, Filter "OFF")	kHz	≈ 0 – 200
Weight	kg	≈ 2

A high-speed video camera (MotionPro X4, model no. X4CU-U-4) with a standard F/0.95 – 50 mm lens was used to capture the velocity and displacement of the impactor. The video camera was positioned directly in front of the test specimen to track the movement of the impactor and the deformation of the structures. A high-intensity lamp was used in order to get a clear image of the deformation as well to illuminate the test rig while filming. The recording was initiated at the moment the impactor struck the top surface of the specimen and continued until the specimen was fully crushed and/or the impactor had stopped. As the image output was in pixels, the captured images were calibrated and processed to yield the required parameter, such as displacement and velocity. The calibration was carried out using the motion analysis software (ProAnalyst®). The energy to cause failure of the specimen was determined fromEquation 3.4.

$$E = mgh \tag{3.4}$$

where$E$ = energy (J), m = mass of the impactor (kg), g = gravity (~9.81 ms^{-2}) and h = height (m) of the impactor above the specimen. The same method used to calculate the total energy absorption, the specific energy absorption andthe specific strength that were used for the quasi-static tests were used in dynamic tests.

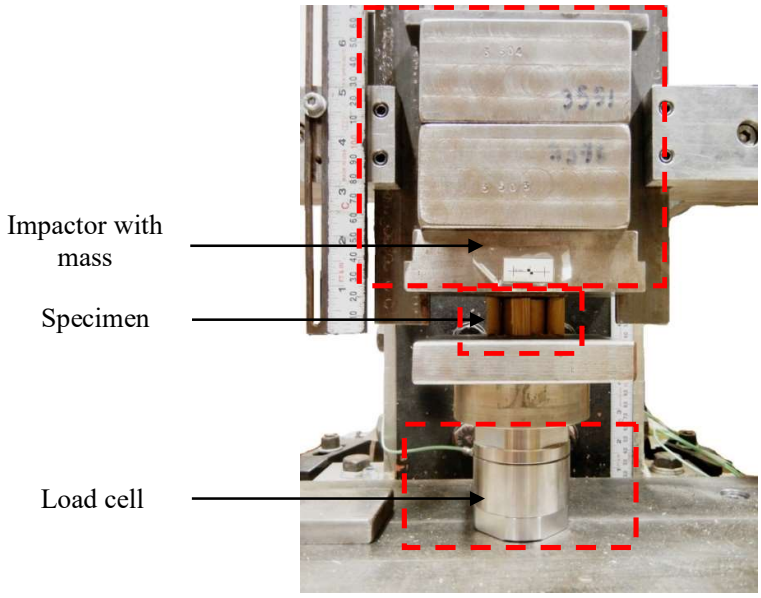

Figure 3.21. A close-up view of the test area for the low-velocity impact test.

3.4 Interim Conclusions

The details of manufacturing procedures for the skin material and the natural fibre-based sandwich structures have been presented in Chapter 3. This chapter also describes the experimental set-up, as well as the testing procedures for both the quasi-static and dynamic tests. Two types of material were tested in order to investigate the material properties, these being flax-based composites and natural bamboo tubes. These materials then were used to fabricate the core and skins for the sandwich structures. The fabrication includes the compression moulding (hot press) and cutting processes. Following this, the sandwich core structures were tested under the quasi-static loadingby using an Instron machine. The dynamic loading conditions was carried out using a drop-weight impact with impactor mass up to 30 kg, dropped from a height up to 1.5 m. A detailed explanation of the fabrication procedures used to make the structures is also included in this chapter.

CHAPTER 4 : MECHANICAL PROPERTIES OF NATURAL FIBRE-BASED SANDWICH STRUCTURES

4.1 Mechanical Properties of Flax-based Composites

4.1.1 The Influence of Processing Temperature on Flax-based Composites

Figure 4.1 shows the tensile stress – strain traces for the flax/PP and flax/PLA composites at various temperatures. It is apparent that all of the flax/PP composites show similar trends, initiated with linear and continued witha non-linear response up to the maximum stress value. The flax/PP composite failed in a catastrophic manner across the width of the sample, as a result, the stress dropped rapidly. It is clear that the flax/PP composite tested at 170 ºC offer a high strain to failure, approximately 0.05, compared to samples tested at 190 ºC and 200 ºC, which failed at strain approximately 0.022 and 0.013, respectively. The highest tensile strength for the flax/PP appears to be at 190 ºC measured, this being approximately 30 MPa.

In Figure 4.1b, the samples of flax/PLA composite at temperatures of 180 ºC and 190 ºC failed at strains of 0.05 and 0.024, respectively. It is evident that the stress level of the flax/PLA dropped gradually after reaching their maximum values. However, the stress at a temperature of 200 ºC found to drop rapidly and this might be related to the loss of matrix during the manufacturing process. The highest tensile strength for the flax/PLA composite was found to be 10.6 MPa at a temperature of 180 ºC, approximately 13% higher than at 200 ºC.

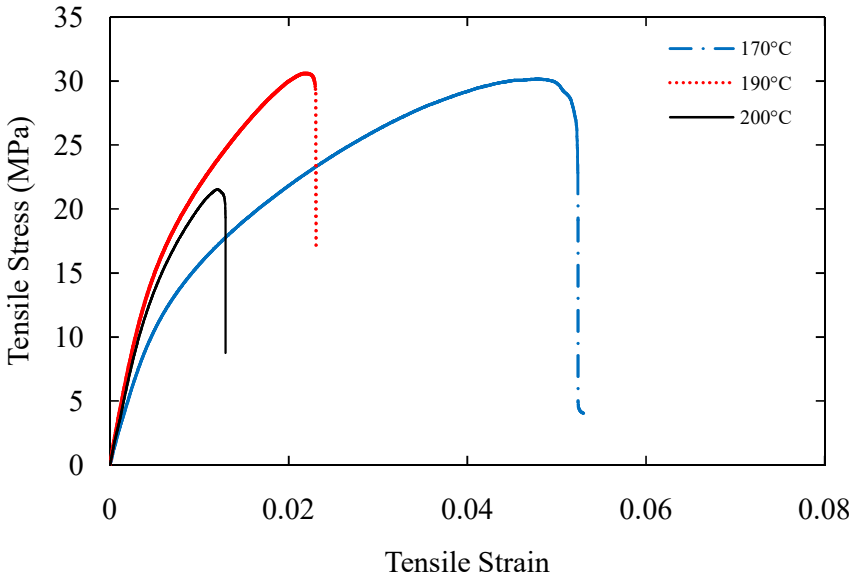

(a)

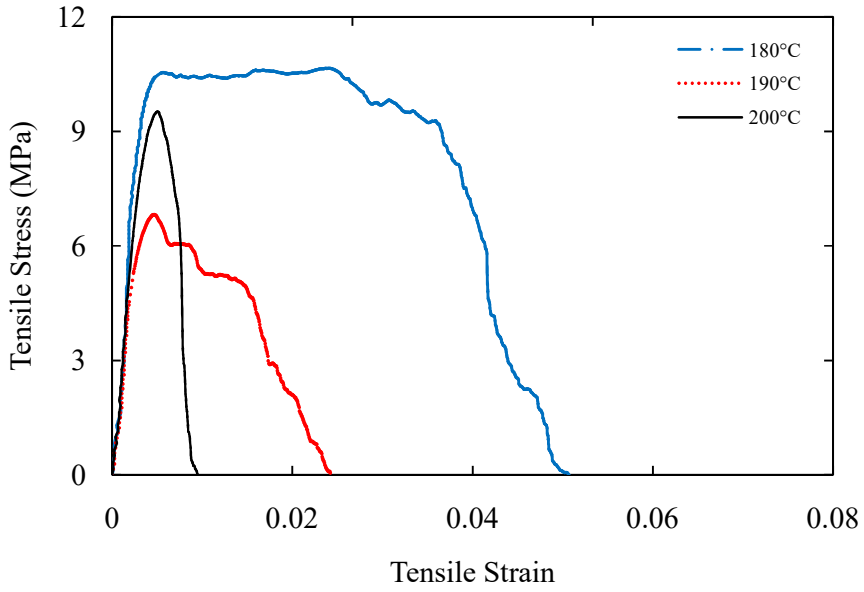

(b)

Figure 4.1.Tensile stress – strain curves for (a) flax/PP and (b) flax/PLA.

Figure 4.2 shows the variation of tensile strength with the processing temperature for the flax-based composite. Close examination of the flax/PP data shows that for processing temperatures of 170 ºC, 180 ºC and 190 ºC, the strength is averaging approximately 26 MPa. However, a noticeable drop occurs at 200 ºC, that is probably due to degradation of the PP matrix at this elevated processing temperature. It is evident that there is some dispersion in the set of data values in those samples processed at 180ºC. The reason for this is not clear, although such effects are not considered to be associated with any microstructural effects within the composite. This also could be attributed to the alignment of the flax fibre yarn in the composite. Here, the flax/PP composite significantly outperforms its flax/PLA counterpart at all temperatures.

The values for the flax/PLA are relatively constant across the range of temperatures, although there is a maximum value at 180 ºC. The pronounced difference between the two types of composite is likely to be associated with the brittle nature of the PLA matrix. Previous work on neat biopolymers [133] has shown that the tensile strain of PLA lies between 2.5% and 6%, significantly lower than those values measured on much more ductile PPpolymers. Given that damage in 0º/90º laminates often initiatesbetween the transverse fibres, it is likely that increasing theductility of the polymer will lead to improvements in the ultimateproperties of the composite. Indeed, Garrett and Bailey [134] investigatedthe effect of matrix failure strain on the tensile propertiesof 0º/90º glass fibre reinforced/polyester laminates. Their results showedthat increasing the strain to failure of the thermosetting matrixfrom 1.75% to 11.1% served to increase the transverse crackingstrain of the cross-ply composite by more than 600%.

In Figure 4.3, it shows that PP-based system tends to offer superior mechanical properties at temperatures between 180 ºC and 200 ºC, although the differences are not as significant as in the previously-reported tensile strength data. The stiffness properties of the PLA-based material are relatively constant across the range of processing temperatures. It is evident that the stiffness of PLA-based composites at 170 ºC is higher than the PP-based counterpart. This could be associated with the PLA matrix that is not completely melted at this elevated temperature. As a result, the specimen failed as fibre-by-fibre rather than a catastrophic failure as in the PP-based composite. In contrast, the modulus of the PP-based composite increases with temperature, reaching a maximum value of 3.7 GPa at 190 ºC. Hence, all subsequent manufacturing of the PLA-based composite was undertaken at a temperature of approximately 180 ºC and the PP-based composite at approximately 190 ºC. The images of fractured flax-based composite following a tensile testing are shown in Table 4.1.

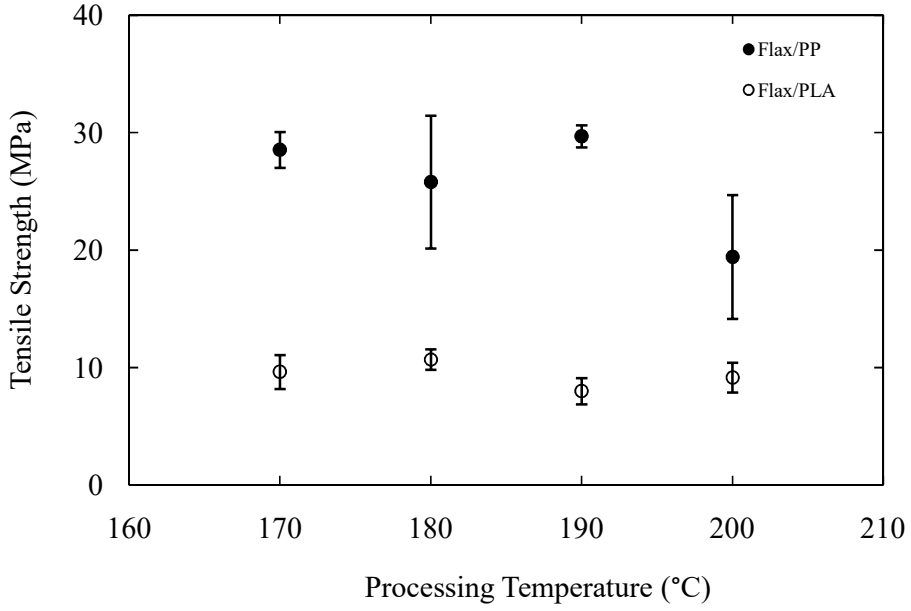

Figure 4.2.Tensile strength of flax-based composite versus processing temperature.

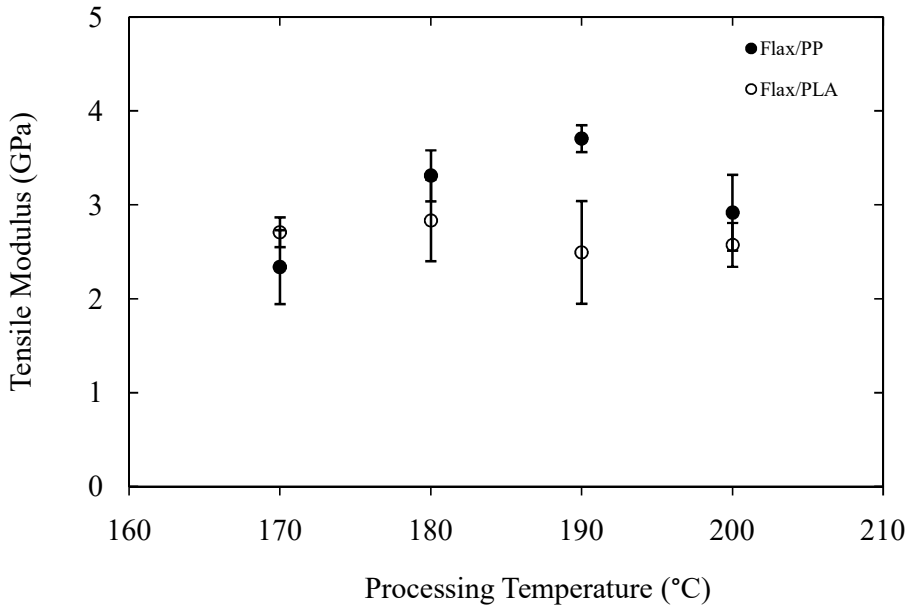

Figure 4.3.Comparison of the tensile modulus for flax/PP and flax/PLA composites as a function of processing temperature.

Table 4.1.The failure regions in the flax/PP and flax/PLA composite following the tensile tests at various temperatures.

Temperature (ºC)	Flax/PP	Flax/PLA
170		
180	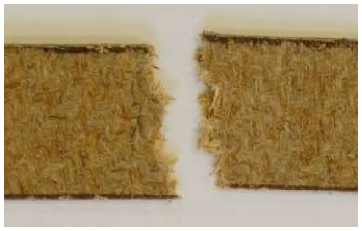	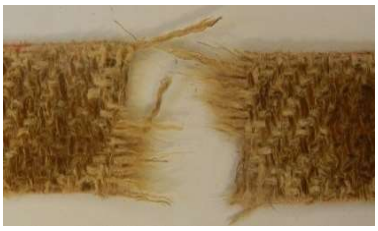
190		
200	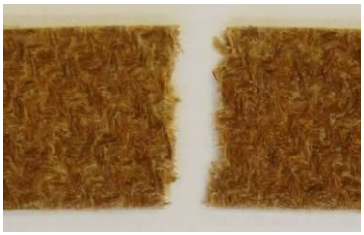	

10 mm

4.1.2 The Influence of Cooling Rate on the Flax-based Composites

The influence of varying cooling rate for these flax-based composites was investigated. Here, the consolidation process was approximately one hour, started once the required temperature had been established. The temperature was monitored by using a thermocouple, placed inside the mould. The press was then turned off and a pressure of 1.5 bar was maintained (for the slower cooling time). Fast cooling time was achieved by removing the mould after the consolidation process, followed by placing weights (~5 kg) on top of the mould. The cooling time was measured until the temperature had been cooled to approximately 80ºC.

Figure 4.4 shows the processing conditions for the slow and fast cooled flax-based composites. From the graph, the total cooling time periods for the flax-based composites was approximately four hours for slow cooling and six minutes for fast cooling. Following this, a series of tensile tests were undertaken on samples produced at both cooling rates, with a displacement rate of 1 mm/min. Figure 4.5 shows the tensile strength of the flax-based composite processed with slow and fast cooling times. Clearly, the flax-based composite exhibits a higher value of strength at the slower cooling rate, approximately 30% for flax/PP and 24% for flax/PLA.

It is worth noting that the flax-based composite offers greater properties at the slower cooling rate. This result may be associated with the crystalline nature of the matrix, as thermoplastic matrices often develop highly crystalline regions at a slow cooling rate. Previous work has shown that during fast cooling, the level of crystallinity was low and this affected the tensile strength to some degree [135]. Furthermore, the fibre-matrix interface also plays a fundamental role in determining the composite properties. Le Duigo *et al*. [136] stated that the interfacial properties between the fibre and matrix are lower under the rapid cooling rate, where the matrix structures that show the visco-elastic behaviour does not have time to relax. Here, the interfacial properties are being controlled by the residual stresses that appear during this phase, where at a slow cooling rate, the friction stress is increased.

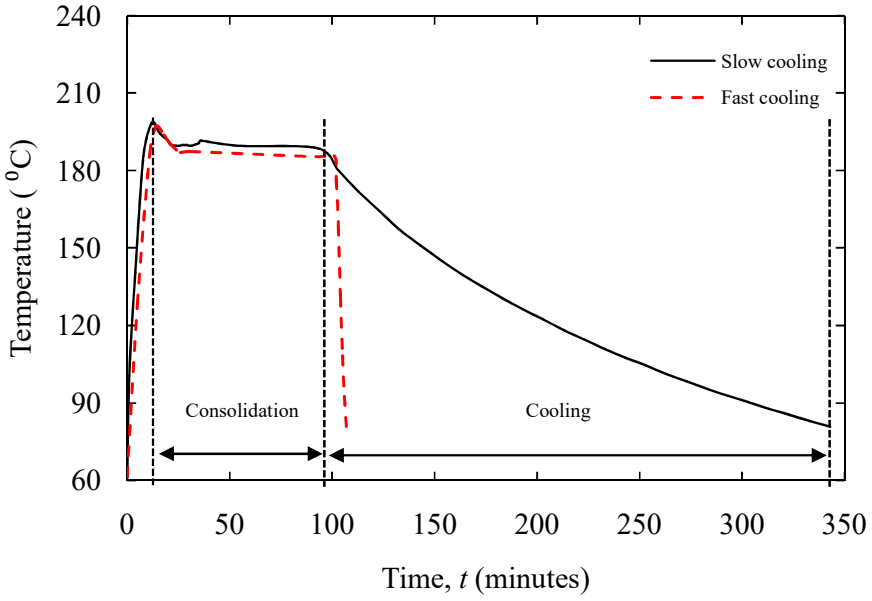

(a) flax/PP

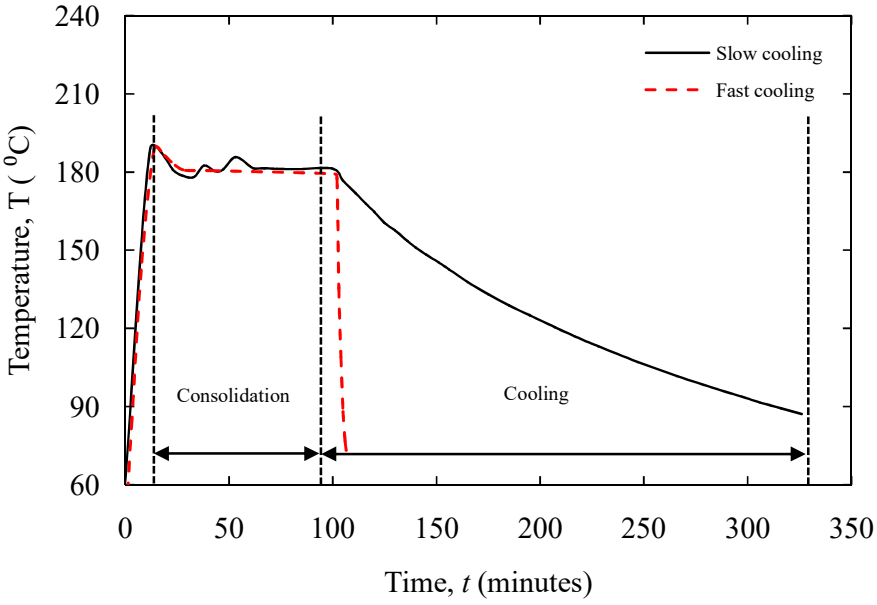

(b) flax/PLA

Figure 4.4.Processing temperature with processing time for slow and fast cooled flax-based composites.

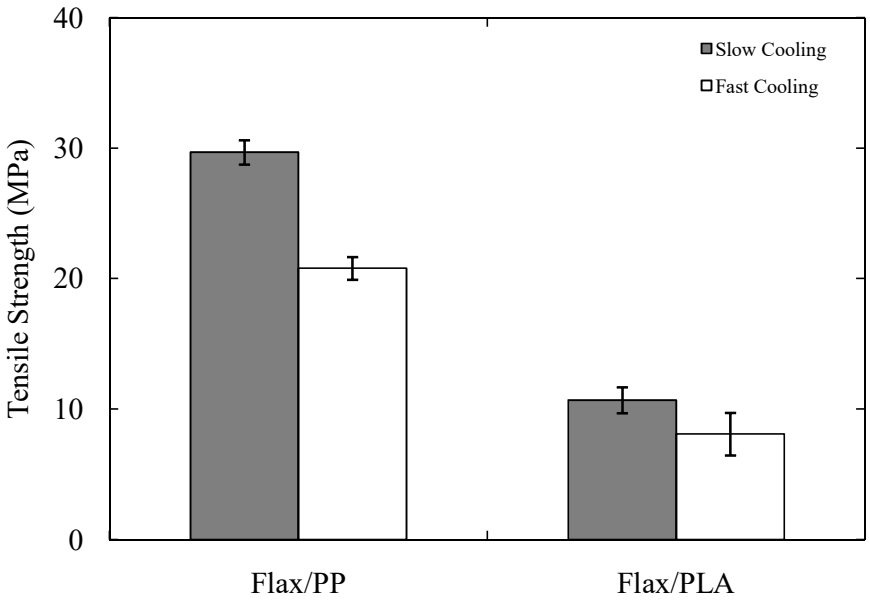

Figure 4.5. Tensile strength at different cooling rates for the flax-based composites.

4.2 Mechanical Properties of Bamboo Tubes

4.2.1 The Effect of the Geometry Size under Quasi – Static Loading

Another attempt to develop an environmentally-friendly structure was undertaken on a natural bamboo tube. Bamboo is a typical natural tube structure and hence, every segment of the outer and inner diameter are not the same size. Therefore, it has to be assumed to be a perfect cylinder in order to calculate the diameter-to-thickness ratio as well as the compressive strength. It should also be noted that bamboo is a functionally graded composite material that consists of vascular bundles. Here, the crush behaviour of the individual bamboo tubes based on small and large diameters was investigated. The initial focus was to understand the influence of tube geometry on the strength and energy-absorbing characteristics of the bamboo tubes. The effect of varying the ratio of the internal tube diameter to the tube wall thickness, D/t, on the energy absorbing capability was investigated.

Figure 4.6 shows typical load-displacement traces following compression tests on tubes with small and large diameters at a length of 20 mm. On close examination, the peak loads for the small diameter tube range between 1.3 and 11 kN, whereas the large diameter lies between 17 and 31 kN, with all tubes exhibiting similar trends. Figure 4.7 compares the load-displacement traces for both bamboo geometries. Here, the trace for the smallest diameter tube increases rapidly to approximately 11 kN, before decreasing steadily with increasing crosshead displacement. This response contrasts with that of the larger diameter tube, where the force rises rapidly to approximately 31 kN before dropping to 25 kN and then rapidly to below 10 kN. Complete failure of the tubes (small and large) occurred at a displacement over 6 mm.

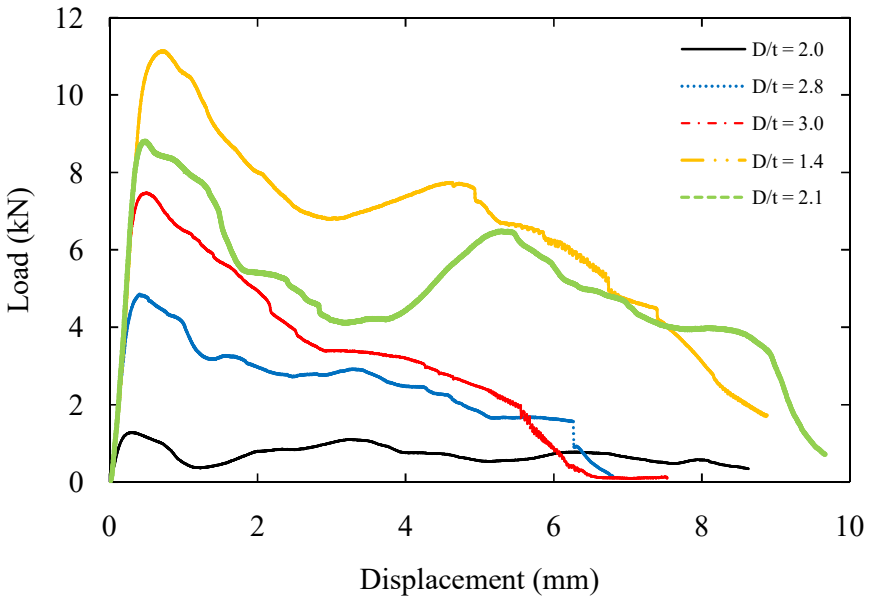

(a)

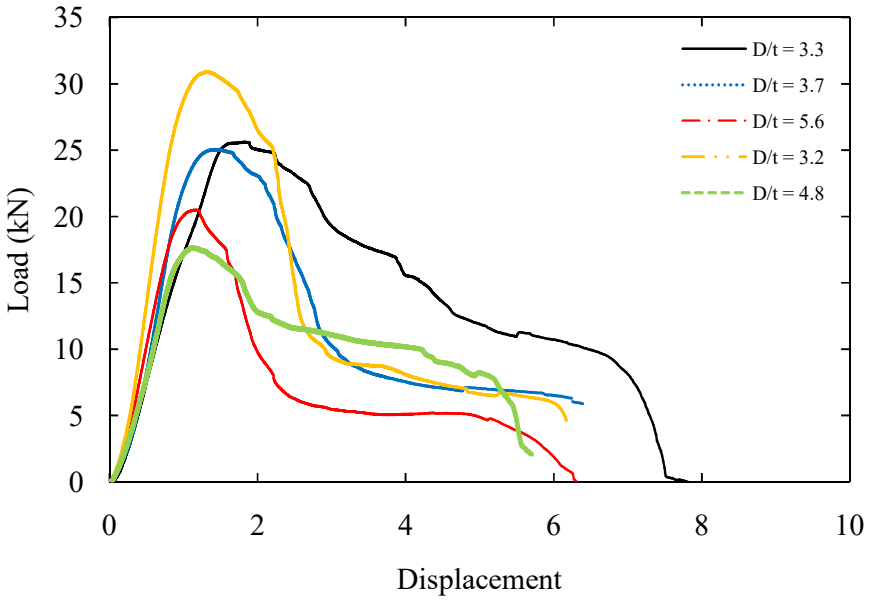

(b)

Figure 4.6.Typical load-displacement curves for (a) small and (b) large bamboo tubes.

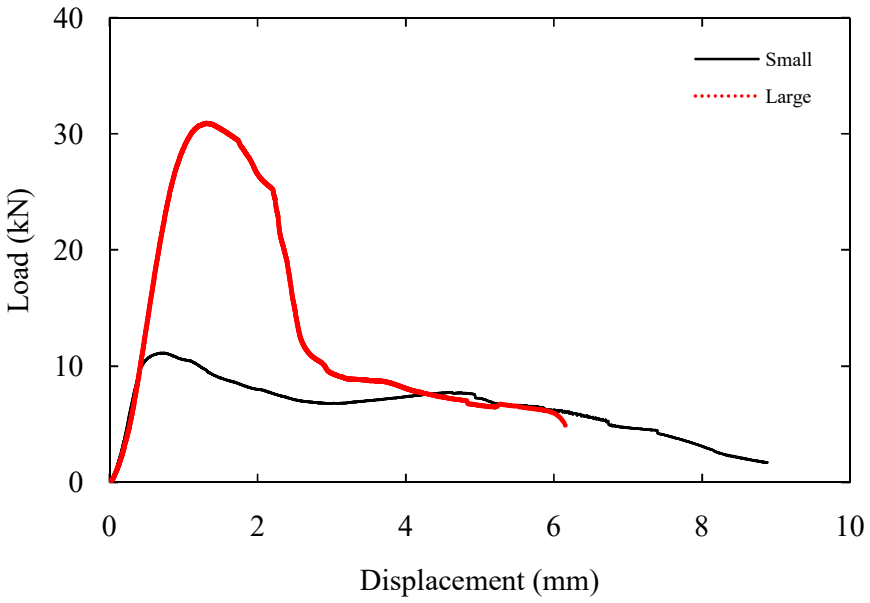

Figure 4.7.Comparison of load-displacement curves for the small and large bamboo tubes.

Figure 4.8 shows the plan and side views of the small and large bamboo tubes after testing. Greater levels of crushing are apparent in the small diameter bamboo tube, Figure 4.8(a), which reflects the long and steady decline in the load-displacement traces in Figure 4.7. A closer inspection of the sample indicates that a large amount of material has splayed inwards and outwards during the crushing process. An examination of the larger test sample highlights some top-surface crushing of the bamboo substrate, as well as a number of vertical splits extending along the length of the specimen. The initial crushing process occurred between the maximum load and the knee at 25 kN. It is believed that this mode of failure is capable of absorbing reasonably high levels of energy. The sudden drop in the load-displacement trace is associated with the low energy splitting mechanism in evidence on the sides of the sample. The strength and failure mode of bamboo tubes are associated with the distribution of vascular bundles in the bamboo tube. It is found that the outside regions of a bamboo tube has a higher fibre density than the inside regions. Zhang *et al*. [137]proved that the area ratio of vascular bundles in small diameter of bamboo

tube is higher than that in large diameter, which affected their final compression results.

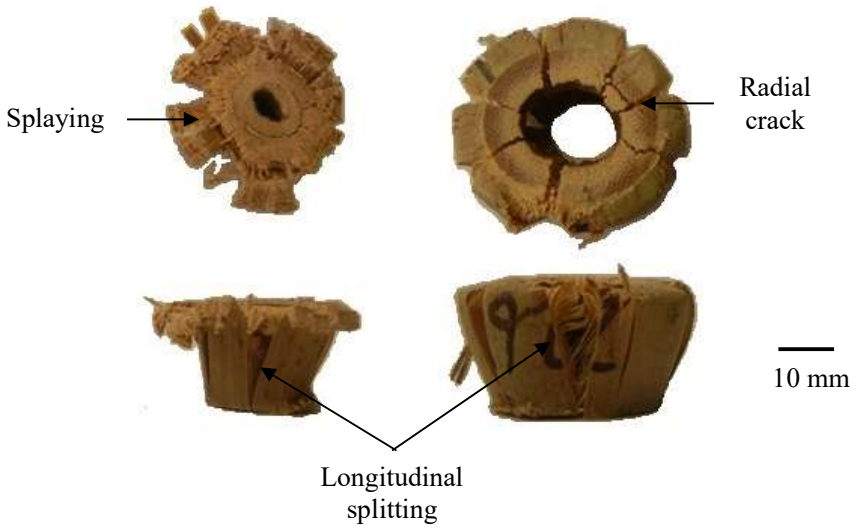

Figure 4.8.Photograph of failed samples for (a) small diameter and (b) large diameter bamboo tubes following quasi-static testing.

The area under each of the load-displacementtraces was used to calculate the energy absorbed during the crushing process. These values were divided by the initial masses of the specimens to yield specific energy absorption values. Figure 4.9 shows the variation of specific energy absorption (SEA) with the tube D/t ratio. An examination of the figure highlights significant scatter in the experimental data. This is most pronounced for low values of D/t, partly due to difficulties in clearly identifying the values of "D" and "t" in tubes that appeared to be almost completely filled (Figure 3.5(a) in Chapter 3).

In spite of the level of scatter in Figure 4.9, it is evident that the SEA decreases with increasing D/t ratio, an observation that has been made following tests on both Kevlar/epoxy composite[138] and metal tubes [139]. The highest value of SEA approached 26 kJ/kg, which is similar to that reported by Farley [140] following tests

on glass and Kevlar fibre reinforced epoxy tubes. It is clear that the lower value of D/t ratio exhibit a superior energy absorption performance to their higher value counterparts.

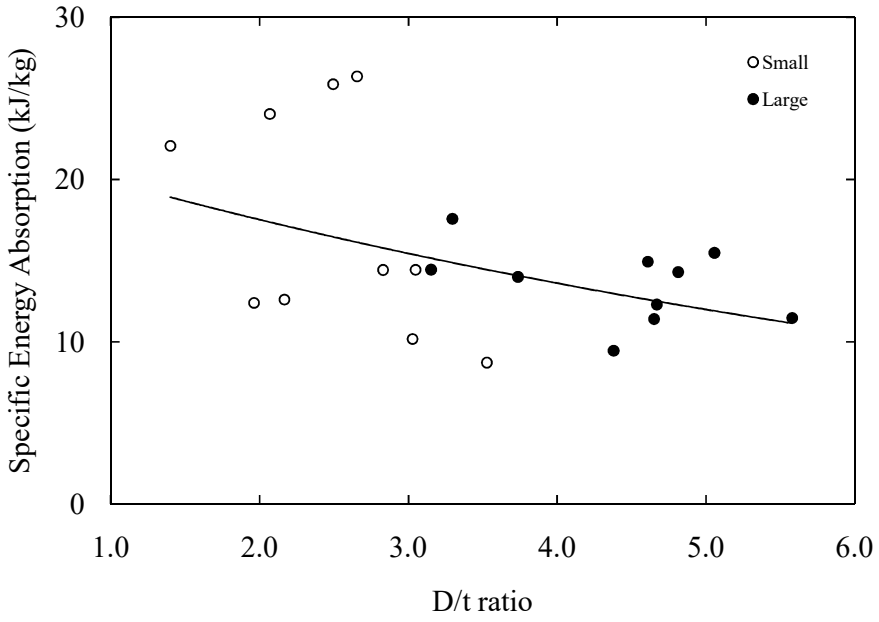

Figure 4.9.The SEA values of small and large bamboo tubes as a function of the D/t ratio.

4.2.2 The Effect of the Geometry Size under Dynamic Loading

Figure 4.10 shows the load-displacement traces for the small and large diameter tubes under impact loading. The dynamic responses were similar to those observed under quasi-static loading (Figure 4.7). The force associated with the tests on the smaller diameter tubes increased to a value of approximately 21 kN before decreasing steadily during the second part of the test. In contrast, the initial response of the large tube was relatively linear rising to a maximum value around 38 kN. A sudden drop occurred after the peak point, associated with longitudinal cracking between the bamboo fibres. Here, localised crushing occurred in the uppermost part of the tube, leading to localised splaying and some splitting. Figure 4.11 shows photos of both types of tube following dynamic crushing. A comparison of the

figures with those shown previously in Figure 4.8 highlights many similarities in the failure modes at these two strain rates.

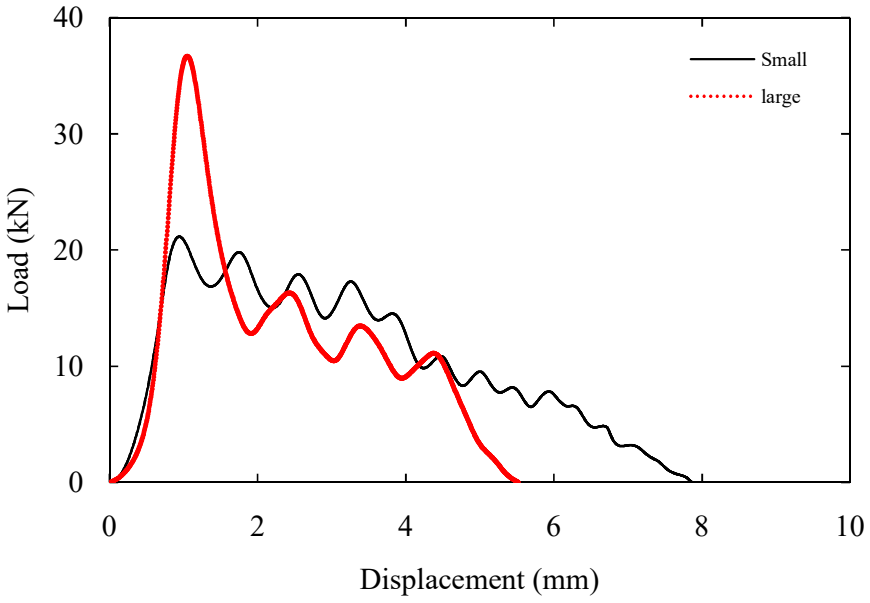

Figure 4.10. Typical load-displacement traces for the small and large diameter bamboo tubes following dynamic testing.

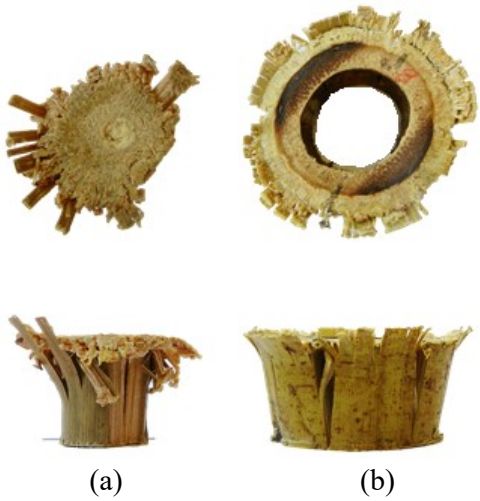

Figure 4.11. Photograph of failed bamboo tubes for (a) small diameter and (b) large diameter bamboo tubes following dynamic testing.

Figure 4.12 shows the variation of SEA with tube D/t for the dynamically-loaded bamboo samples. Here, the trends in energy absorption with tube geometry are less pronounced than that observed following quasi-static testing (Figure 4.9). An examination of the figure does, however, suggest a slight upward trend as D/t is decreased. A comparison with the data in Figure 4.9 indicates that the SEA values are higher at impact rates of strain, highlighting a distinct rate-sensitivity in these materials.

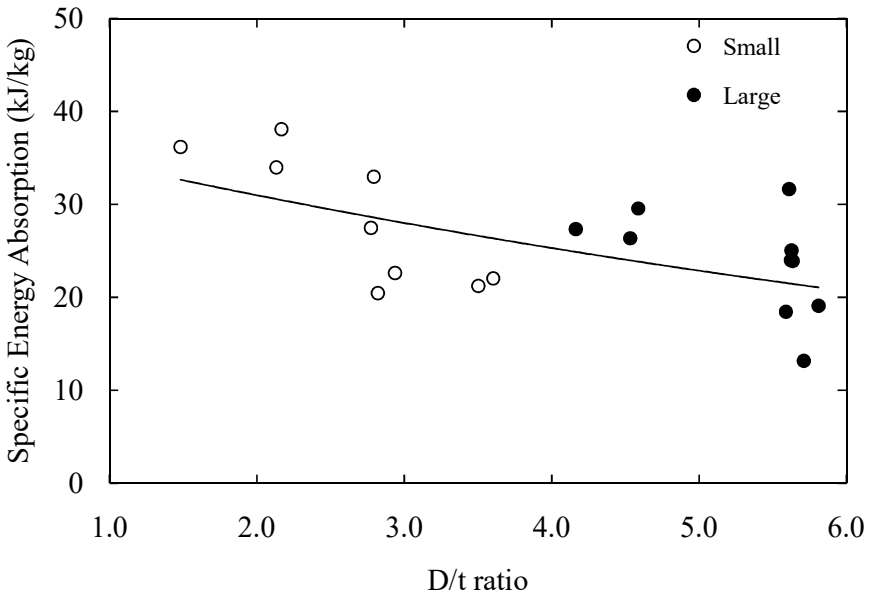

Figure 4.12. The variation of SEA with D/t for small and large diameter bamboo tubes following impact testing.

4.2.3 The Effect of the Triggering System on the Bamboo Tubes

The next stage of this study was to investigate the effect of the triggering system for the large bamboo tubes. Here, two types of geometry were considered, these being unchamfered (non-triggered) and chamfered (triggered) tubes. The triggering system was carried out by making a taper at one end of the tube at an angle of 45º. A comparison of the load-displacement response under compression loading for the unchamfered and chamfered tubes is shown in Figure 4.13. The presence of the triggering profile was observed to change the stiffness of the tube.

Closer inspection showsthere is evidence of a reduction in thepeak load in the chamfered tube. The peak load values of the triggered tube are approximately 9% lower than for its counterpart. Here, the chamfered tube initiated progressive crushing during the initial stage before reaching the highest value at approximately 28 kN, following a sudden drop. The tube completely failed at a displacement of 6 mm. It is apparent that the chamfer can significantly increase the trigger length, where the peak load occurred at a displacement of 5 mm.

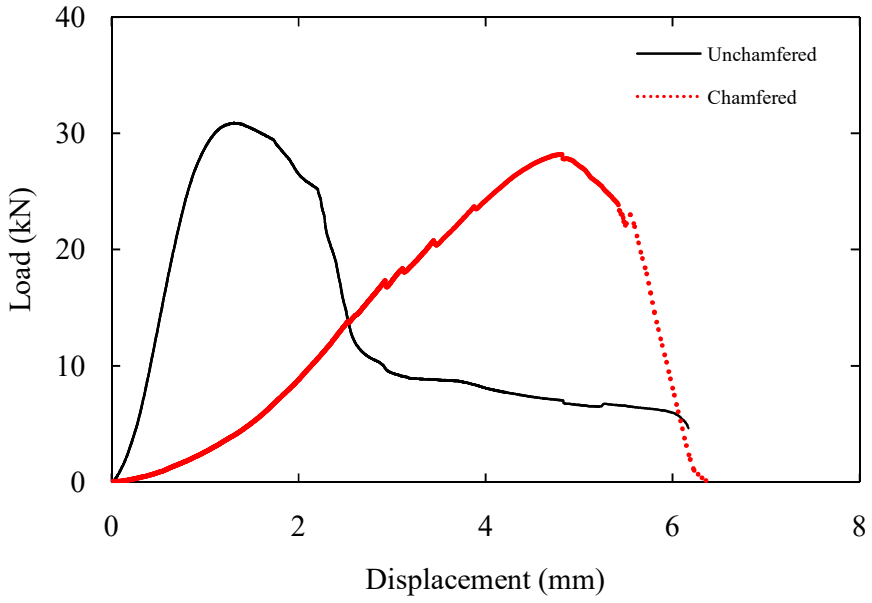

Figure 4.13.Load-displacement traces for the unchamfered and chamfered bamboo tubes.

Figure 4.14 summaries the average values of the peak load (left) and specific energy absorption (right) for both geometries conditions. As discussed earlier, the effect of the triggering system will reduce the peak load. Nonetheless, the SEA values for the triggered tubes are greater than those for the non-triggered tubes, approximately by 16%.

Previous work has shown that the trigger mechanism can reduce the initial peak load while maintain the stability of the crushing load [141,142]. Indeed, the presence of trigger mechanism can significantly increase the energy absorbed by the bamboo tubes. The trigger system for this natural bamboo tube can be seen clearly in the earlier stages of the crushing load, before continuing in a splitting failure mode. Yan *et al*. [143] studied the effect of triggering system in flax/epoxy composite tubes. They reported triggering the tube increased the SEA values remarkably. The sequence of failure in the large bamboo tube for triggered and non-triggered samples is presented in Figure 4.15. In the figure, both geometries fail in a similar fashion, initiated by localised crushing and followed by a splitting mode. Images of the failure process in the non-triggered and triggered specimens during crush can be seen in Figure 4.16.

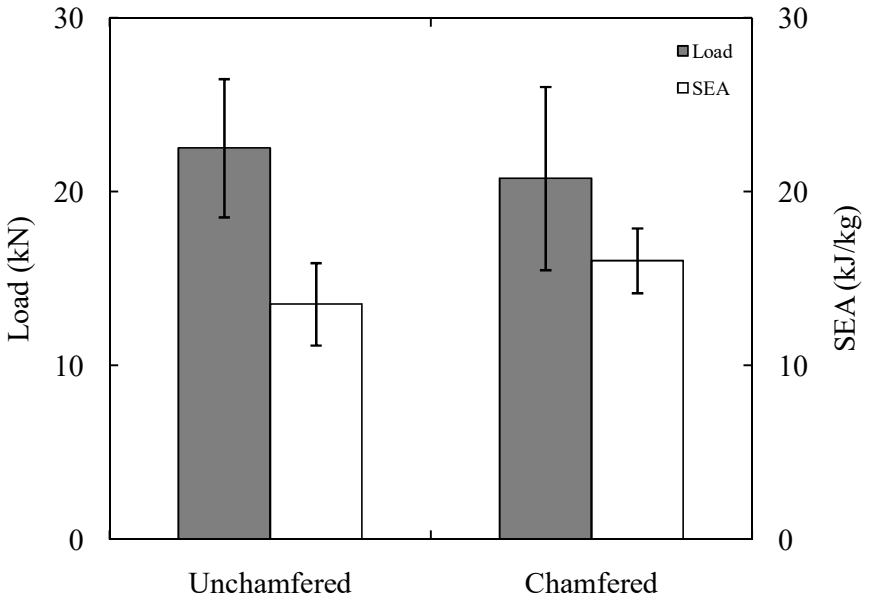

Figure 4.14.Comparison of the average values of the unchamfered and chamfered bamboo tubes following quasi-static testing.

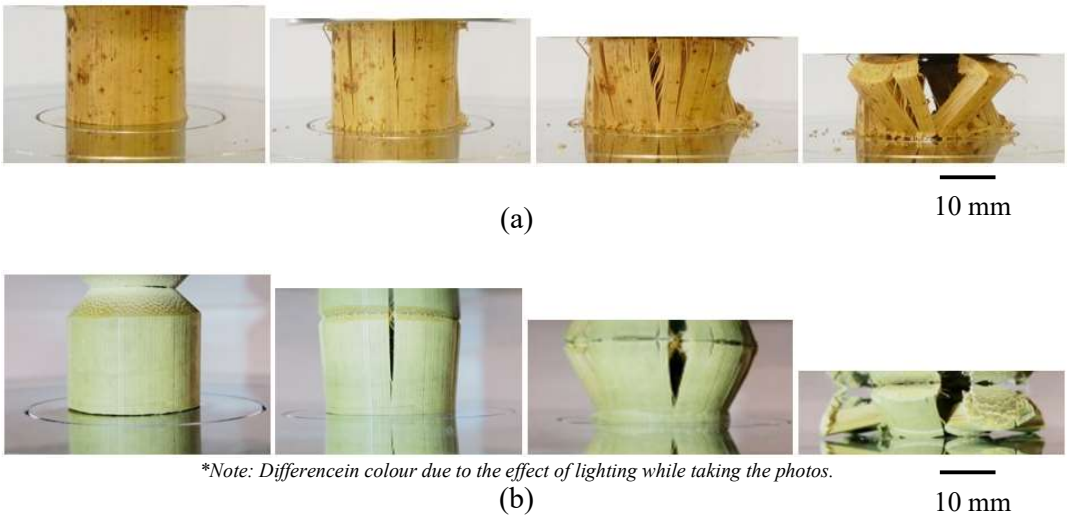

Figure 4.15.Compression tests on (a) unchamfered and (b) chamfered large bamboo tubes.

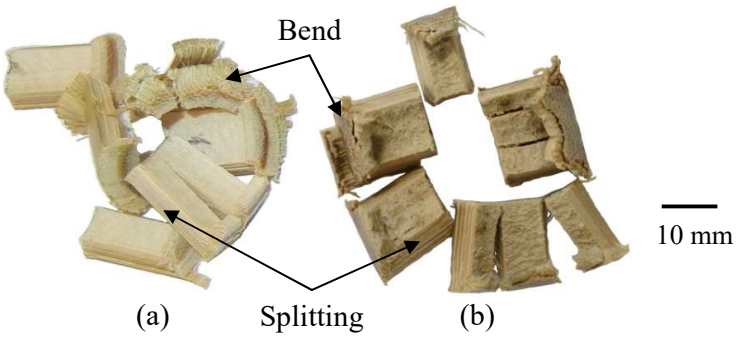

Figure 4.16. Photograph of failure in (a) unchamfered and (b) chamfered bamboo tubes following compression tests.

4.3 Bamboo Honeycomb

4.3.1 Quasi – Static Tests

Compression tests were conducted on square core samples with an edge length of 40 mm and both flax/PP and flax/PLA skins. Figure 4.17 shows typical load-displacement traces following compression tests on samples based on small and large bamboo tubes, with both types of skin. An examination of the figure indicates, as expected, that both types of skin material exhibit a similar load-displacement response.

In both cases, the force rises in a linear and non-linear fashion to a maximum, at which point the force reaches a plateau. During this phase, the uppermost surfaces of the tubes are being crushed in a similar manner to that observed previously in the individual tubes. With continued loading, the force begins to decrease rapidly as the bamboo tubes undergo the splitting mode, as previously-discussed. Here, the decline in force is less rapid than in Figure 4.7, due to the constraint applied by the neighbouring tubes (see Figure 3.5 in Chapter 3) as well as the two composite skins. This may also be related to the failure displacements corresponding to the peak loads in both Figure 4.7 and Figure 4.17. The individual tube failed at a displacement well below 2 mm (less than 1 mm for the small tube), whereas the bamboo cores failed at about 2 mm. The tests were interrupted when all of the tubes had completely failed in a splitting mode. As the result, the force did not drop to zero. However, a distinctive difference in the residual forces between these two flax composite sandwich structures is noticeable in the later stages of crushing. Here, the flax/PLA still exhibits higher values, largely because of the more compacted stacking of the split tubes than its PP counterpart.

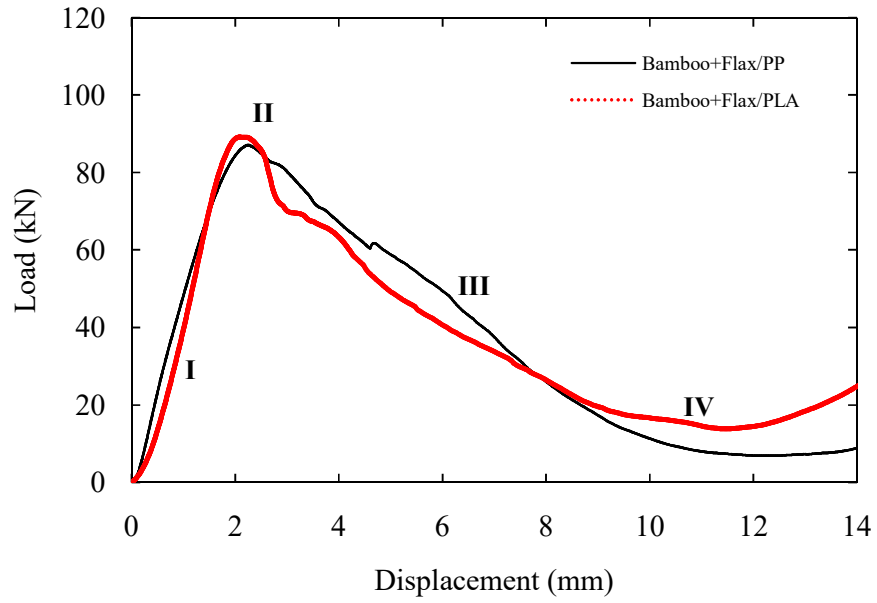

(a)

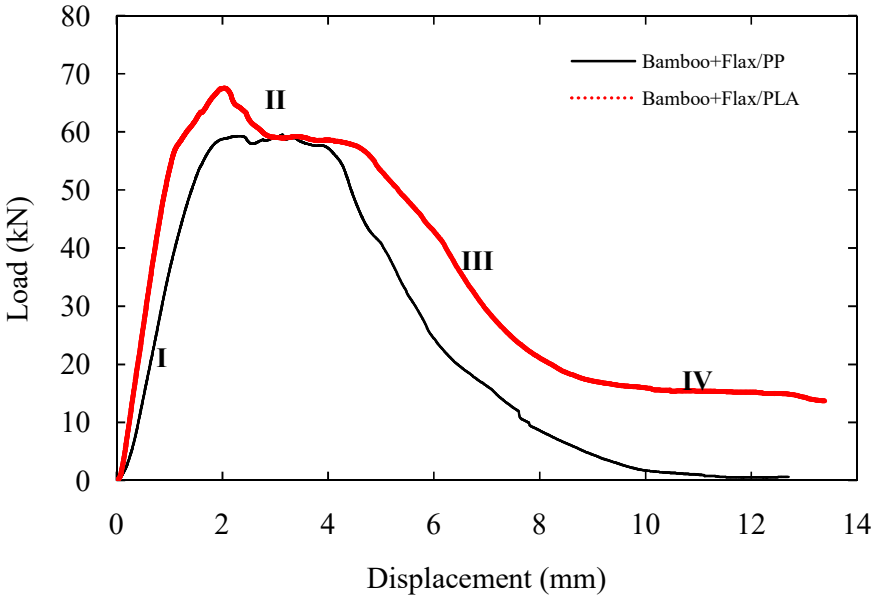

(b)

Figure 4.17.Typical load-displacement curves forthe (a) small and (b) large diameter bamboo honeycomb structures based on flax/PP and flax/PLA skins.

Figure 4.18 summarises the compression strengths of the flax/PP and flax/PLA sandwich structures based on cores with small and large diameter bamboo tubes. The figure indicates that there is little difference between the PP and PLA-based sandwich structures. It is interesting to note that the samples based on the small diameter tubes offer higher compressive strengths than those based on large diameter tubes. It should be noted that the density of the cores based on small diameter tubes was 540 kg/m^3, somewhat higher than the value of 400 kg/m^3 for its large diameter counterpart. It is also observed that the strength of the large bamboo core with flax/PLA skins is higher than the flax/PP skins counterpart, whereas this is reversed for the small cores. This could be attributed to the effect from various D/t ratios of the individual tubes in the cores as the structures were fixed only with pre-defined specimen size, as well the various ratios of vascular bundles in each tube. Figure 4.19 presents the specific energy absorption (SEA) values of the PP and PLA-based sandwich structures. Here, a distinct difference is observed between the two types of material manufactured using large diameter tubes. Such differences are not apparent in the smaller diameter systems, with both material types exhibiting similar values of SEA. The values of SEA evident in Figure 4.19 compare favourably with values measured on silk fibre reinforced epoxy(5 kJ/kg) [144] and jute fibre/epoxy tubes (10 kJ/kg) [145].

Figure 4.20shows the sequence of failure during quasi-static testing on the small and large diameter bamboo honeycomb structures with flax/PLA composite skins. An examination of the figure highlights the presence of longitudinal splits in the small diameter tubes, leading to lateral movement of the tubes during the crushing process. Failure, in the form of localised splitting and crushing at the lower surface, is in evidence in the larger diameter tubes.As previously discussed, the stacking of the split tubes related to PLA skins can also be clearly observed in the images no. IV in Figure 4.20, whereas the comparisons of stacked split tubes for both flax-based composite structures after crushed are shown in Figure 4.21.

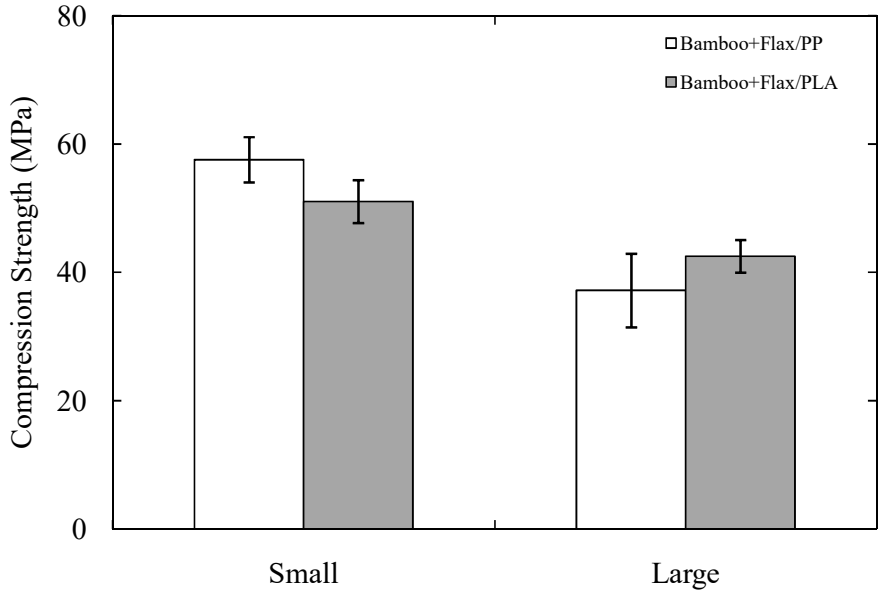

Figure 4.18.The compression strength following the quasi-static tests on the small and large diameter bamboo honeycomb with flax/PP and flax/PLA skins.

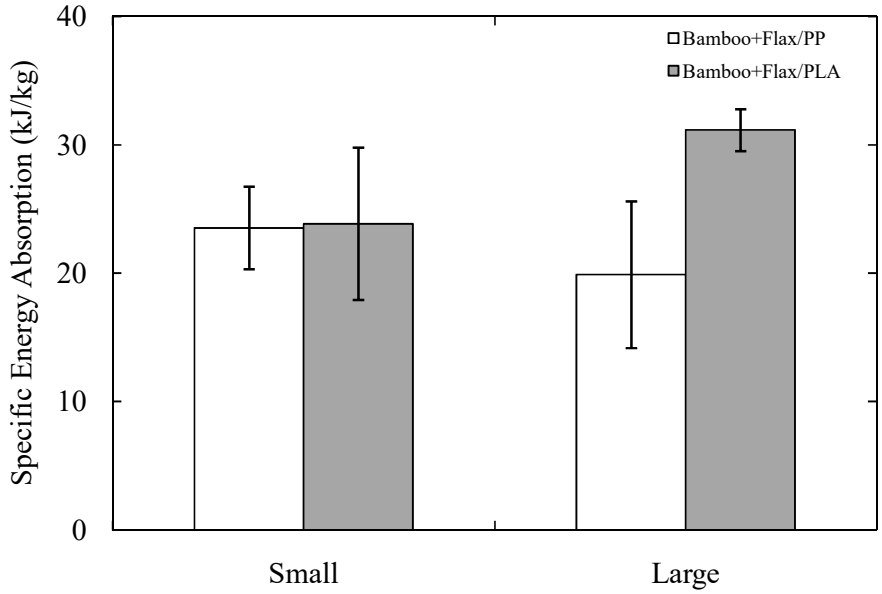

Figure 4.19.The SEA values following the quasi-static tests on the small and large diameter bamboo honeycomb with flax/PP and flax/PLA skins.

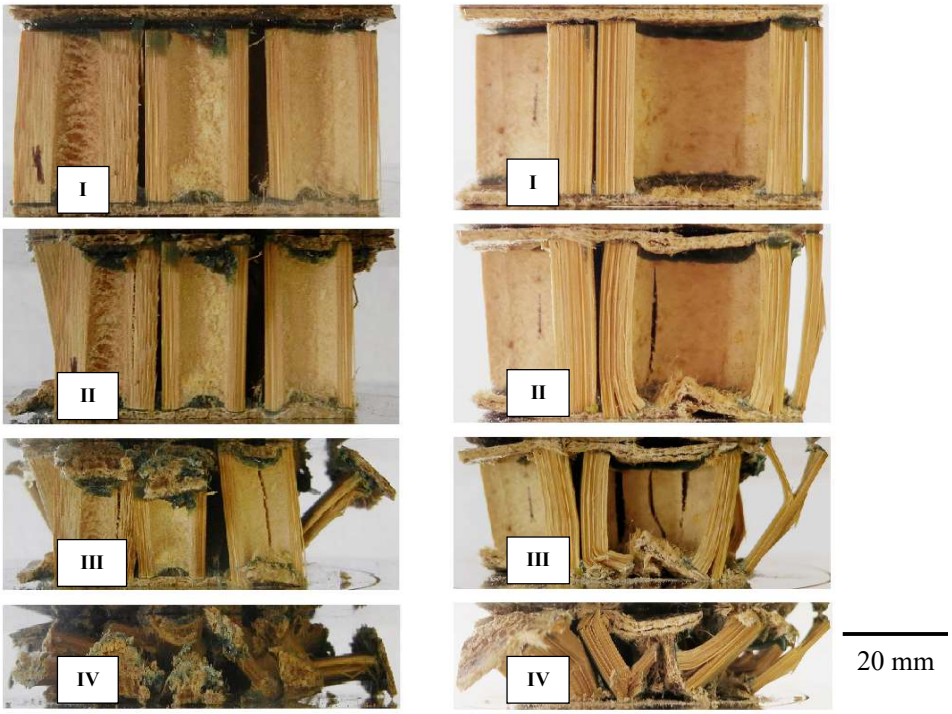

Figure 4.20.Failure sequences in cores based on (a) small and (b) large diameter bamboo honeycomb structures following quasi-static testing. Both structures have flax/PLA skins.

Figure 4.21. Comparison of the crushed sandwich structures made with large bamboo cores subjected to quasi-static compression, (a) flax/PP skins, (b) flax/PLA skins.

4.3.2 Dynamic Tests

Figure 4.22 shows typical load-displacement traces following dynamic crushing tests on the square bamboo core laminates based on small and large diameters. For both material systems, the force initially increases in a linear and non-linear fashion, before reaching a peak value that ranges from 70 to 90 kN for the small core, and 60 to 70 kN for the large core. The force then drops rapidly as the core begins to fail and fragment under the continued movement of the crosshead. However, there is a higher residual load in the PLA sample, due tomore compacted split tube of PLA-based skins than the PP-based skins, as discussed previously. This system offers a higher crush resistance than its more brittle PP counterpart. A comparison of the dynamic traces in Figure 4.22 with the equivalent earlier traces in Figure 4.17, suggests that the impact-loaded samples absorb less energy than their quasi-static counterparts. This is confirmed when the SEA values are calculated and compared.

Figure 4.23 presents a comparison of the impact strength of both material systems. The results indicate that the small cores offer a greater impact strength than the larger counterparts, as observed following quasi-static testing. Under dynamic loading, the strength for large bamboo core with flax/PLA skins is slightly lower than the flax/PP skins. Again, this could be the D/t ratio effect of the individual tubes as well as the material rate-effect. Figure 4.24 summarises the SEA values for the small and large diameter bamboo cores based on the two skins materials. A comparison with Figure 4.19 suggests that these values are lower than those measured at quasi-static rates. This evidence contradicts the results from the tests on the plain tubes, where higher values of SEA were recorded at impact rates of loading.

The cause of this inconsistent behaviour may be related to the imperfection sensitivity of the cores under quasi-static and dynamic loading conditions. In addition, the age of the bamboo, inconsistences in the diameter andthe fibre density in each tube, also play some part in their mechanical test results. Given that the core structures are made from an assembly of bamboo tubes, it is inevitable that there are greater numbers of imperfections than in a single tube. These so-called imperfections include tube positioning errors and flatness inconsistencies at both ends of individual tubes within the cores. When resulting core is subjected to quasi-static loading, the core has more time to engage and realign to the loading process. In contrast, under dynamic loading conditions, there is less time to respond to the applied stress field through local re-organisation of the tubes and re-alignment of the core etc., potentially leading to a poorer overall energy-absorbing capability.

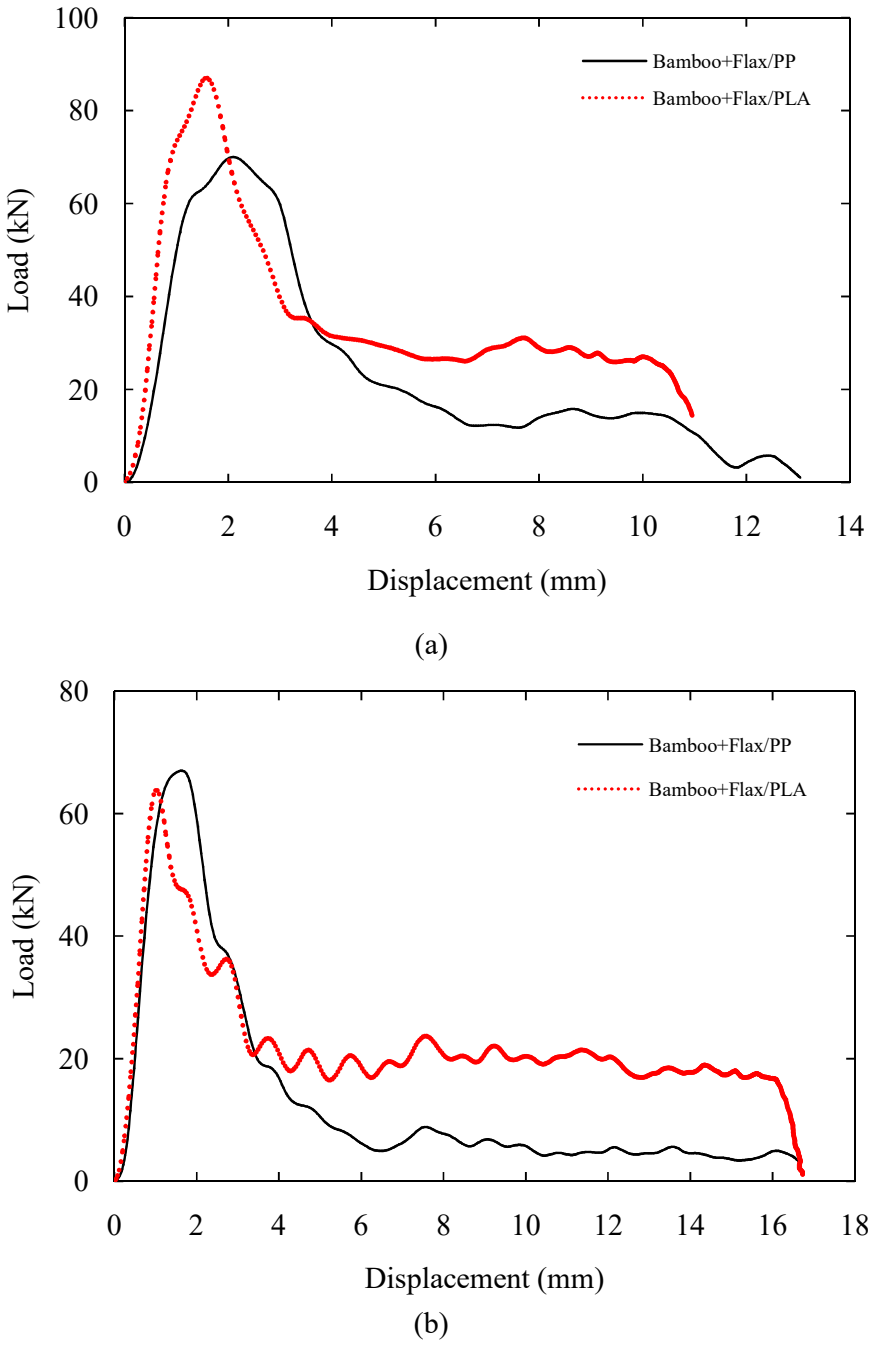

Figure 4.22.Typical load-displacement curves following dynamic loading for (a) small and (b) large diameter bamboo cores with flax-based composite skins.

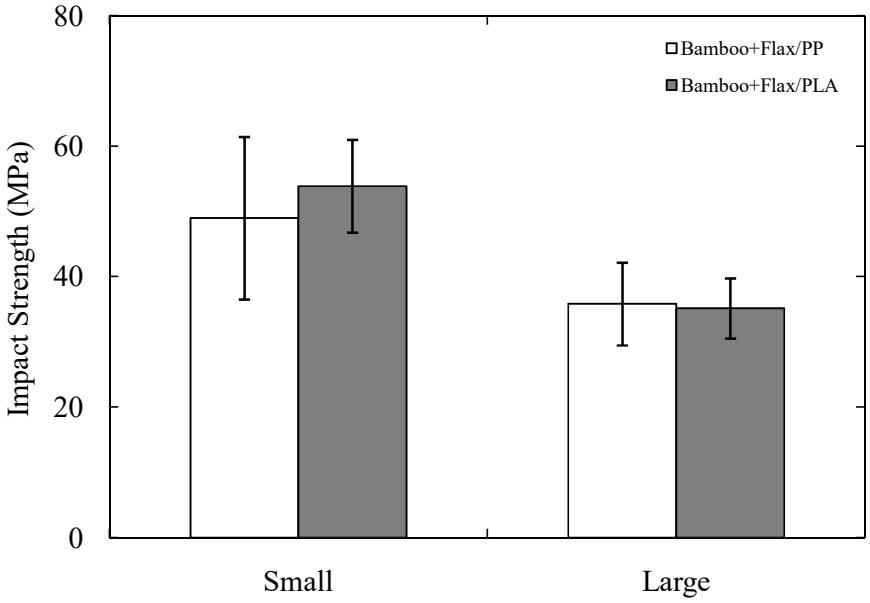

Figure 4.23.Impact strength of small and large bamboo honeycomb structures.

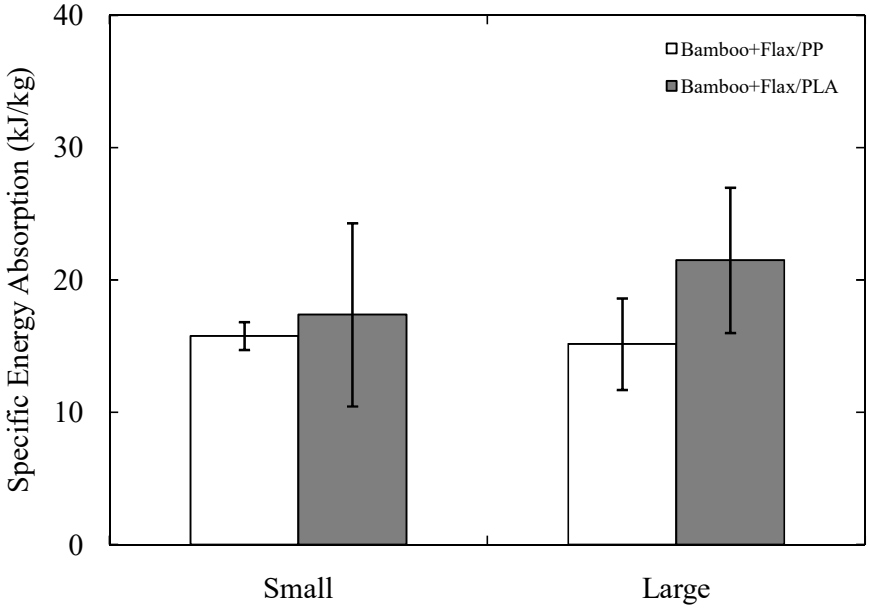

Figure 4.24.The SEA values of the small and large bamboo honeycomb structures under dynamic loading conditions.

4.4 Bamboo Tube-reinforced Foam

4.4.1 Quasi – Static Tests

A typical load-displacement trace following a compression tests on the bamboo tube reinforced foams is presented in Figure 4.25. Here, foams with different densities ranging from 15.6 kg/m^3 to 128 kg/m^3 were used to support a single bamboo tube. Under uniaxial compression loading, all tube-reinforced foams exhibit a linear and non-linear response until initial fracture of the tube occurred, as a result, the stiffness reduced. Initial fracture of the tube is clearly seen at intermediate displacements between 1.5 and 4 mm. The load required to further deform the specimen gradually decreases after reaching the peak load, and rises again until its densification phase. Figure 4.26 shows typical load-displacement traces for a bamboo tube reinforced foam with a density of 128 kg/m^3. Also included in the figure are the corresponding traces for the individual bamboo tube and the equivalent unreinforced foam. Clearly, the response of the tube and foam are markedly different from the constituent materials. An integrated response was observed during the initial stages before the load was transferred to the foam (following fracture of the tube). It is also observed that strength of the integrated structure is higher than the combination of both constituent materials. This could be attributed to the constrained failure of the tube offered by the foam.

Figure 4.27 shows that the specific measure of energy absorption for integrated bamboo and foam does not change greatly with the increasing of foam density, with all values averaging 17 kJ/kg. An estimation of the energy absorbed by the individual tube was undertaken by removing the contribution of the foam from the energy under the load-displacement traces in the bamboo-foam combination. The value then was normalized by the mass of the tube, also included in Figure 4.27. It is evident that the energy absorbed by the bamboo tubes increases with increasing foam density. The SEA value of the individual tube in the highest foam density is approximately 35 kJ/kg. It is interesting to note that the foam has been successful in suppressing longitudinal failure and enhancing the specific energy absorption capability of the tube (following removal of the energy contributed by the foam).

Figure 4.28 shows the plan view of the bamboo reinforced foam structure at several densities ranging from 15.6 kg/m^3 to 128 kg/m^3. On close examination, the low-density foam highlights the presence of several radial cracks, due to the presence of longitudinal splitting in the tubes. The foam may not trigger a splaying type of fracture, however, it serves to constrain the lateral movement of the embedded tube.

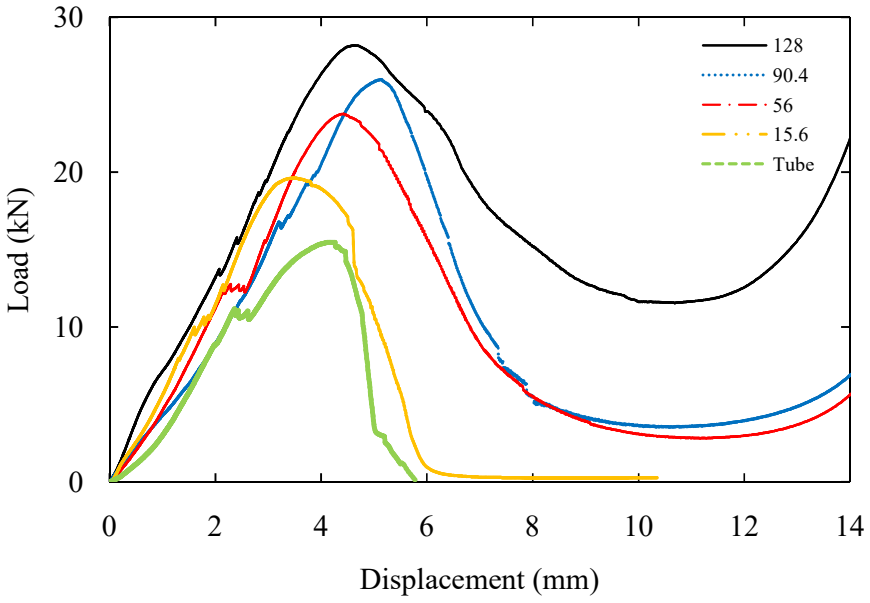

Figure 4.25. Typical load-displacement traces for bamboo reinforced foam for various densities of foams (Unit: kg/m^3).

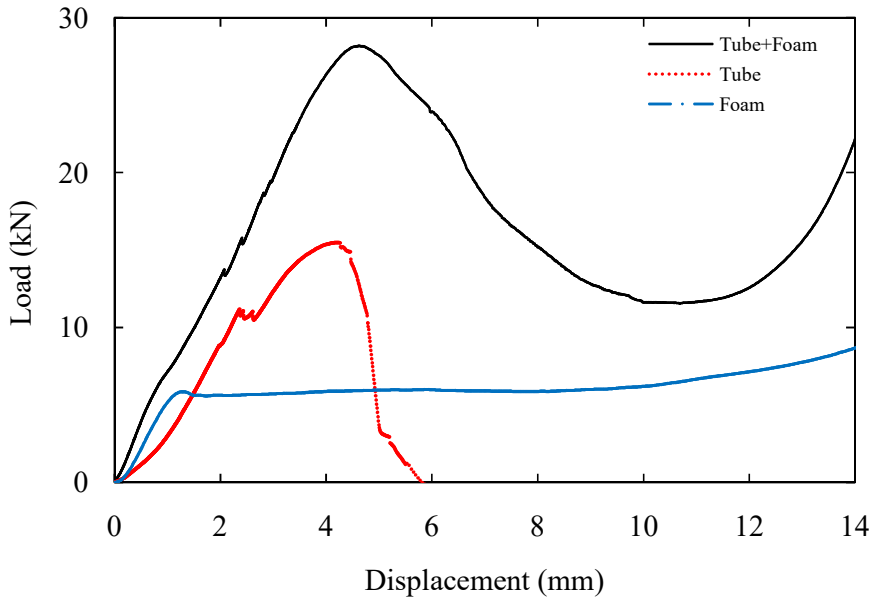

Figure 4.26. Typical load-displacement traces following tests on the bamboo reinforced structures (bamboo outer diameter = 24 mm and foam density = 128 kg/m^3).

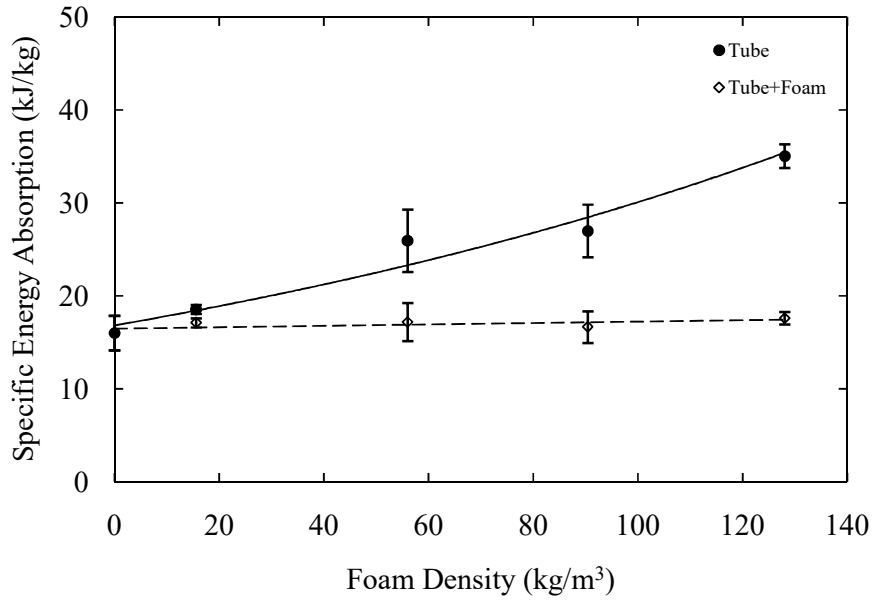

Figure 4.27.The variation of the SEA value of individual tubes inside the foam and the combination of bamboo – foam structures following compression tests.

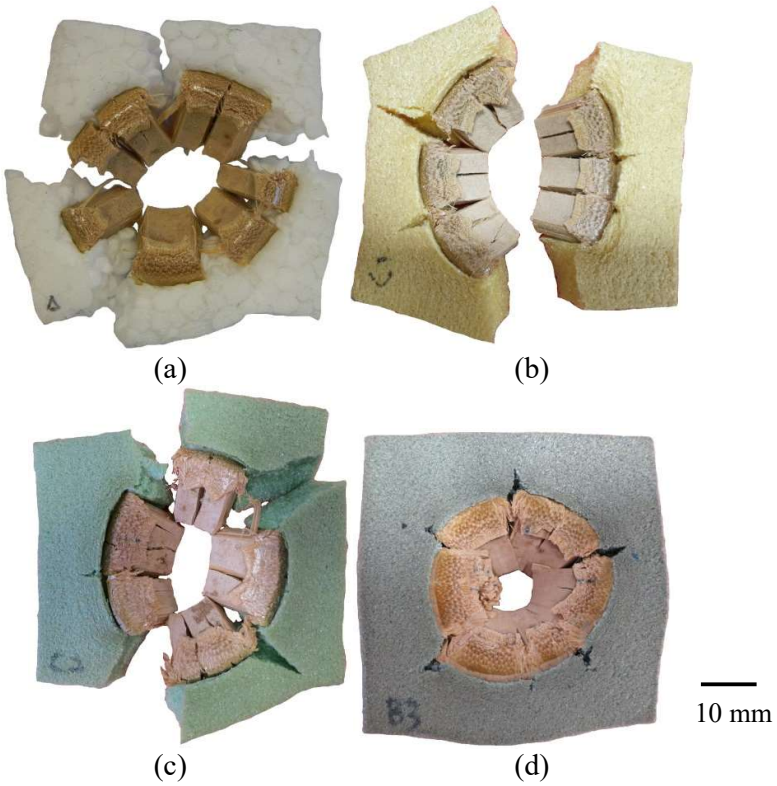

Figure 4.28. Photographs of the plan views of bamboo tube-reinforced foams for foam densities of (a) 15.6, (b) 56, (c) 90.4 and (d) 128 (Unit: kg/m^3).

4.4.2 Dynamic Tests

The capability of the bamboo reinforced foams to absorb energy under dynamic loading conditions has been investigated. The results of the dynamic test are presented in Figure 4.29. A comparison of the bamboo-foam structure (density foam = 128 kg/m^3) with the corresponding individual tube and equivalent plain foam is also included in the figure. Closer inspection of the trace indicates that the tube-reinforced foam reaches the maximum value at approximately 37 kN. Subsequently, the applied loading decreases due to fracture of the tube, remaining constant up to the onset of densification at about 15 mm. The dynamic traces in Figure 4.29 can be compared with the previous load-displacement response under quasi-static loading (Figure 4.26). There is evidence of an increase in the maximum value, and this may

be due to material rate-effects. It is also evident that the dynamic traces show some oscillation compared to the smooth quasi-static traces.

Figure 4.30 presents the energy absorbed by the individual tube and the combination of tube with foam. The method used to "correct" the SEA values in the quasi-static tests was applied to these dynamic results. It is clear that by increasing the foam density, the "corrected" SEA values for the individual tubes also increases. Figure 4.31 compares the capability of the individual tube to absorb energy under dynamic and quasi-static loading conditions. It is apparent that the dynamic response is higher for all foam densities than the quasi-static response, by over 40%. Both tests exhibit almost identical trends, with increasing the foam density there is an increase in the SEA values of the tube.

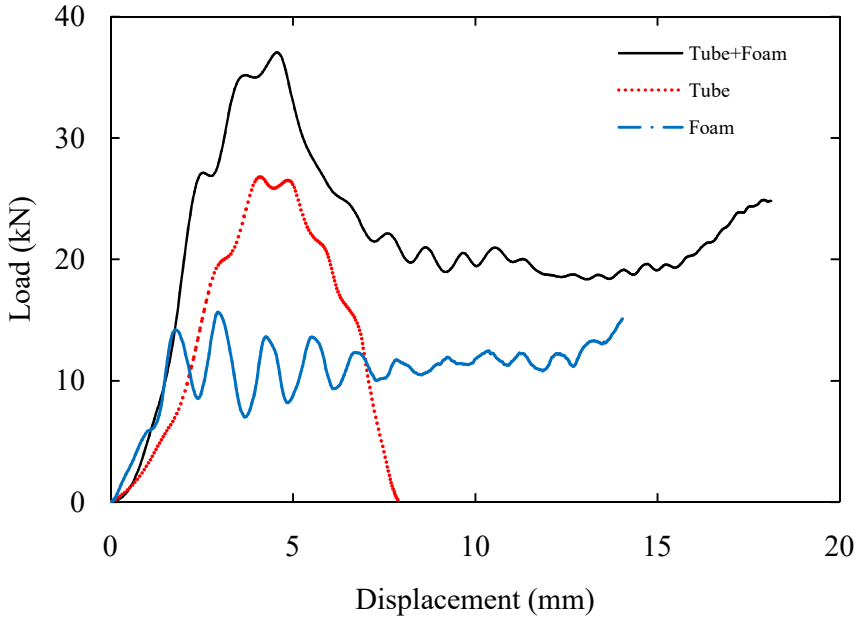

Figure 4.29. Comparison of tube reinforced foam, individual tube and individual foam (for a foam density 128 kg/m^3).

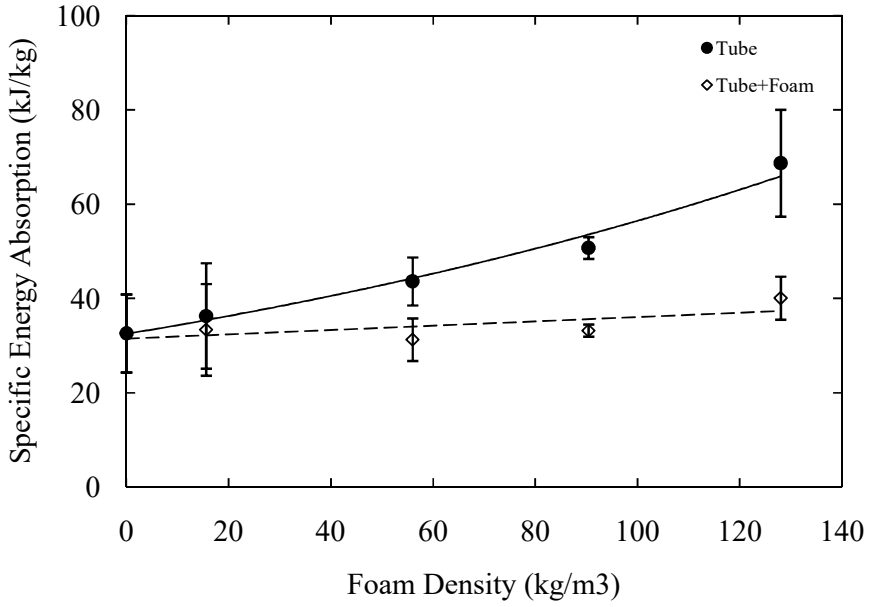

Figure 4.30.The variation of the SEA values of the individual tubes inside the foam and the combined tube andfoam structures following impact tests.

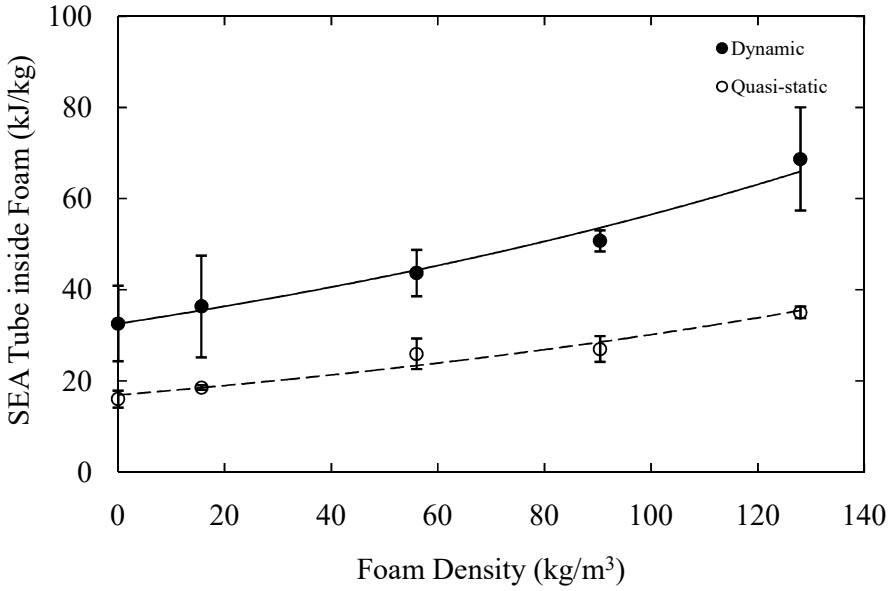

Figure 4.31.Comparison of the SEA values of individual tubes embedded in foam under quasi-static and dynamic loading conditions.

4.5 Corrugated of Flax-based Composite Core

4.5.1 Quasi – Static Tests

Figure 4.32(a) shows typical load displacement traces following compression tests on the flax/PP corrugated core with five unit cells. There are four distinct regions, these being linear, non-linear, plateau and densification. In region I, the load initiated with non-linear response and continues in a linear fashion up to the first peak. The effects of machine compliance and skins that are not aligned parallel to each other has resulted in this initial "stiffness". Hence, upon loading, the structures exhibit an effective flattening deformation during this initial contact. At the peak load, the core deformed almost symmetrical about the axis of loading. In region II, the response becomes non-linear and following this, the structure started to lose its stability due to the buckling mode. As a result, a gentle drop in the applied load occurred. In region III, the corrugated core turns into trapezium shape, followed by the initiation of a small region of fracture close to the uppermost core area (in certain cases). This is due to the surfaces of the cell walls coming into contact with the uppermost skin, slightly increasing the applied load. Further applied loading resulted in the structure becoming completely densified (region IV). Here, in certain cases, debonding at the edges of the structure occurs, due to insufficient levels of adhesion for transmission of the shear force to the core.

In contrast, the flax/PLA corrugated core exhibits extensive crushing, as shown in Figure 4.32(b). Similar non-linear and linear responses were observed in the PLA-based system in region I as were observed in the PP-based materials. However, in this case, delamination between the core plies was visible, rather than buckling. Such delamination became more visible as the movement of the crosshead continued. This resulted in a dramatic drop in force and a long plateau zone (region II – III). Finally, in region IV, the completely crushed structure, with wrinkling of the core, is in evidence (following delamination failure).

An attempt to further investigate the mechanical response of the core was carried out using different numbers of unit cell, i.e. two, three and five cells. Figure 4.33 shows the typical compression response for both PP and PLA-based corrugated core system with different numbers of unit cells. Based on these observations, all unit cells show an acceptable load-displacement trace. It is evident that the load increases as the number of unit cells increases. Figure 4.34 shows the process of failure in the flax-based composite specimen during compression testing. Close examination of the failure mechanismsin the PP-based system, is predominantly associated with buckling, fibre fracture and debonding at the edge, whereas failure in the PLA-based material involved a combination of fibre micro-buckling and delamination. Complete failure of the specimens with different numbers of unit cellsare shown in Table 4.2. In the table, all unit cells exhibit a similar failure mode, this being fibre fracture and debonding for the PP-based system and delamination for the PLA-based material.

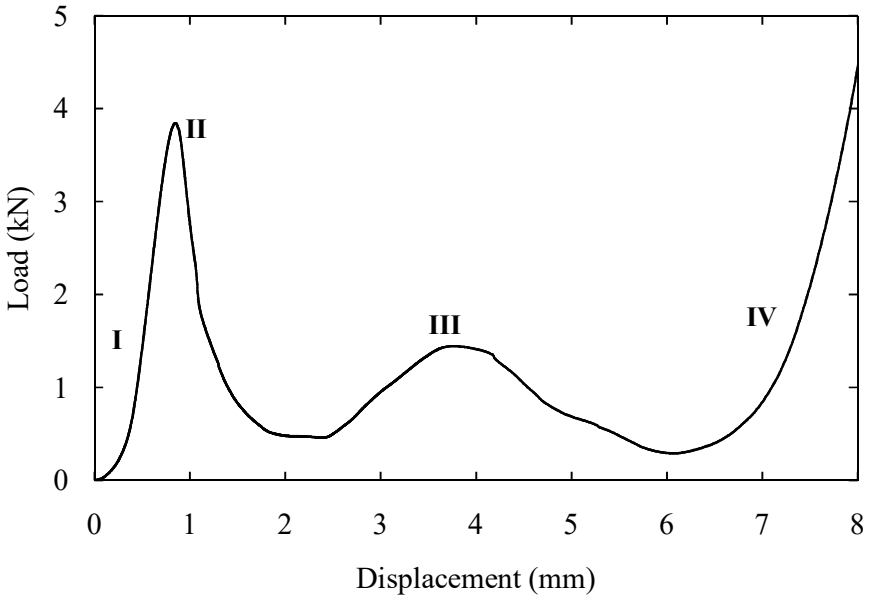

(a)

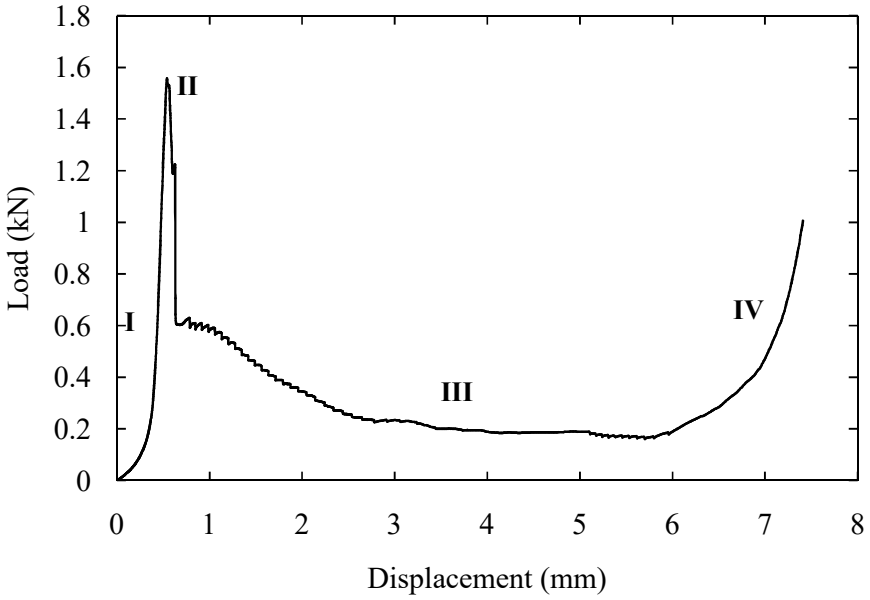

(b)

Figure 4.32. Typical load-displacement curves for (a) flax/PP and (b) flax/PLA corrugated core structures.

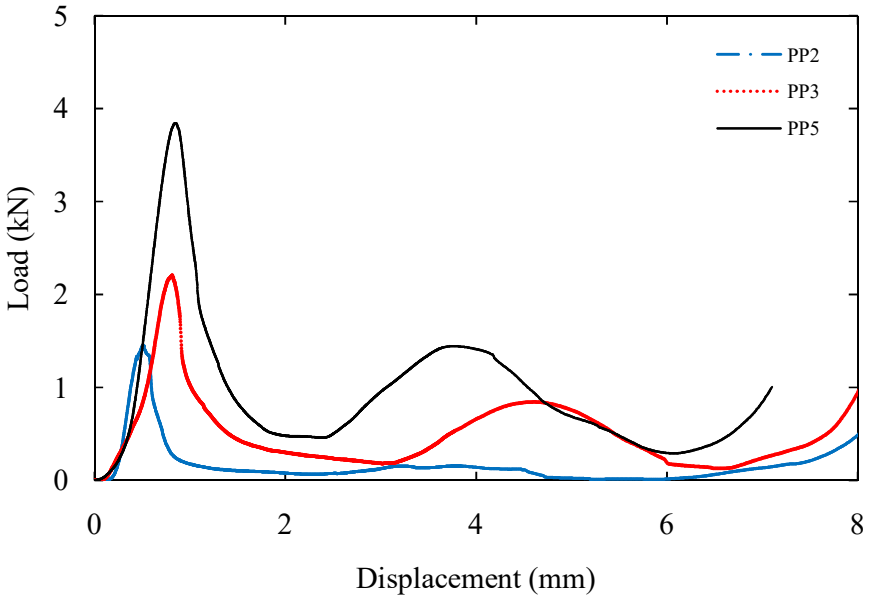

(a)

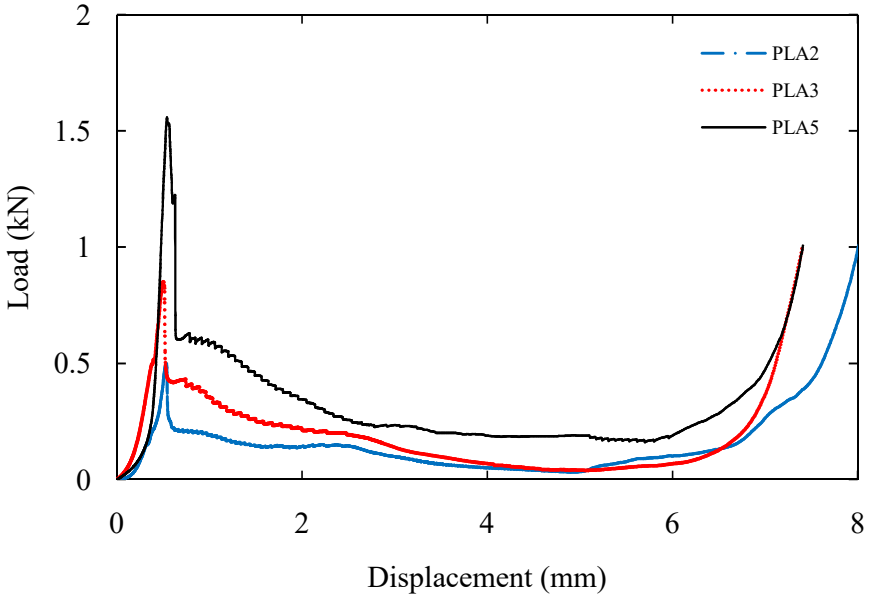

(b)

Figure 4.33. Comparison of load-displacement traces for (a) flax/PP and (b) flax/PLA corrugated core based on 2, 3 and 5 unit cells.

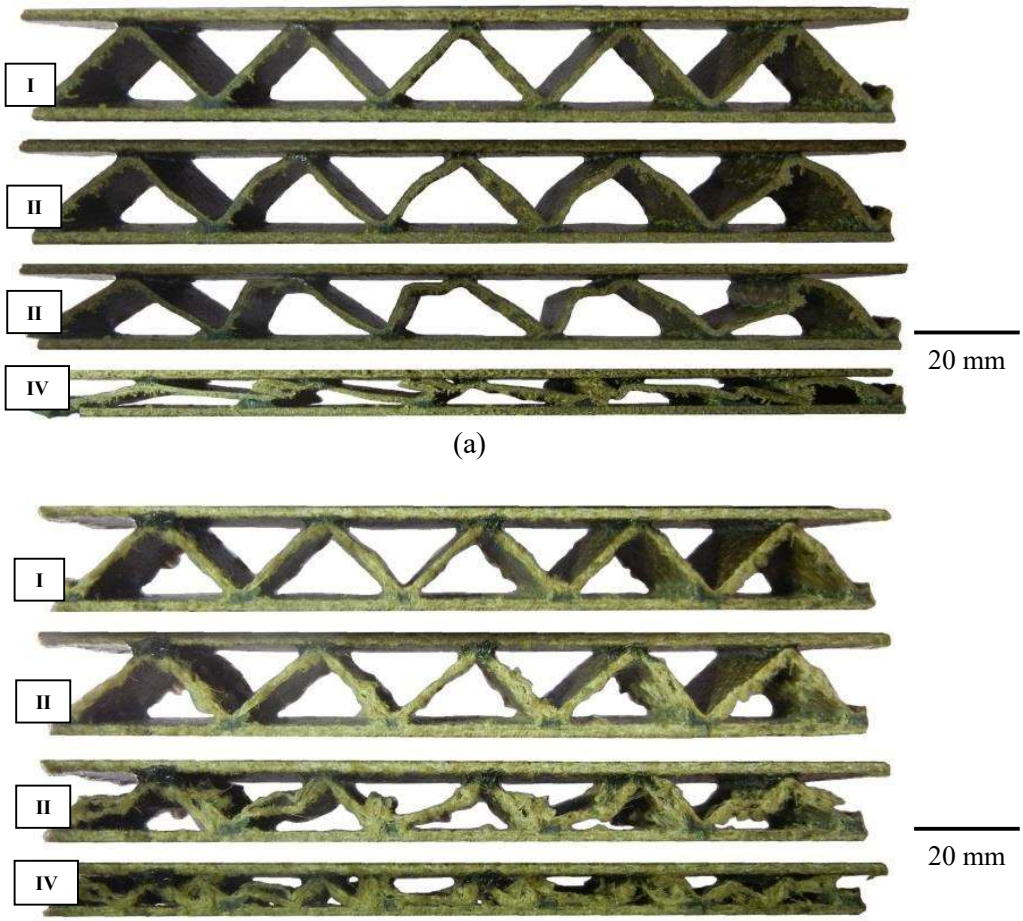

Figure 4.34. Photographs of progressive damage development in structures based on five unit cells of (a) flax/PP and (b) flax/PLA.

Table 4.2. Photographs of the flax-based composite specimens based on 2, 3 and 5 unit cells after crushing under quasi-static loading.

Composite materials	Number of unit cells	Photographs of failed specimens
Flax/PP	2	
	3	
	5	
Flax/PLA	2	
	3	
	5	

The effect of varying the number of unit cells on the compression strength of the flax-based composite corrugated core is presented in Figure 4.35. The figure clearly indicates that as the number of unit cells increases, the strength also increases. A comparison between the two flax fibre corrugated cores suggests that the flax/PP composite offers superior properties to its flax/PLA counterparts. For example, the strength of the flax/PP corrugated core was approximately 57% greater than the flax/PLA corrugated core, for the five unit cell geometry. Figure 4.36 compares the SEA values for the flax/PP and flax/PLA corrugated core. As expected, the SEA of the PP-based core is higher than the PLA-based core. Obviously, the increasein the value of SEA for the PP-based core is more significant than the PLA-based core. The effect of the buckling-dominated failure in the elastic region, allows more energy to be absorbed by the PP-based core (Figure 4.33). Moreover, the presence of the buckling failure mechanism means that the core experienced a substantial increase in strength, as has been proposed by Kazemahvazi *et al*. [30]. The poorer mechanical properties of the flax/PLA composite, discussed earlier, may also contribute to this result. All of the specimens were deformed to a similar level of crosshead displacement, where the instability of the core struts (or buckling) occurred during the initial failure.

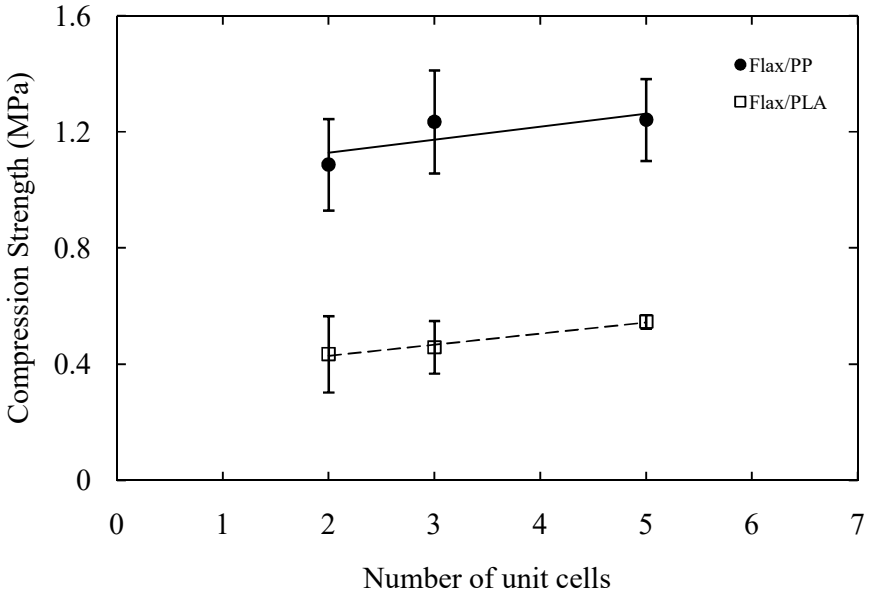

Figure 4.35. Comparison of compression strength of the flax-based corrugated core based on different numbers of unit cells.

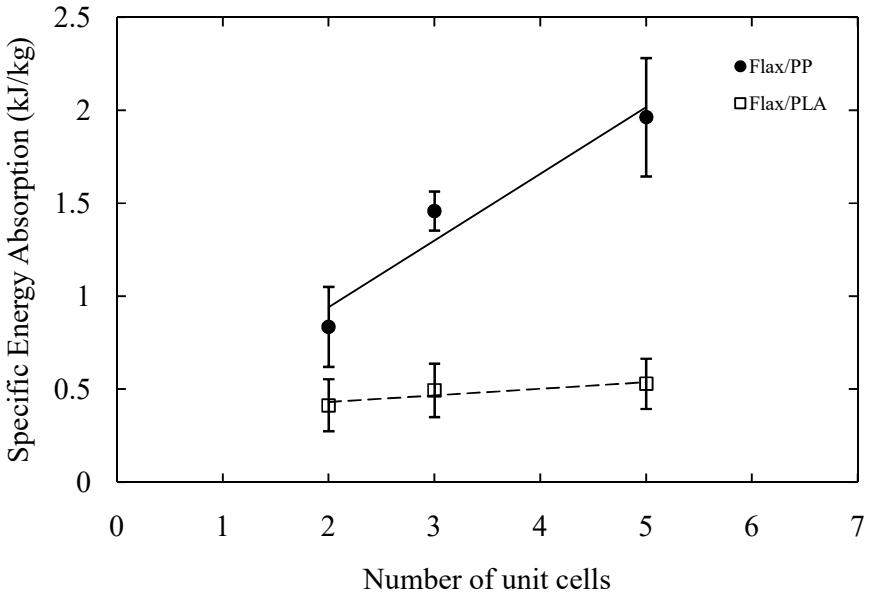

Figure 4.36. Comparison of the SEA values of the flax-based corrugated core with different numbers of unit cells.

4.5.2 Dynamic Tests

The dynamic loading response of the flax-based composite has been evaluated on samples with five unit cells of corrugated structure. The results shown in Figure 4.37 indicate similar trends to those presented in Figure 4.32. Initially, the load rises linear and non-linear up to their maximum values, this being about 3.6 kN for the PP-system and 0.64 kN for the PLA-system. With continuing loading, the specimens begin to fail and sustain the load until densification.

A comparison of the compression and impact strengths of the flax-based composite corrugated structures is shown in Figure 4.38. In the figure, it is evident that the PP-system offers a superior performance to its PLA-system counterpart. The dynamic strength of the PP-system is observed to be higher than those under static loading. However, the PLA-system exhibited a lower strength under dynamic loading than under static loading, the difference being more than 50%. This might be related to the failure mode, which is buckling and delamination.Also, the material rate-dependencemay occur during the crushing event. Figure 4.39 presents the energy-absorbing capability of the flax-based composite structures under static and dynamic loading conditions. Both flax composite structures exhibit higher values under the dynamic loading. The higher energy absorption capability of the PP-system is likely to be influenced by the inertia effect, as well the buckling-dominated failure mechanism. In contrast, the more angular deformation of the corrugations in PLA-system indicates a small difference in the failure mechanisms from that seen under quasi-static loading. For dynamic compression, the PLA-system experienced micro-buckling and subsequently delamination failure. Previous work has reported that buckling-dominated failure can be affected by inertia stabilisation, whereas compressive failure (following delamination and fibre micro buckling) influenced by the material strain-rate sensitivity [51]. Table 4.3 summarises the failure mechanisms for both static and dynamic testing.

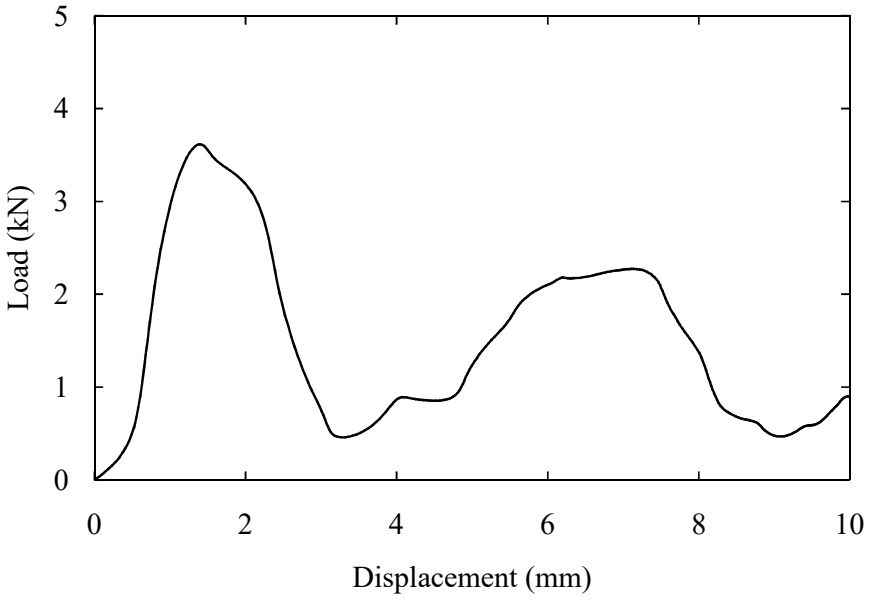

(a)

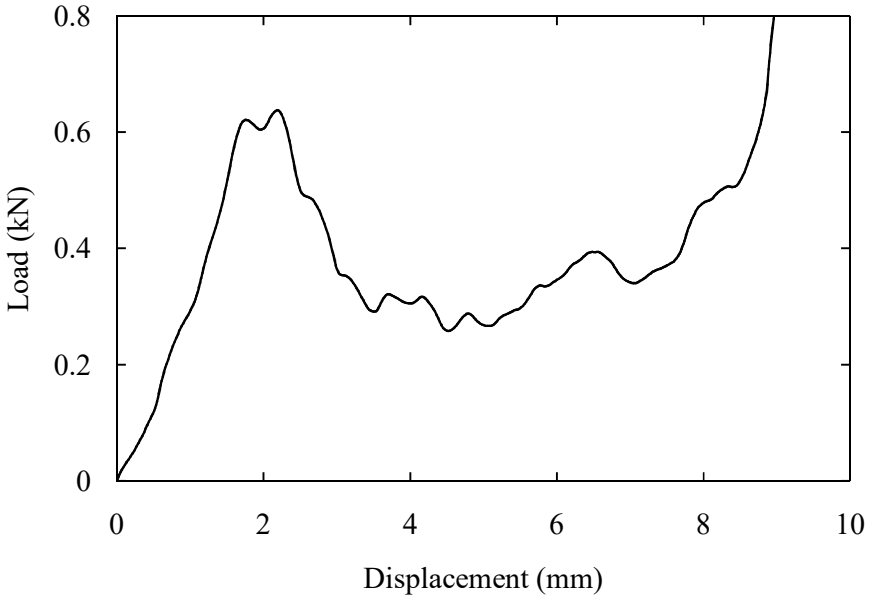

(b)

Figure 4.37. Typical load-displacement response under dynamic loading conditions for the (a) flax/PP and (b) flax/PLA corrugated structures.

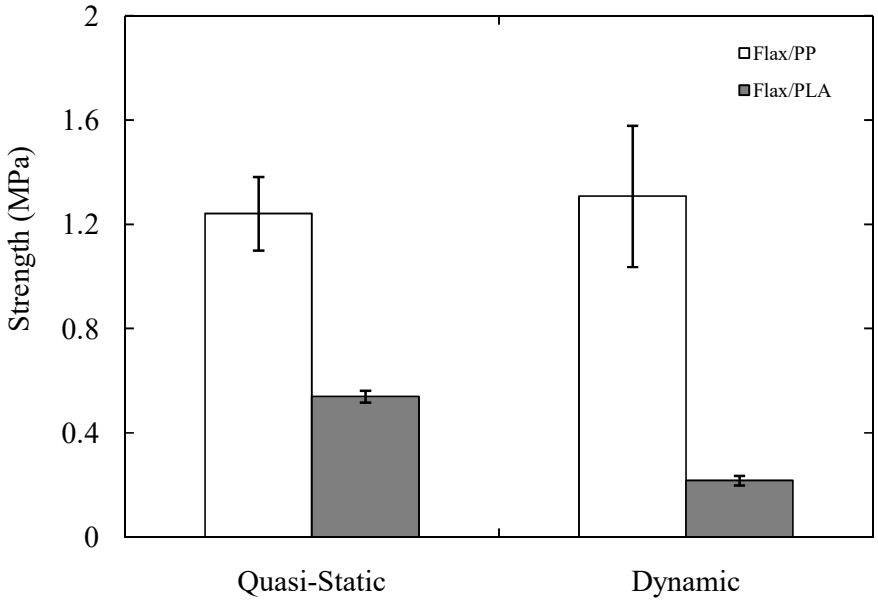

Figure 4.38. Comparison of strength of flax-based corrugated structures under quasi-static and dynamic loading conditions.

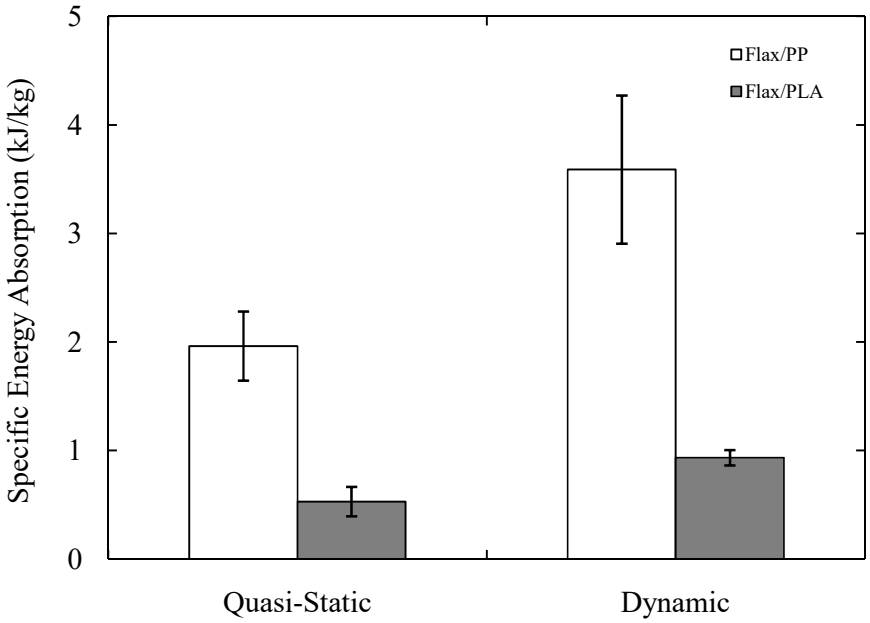

Figure 4.39.The specific energy-absorbing characteristics of flax-based corrugated structures under quasi-static and dynamic loading conditions.

Table 4.3.Comparison of failed flax-based composite specimens under quasi-static and dynamic loading conditions for the corrugated structures based on five unit cells.

Composite materials	Loading Conditions	Photographs of failed specimens
Flax/PP	Quasi-static	
	Dynamic	
Flax/PLA	Quasi-static	
	Dynamic	

20 mm

4.6 Interlocking of Flax-based Composite Core

4.6.1 Quasi – Static Tests

Typical load-displacement traces following compression tests on the square and triangular honeycomb for the flax/PP structures are presented in Figure 4.40(a). This curve exhibits four distinct regions: linear elastic (region I), nonlinear plastic (region II), plateau plastic (region III) and densification (region IV). Both traces rise rapidly during the elastic loading phase (region I) before reaching a maximum value (region II). This is followed by a rapid drop in the applied load as the walls in the core buckled. In region III, plastic yielding occurs at a plateau value and the wall of the core structure starts to crack. As loading continues, the cracked surface of the cell walls comes in contact with the skins. As a result, the core structure is completely densified (region IV). The load for the triangular core is clearly higher than that of its square counterpart, largely due to the fact that the former offers a higher relative density. The tests were interrupted once the force started to increase at higher crosshead displacements, i.e. following the onset of densification of the core material.

Figure 4.40(b) presents the equivalent load-displacement traces for the PLA cores, from where it is apparent that the maximum force values are significantly lower than those associated with the PP cores in Figure 4.40(a). In contrast, the load in these PLA cores does not drop as rapidly following the peak value, being comparable to that of the PP systems at intermediate displacements. Here, the PLA exhibits a long plateau in region III and the force remains fairly constant up to densification.

An examination of the failure modes during compression loading indicate that all of the PP-based structures failed as a result of buckling of the vertical cell walls within the honeycomb. This can be clearly seen at the edges of the test samples shown in Figure 4.41 for the square and triangular honeycombs. A localised buckling-type mode of failure was also observed in certain regions within the PLA-based composites, although delamination within the vertical webs and local kinking in the skins were also widely observed (Figure 4.41(c) and (d)).

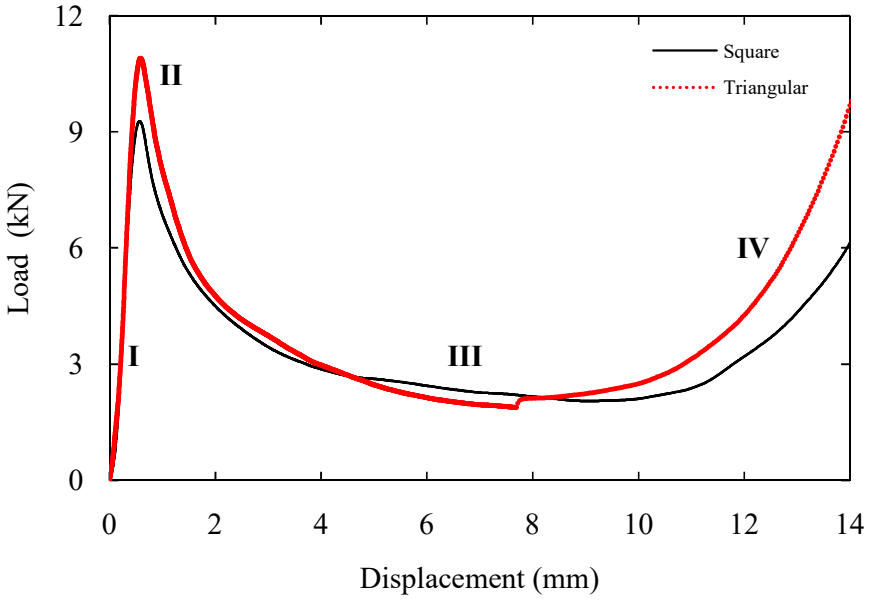

(a)

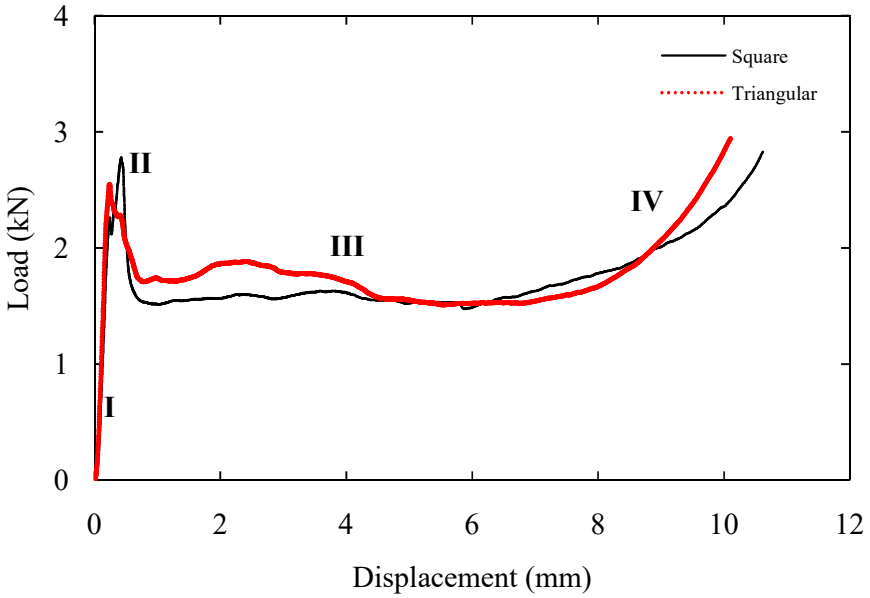

(b)

Figure 4.40. Typical load-displacement traces for the (a) flax/PP and (b) flax/PLA composites.

Figure 4.42 and Figure 4.43 show the load-displacement responses following compression tests on the flax-based composite structures with between two and five layers. It is clear that all of the specimens deformed in a similar fashion. However, the applied load for the five layer PLA cores gradually increasesafter the sudden drop, which associated with large deformation of wrinkling following delamination failure. Clearly, the compression strength increases as the core wall thickness increases, offering a higher energy-absorbing capability compared to the thin wall structures. Previous work has shown that an increasein the honeycomb cell-wall thickness will strengthen the compressive response, as well increases the energy-absorbing characteristics of the honeycomb sandwich panel [146].

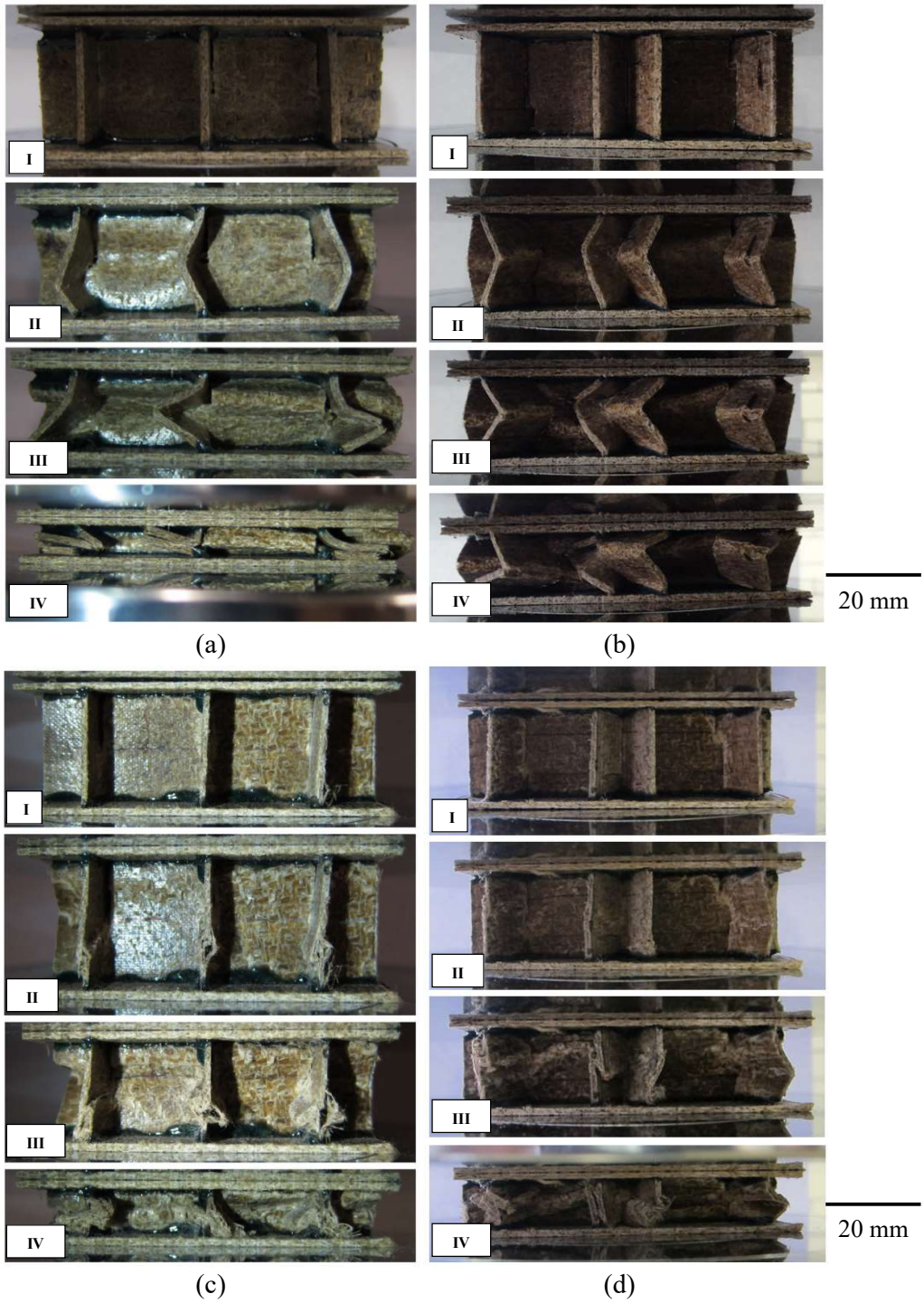

Figure 4.41. Sequences showing the failure modes in the (a) square and (b) triangular core flax/PP structures with a web thickness = 1.5 mm; (c) square and (d) triangular core flax/PLA structures with a web thickness = 1.3 mm.

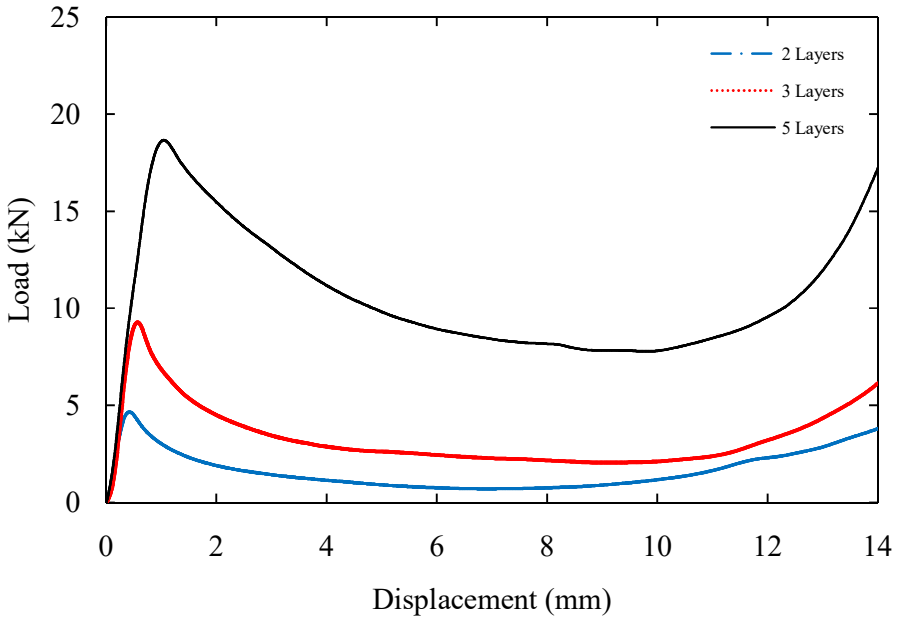

(a)

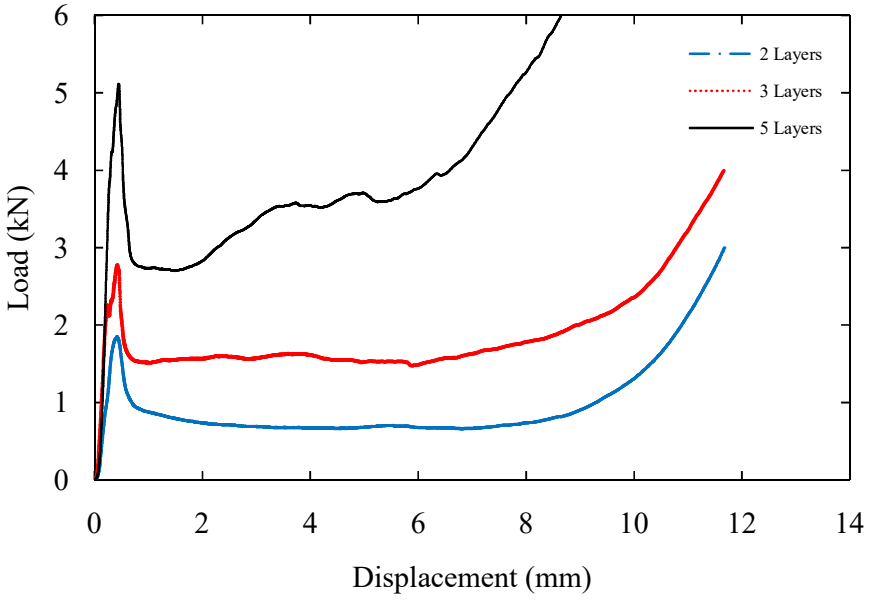

(b)

Figure 4.42. Typical load-displacement traces for the (a) flax/PP and (b) flax/PLA square core interlocking structures based on 2, 3 and 5 layers.

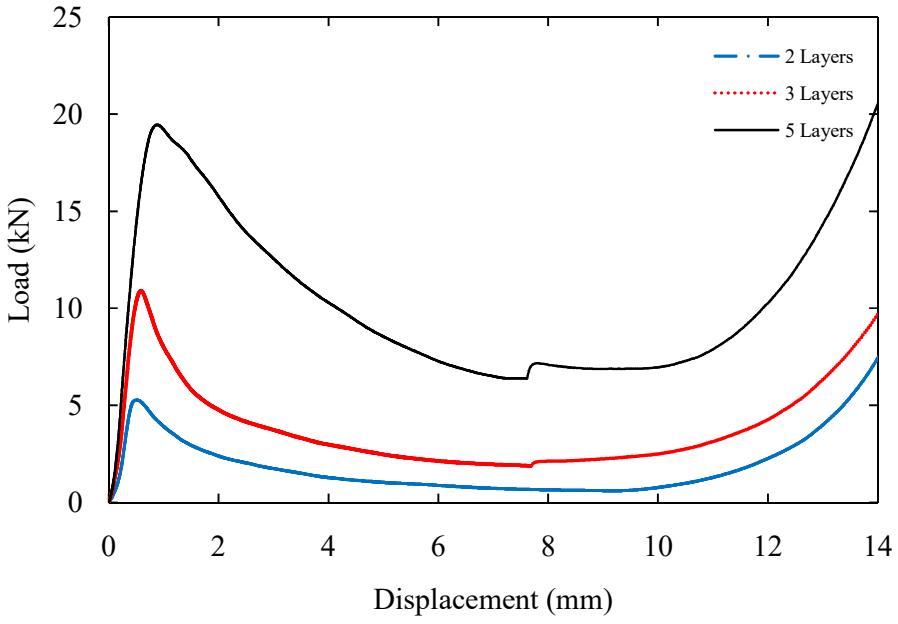

(a)

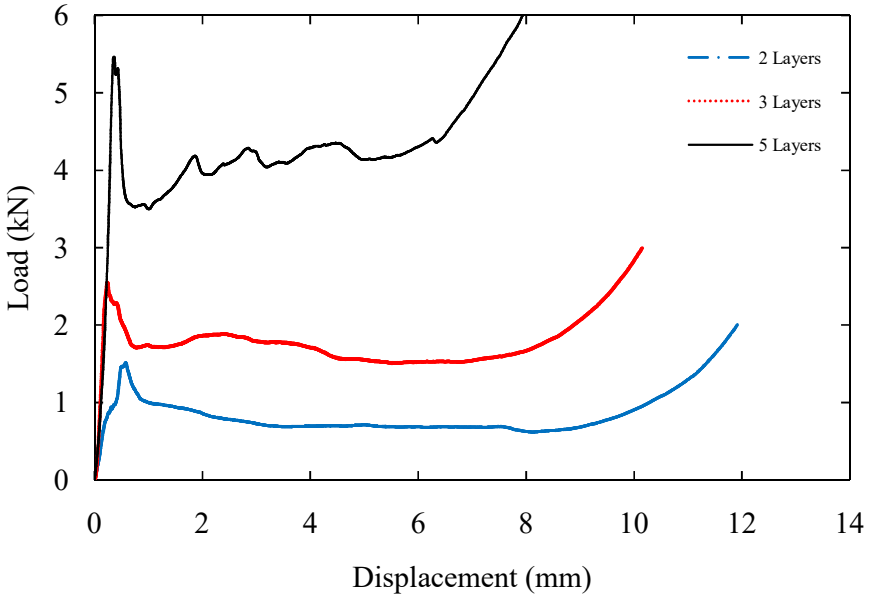

(b)

Figure 4.43. Typical load-displacement traces for the (a) flax/PP and (b) flax/PLA triangular core interlocking structures based on 2, 3 and 5 layers.

The strengths of the square and triangular honeycomb PP-based structures are plotted as a function of relative density in Figure 4.44(a). From the figure, it is clear that the square honeycombs significantly out-perform their triangular counterparts, for a given relative density. The relative density for the square and triangular cores can be expressed as [33]:

$$\text{Square core,} \bar{\rho} = \frac{2t}{l} \tag{4.1}$$

$$\text{Triangular core, } \bar{\rho} = \frac{2\sqrt{3}\,t}{l} \tag{4.2}$$

where*t* is the cell wall thickness and *l* is the length between two strips (as illustrated in Chapter 3).

For example, the compression strength of the square core with a relative density of 0.23 is over thirty percent greater than that of the triangular core with a relative density of 0.26. Similar trends are apparent in the compression data for the PLA-based composites shown in Figure 4.44(b), where the square honeycombs continue to out-perform the triangular systems. This is most evident when the strength of the square core with a relative density of 0.2 is compared with that of the triangular core with a relative density of 0.23. In this case, the former is more than double the latter.It is knownthat when the relative density increases, the cell wall thickness also increases,while the cell pore will decrease.Here, the square core with 5 layers (relative density = 0.23) exhibits a lower relative density than that of triangular corewith a same number of layer (relative density = 0.26). Therefore, the square core is suggested to have a better performance compared to the triangular core.Figure 4.44 again highlights the difference in the relative performances of the two types of material, with the flax/PP structures being between three and four times stronger than the flax/PLA cores.

One potential application of these natural fibre based cores is in energy-absorbing structures and systems. In this study, the energy-absorbing characteristics of the cores are compared by determining the SEA values of the cores. Here, the energy under the load–displacement trace was divided by the mass of the sample. This approach has been used by other authors to characterise the energy-absorbing characteristics of core materials and composite tubes [147,148].

Figure 4.45(a) shows the variation of SEA for the flax/PP honeycomb structures with relative density, where it is again clear that the square cores outperform the triangular cores. Similar trends are in evidence in the SEA data for the flax/PLA core structures, shown in Figure 4.45(b), where it is again clear that the square structure offers superior properties. Once again, the energy-absorbing characteristics of the PLA honeycombs are inferior to that of their PP counterparts, largely due to the poorer mechanical properties of the former.

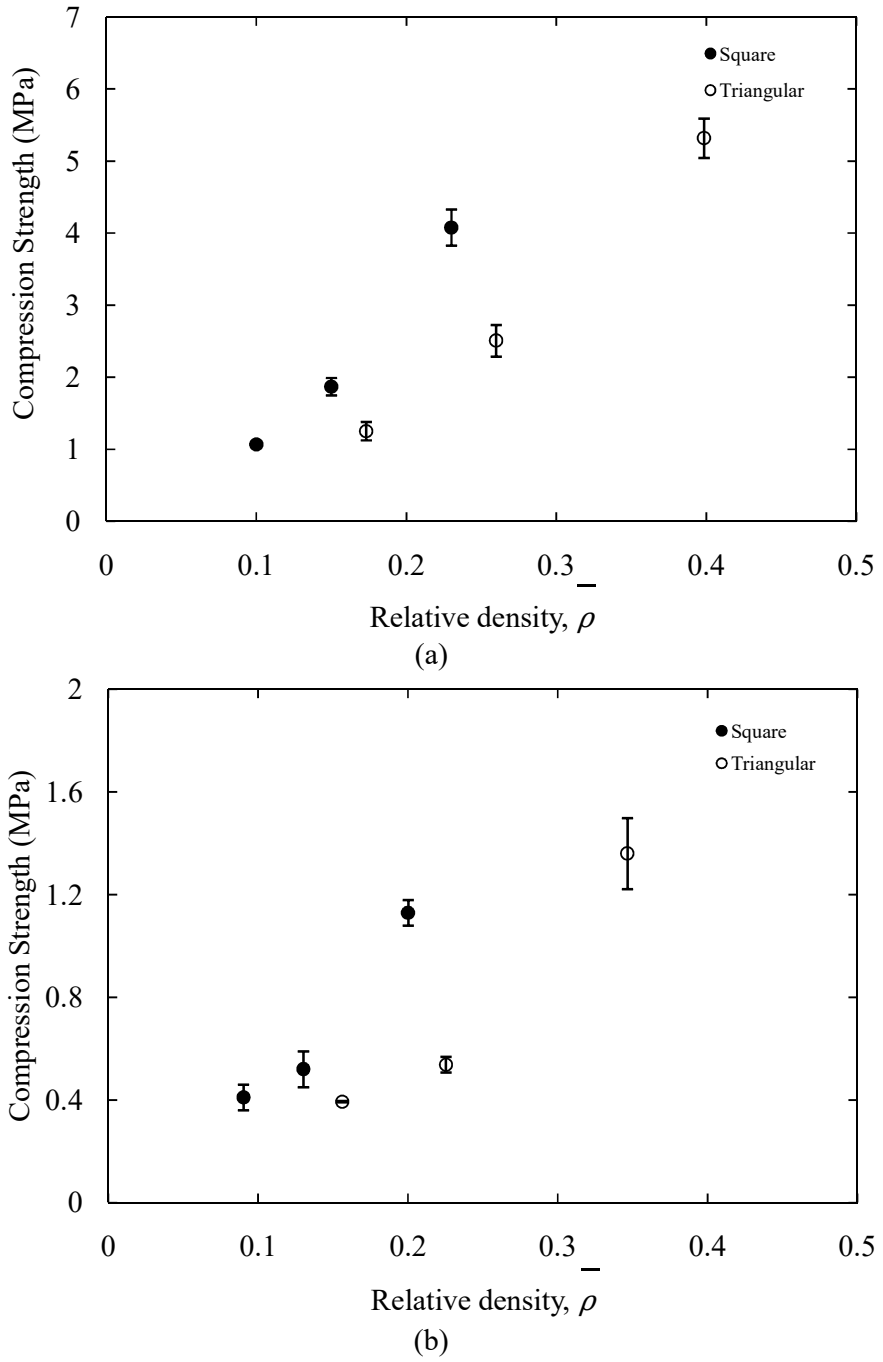

Figure 4.44. The variation of compression strength with relative density for the (a) flax/PP and (b) flax/PLA structures.

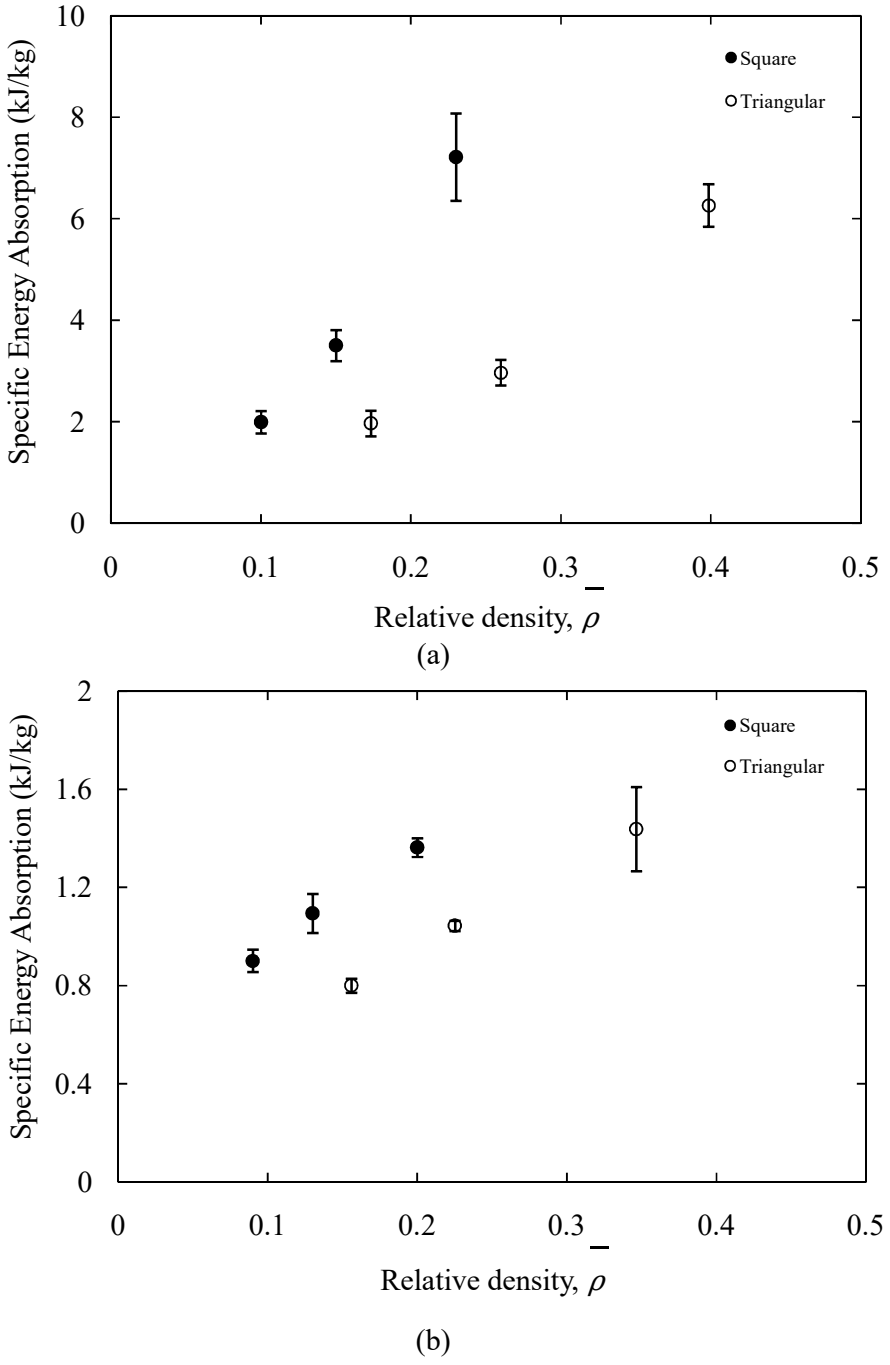

Figure 4.45. Summary of the specific energy absorption values for the square and triangular honeycombs, (a) flax/PP and (b) flax/PLA structures.

4.6.2 Dynamic Tests

Low-velocity impact tests were undertaken on the square interlocking core structures of the flax-based composite. Figure 4.46 presents the dynamic load response of flax-based interlocking structures. In the figure, both curves exhibit a similar response to their static behaviour (Figure 4.40), i.e. the load increases to a maximum value, followed by a subsequent drop, before tending to a plateau force and completely crushed in the compaction zone. Here, the flax/PP structure exhibits its maximum value at approximately 12 kN, about eight times higher than the flax/PLA structure. The failure mechanisms under dynamic loading are similar to those under static loading. This includes buckling and fibre fracture in the flax/PP and delamination and localised buckling in the flax/PLA structure.

Figure 4.47 compares the compressive strength and SEA values of the interlocking structures under quasi-static and dynamic loading conditions. The figure indicates that the dynamic response of the flax/PP structure displayed a greater strength and energy absorption compared to quasi-static response. This is due to the specimen experiencing a greater buckling resistance under dynamic loading. As suggested by Radford *et al*. [50], the enhancement in the dynamic strength can be influenced by the material rate-sensitivity and higher order of buckling modes (due to the inertial stabilisation). An observation of the flax/PLA structure shows no significant difference in the strength and energy absorbing capability between the quasi-static and dynamic data compared to the flax/PP structures. However, a close examination highlights evidence of a slightly lower strength under dynamic loading. It is known that delamination reduces the load-carrying capability of a structure, leading to early failure [149]. Delamination initiated after the peak load and propagated along the vertical webs in the cells of the honeycomb structure, before generating localised buckling. Such failure is associated with the materials rate-sensitivity, as well as the poorer mechanical properties of the flax/PLA composite. Apart from the failure modes, both results are also influenced by small imperfections in the vertical straightness of the core strips.

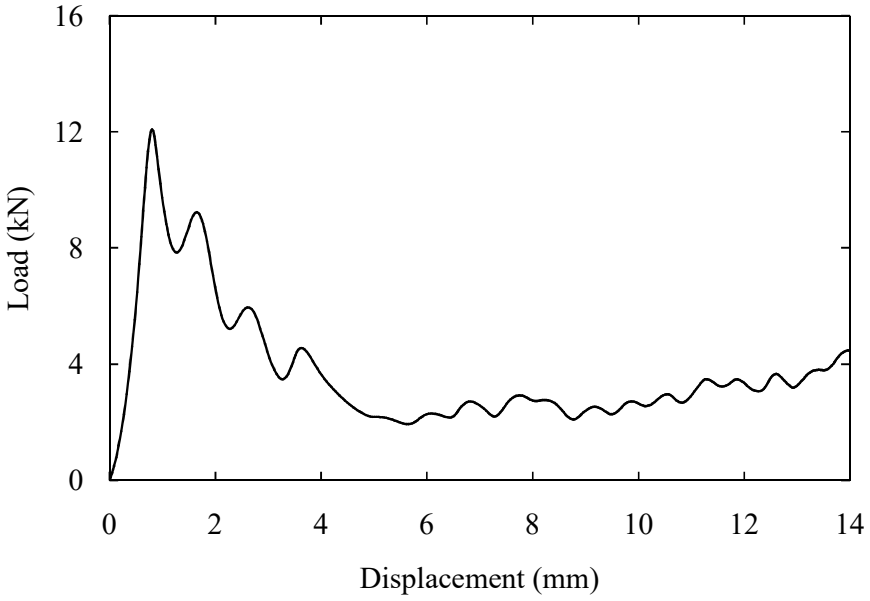

(a)

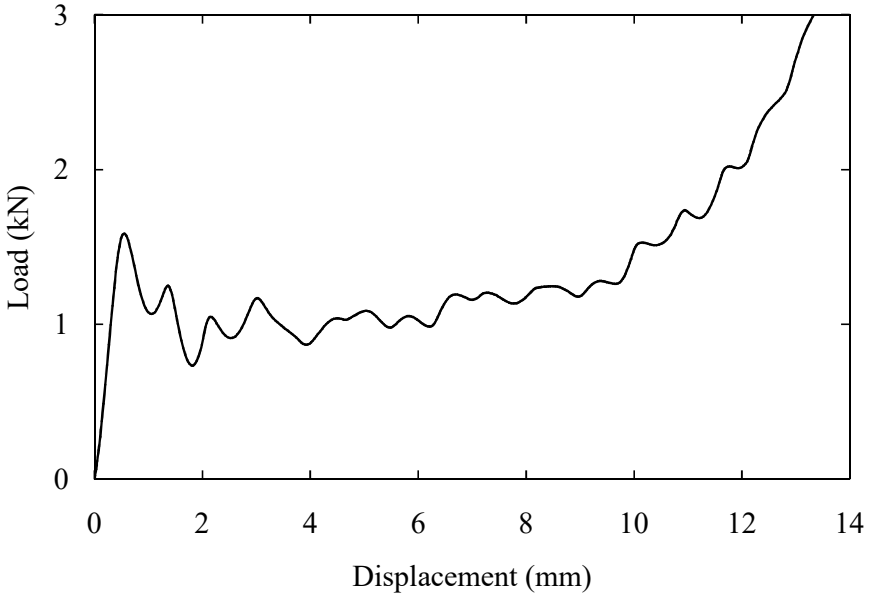

(b)

Figure 4.46. Typical load-displacement traces under dynamic loading for the (a) flax/PP and (b) flax/PLA interlocking structures.

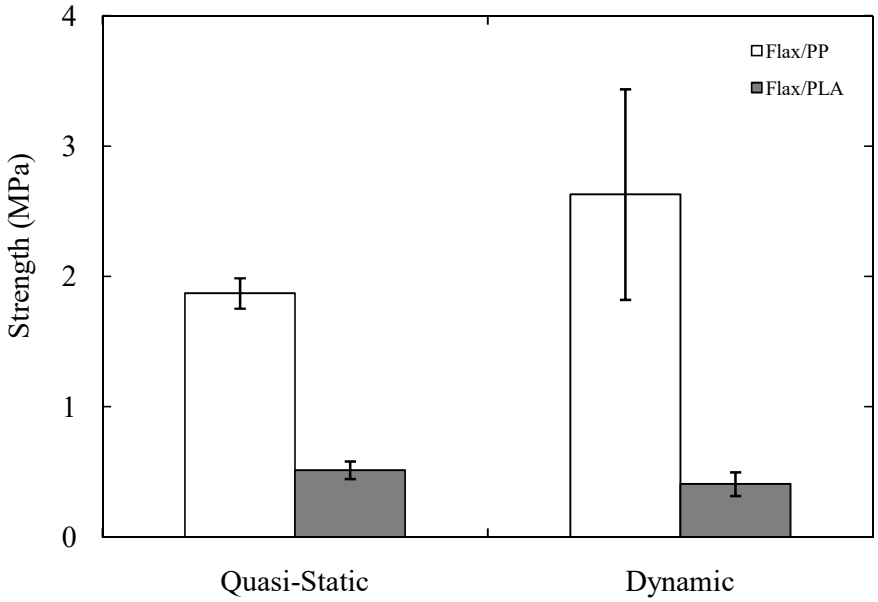

(a) the compressive strength,

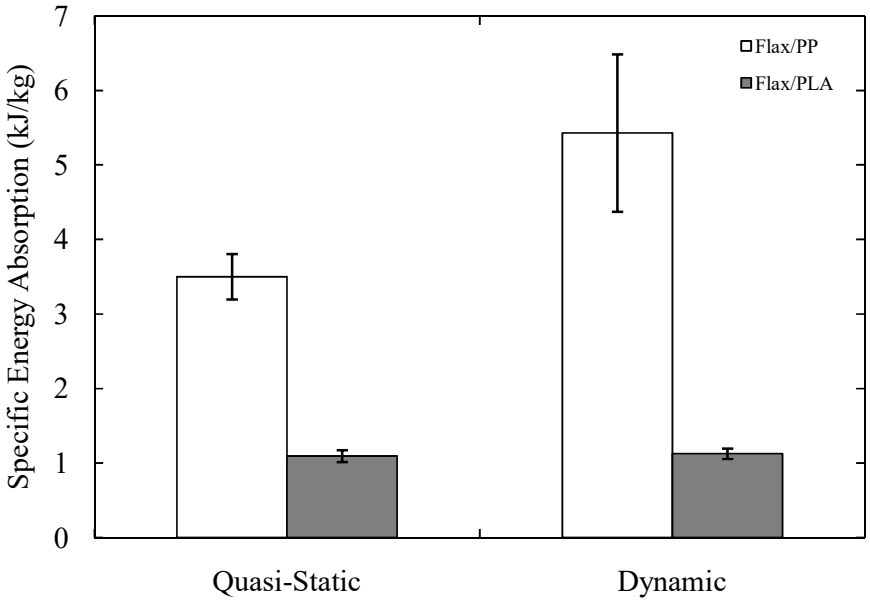

(b) the specific energy absorption

Figure 4.47. The quasi-static and dynamic test results for interlocking core structures based on flax-based composites.

4.7 Corrugated Paperboard

4.7.1 Quasi – Static Tests

Further investigations into the mechanical properties of the corrugated paperboard combined with the flax composite skins have been carried out. Figure 4.48 shows typical load-displacement traces for the corrugated paperboard structures with flax/PP and flax/PLA skins. It is clear that both structures showing a similar compressive response. Here, the load initiates reasonably linearly up to the maximum value. After peak load, the cell walls begin to collapse and a large drop in the load-carrying capability occurs. This drop was caused by local buckling and compression creasing of the cell walls. A close examination of Figure 4.48 indicates that the flax/PLA skin is slightly higher than the flax/PP skin, with a difference of approximately 8%. Figure 4.49 shows the failure sequences in the corrugated paperboard based on flax/PP composite skins. The aforementioned failure modes are observed at the edge of the structure, these being localised buckling and compression creasing.

The strength and energy-absorbing characteristics of the paperboard structures are presented in Figure 4.50. The strength of the paperboard structure was calculated from the compression load response and the surface area of the structure. There is no significant change in the strength properties, even though the flax/PLA value is slightly higher than the flax/PP system. There is a noticeable difference in the SEA values between both skins of about 20%. This may be associated with the onset of densification, as seen in Figure 4.48. It may also be due to the inconsistency in a number of the corrugated cells in the structure, following the cutting processes, that is inevitable. However, since there is evidence of a higher strength in the PLA-skins structures, it suggests that the flax/PLA composite offers greater support to the skins than the flax/PP composite.

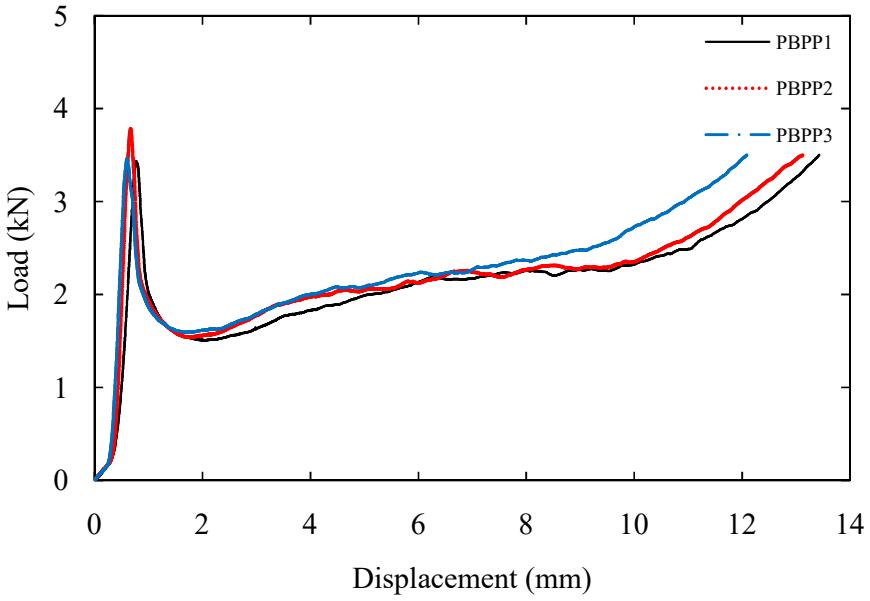

(a)

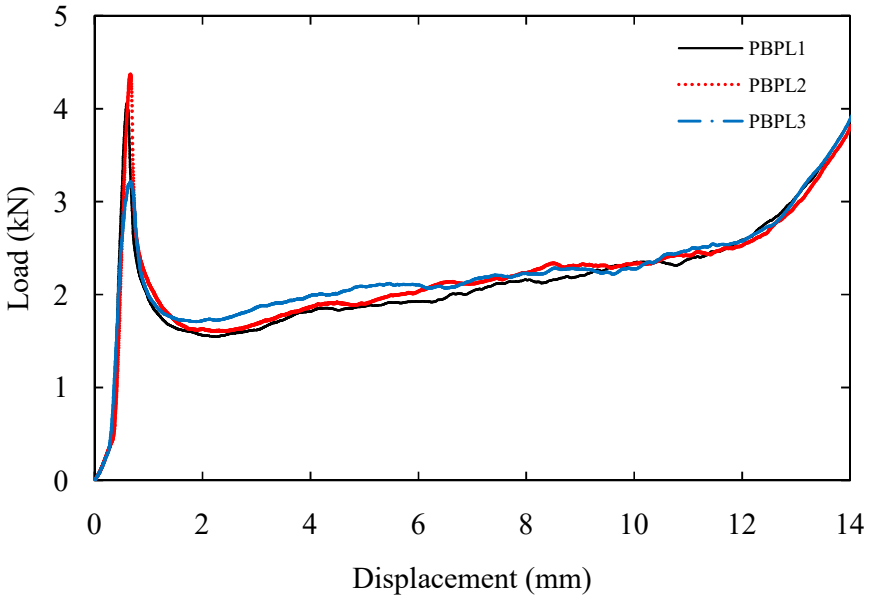

(b)

Figure 4.48. Typical load-displacement traces for corrugated paperboard with (a) flax/PP and (b) flax/PLA skins.

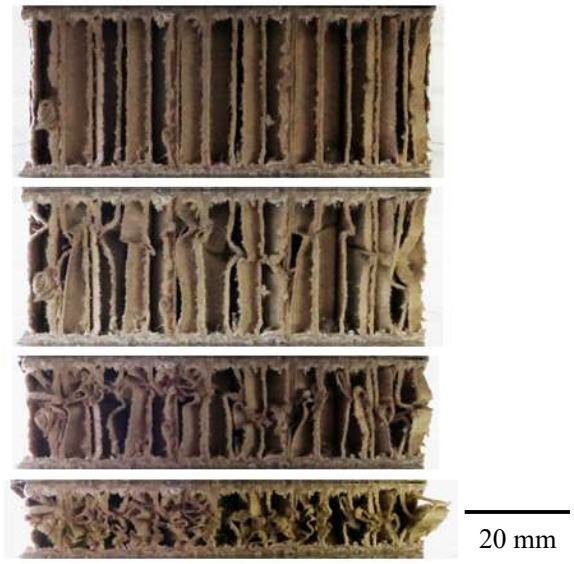

Figure 4.49. Sequence of failure in the corrugated paperboard sandwich structures with flax/PP skins.

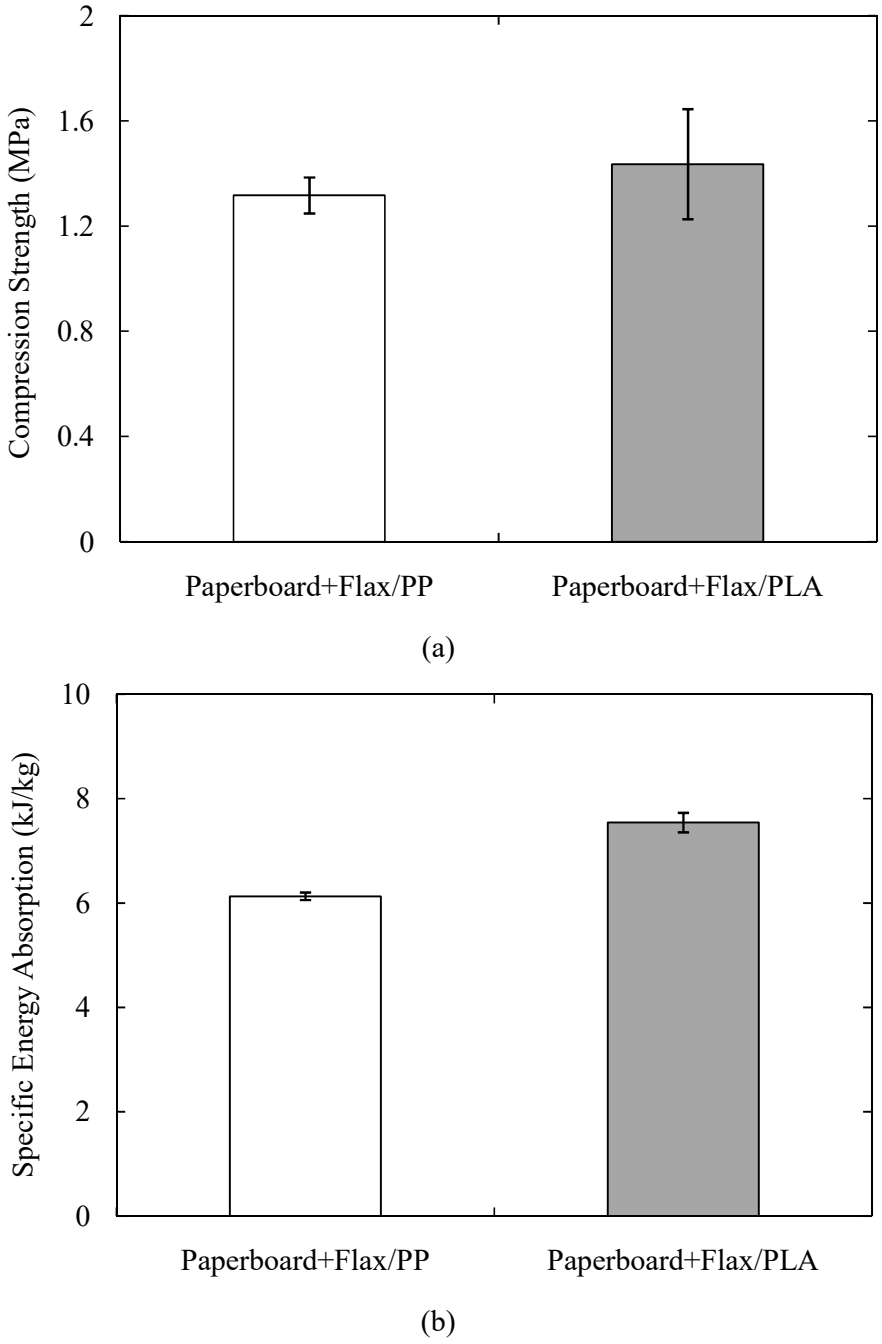

Figure 4.50. Comparison of (a) the strength and (b) the SEA values of corrugated paperboard sandwich structures with flax-based composite skins.

4.7.2 Dynamic Tests

The dynamic responses of the corrugated paperboard structure reinforced with flax-based composite skins were also evaluated under the drop-weight impact tests. Figure 4.51 presents typical load-displacement traces for the paperboard configuration. Both traces show similar loading responses, with a linear and non-linear elastic response to the peak, following the drop in applied load and subsequently continuing until the densification stage. Furthermore, the failure mode for this paperboard core under the dynamic loading, shown in Figure 4.52, is almost identical to that under quasi-static loading (Figure 4.49).

A comparison between both loading conditions is presented in Figure 4.53. Figure 4.53(a) highlights lower strength values under the dynamic loading compared to the quasi-static tests. In contrast, the SEA data for the dynamic tests are higher than the quasi-static values, by a factor of two. The energy absorption values were calculated from the load-displacement traces up to the onset of densification. The higher values from the dynamic tests are associated with the time required to generate folds in the cell walls, particularly during the drop in load. Wang [146] reported that the impact behaviour of the paperboard honeycomb sandwich structures can be affected by a number of factors, such as cell-wall thickness and length, core thickness as well as the skins. Other work carried out by Wang and Wang[150], proposed that the height of the paperboard core also influences its cushioning properties.

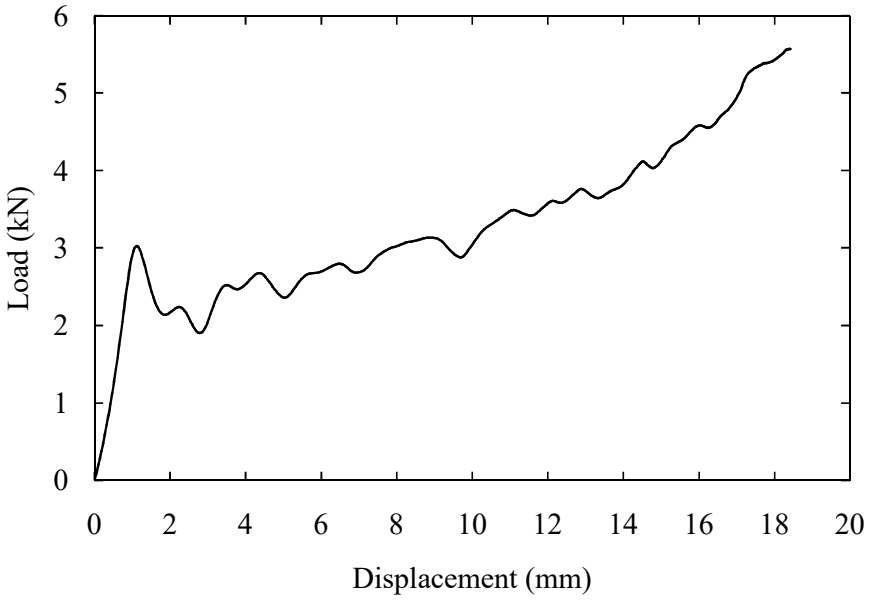

(a)

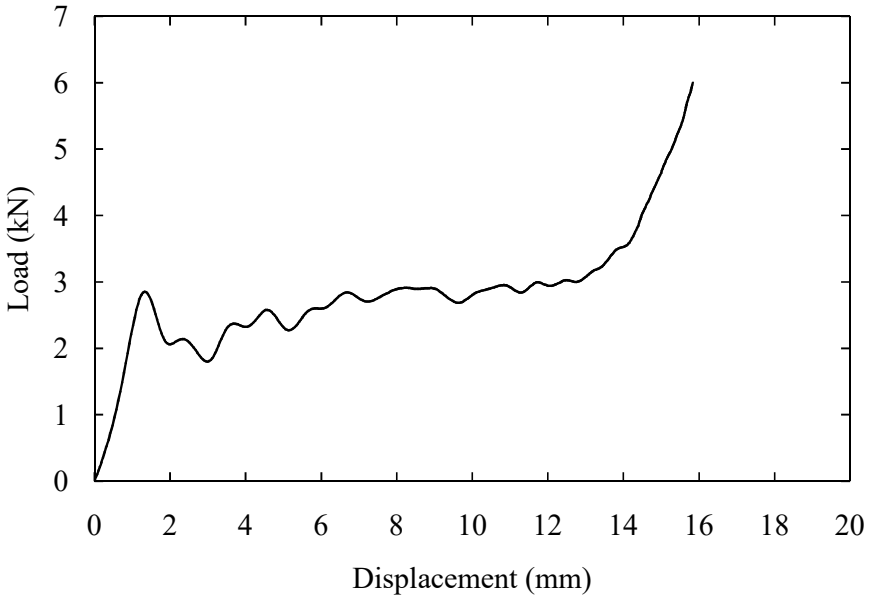

(b)

Figure 4.51. Typical impact load-displacement responsesfor the corrugated paperboard reinforced sandwich structures, (a) flax/PP and (b) flax/PLA skins.

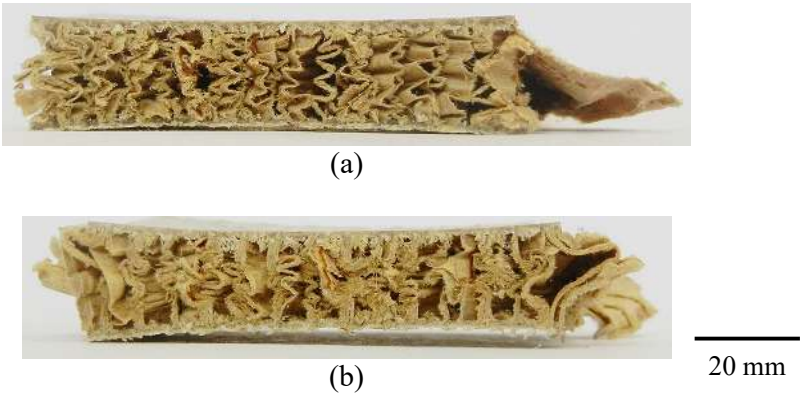

Figure 4.52. Photographed of failed specimens of corrugated paperboard reinforced (a) flax/PP and (b) flax/PLA skins after impact tests.

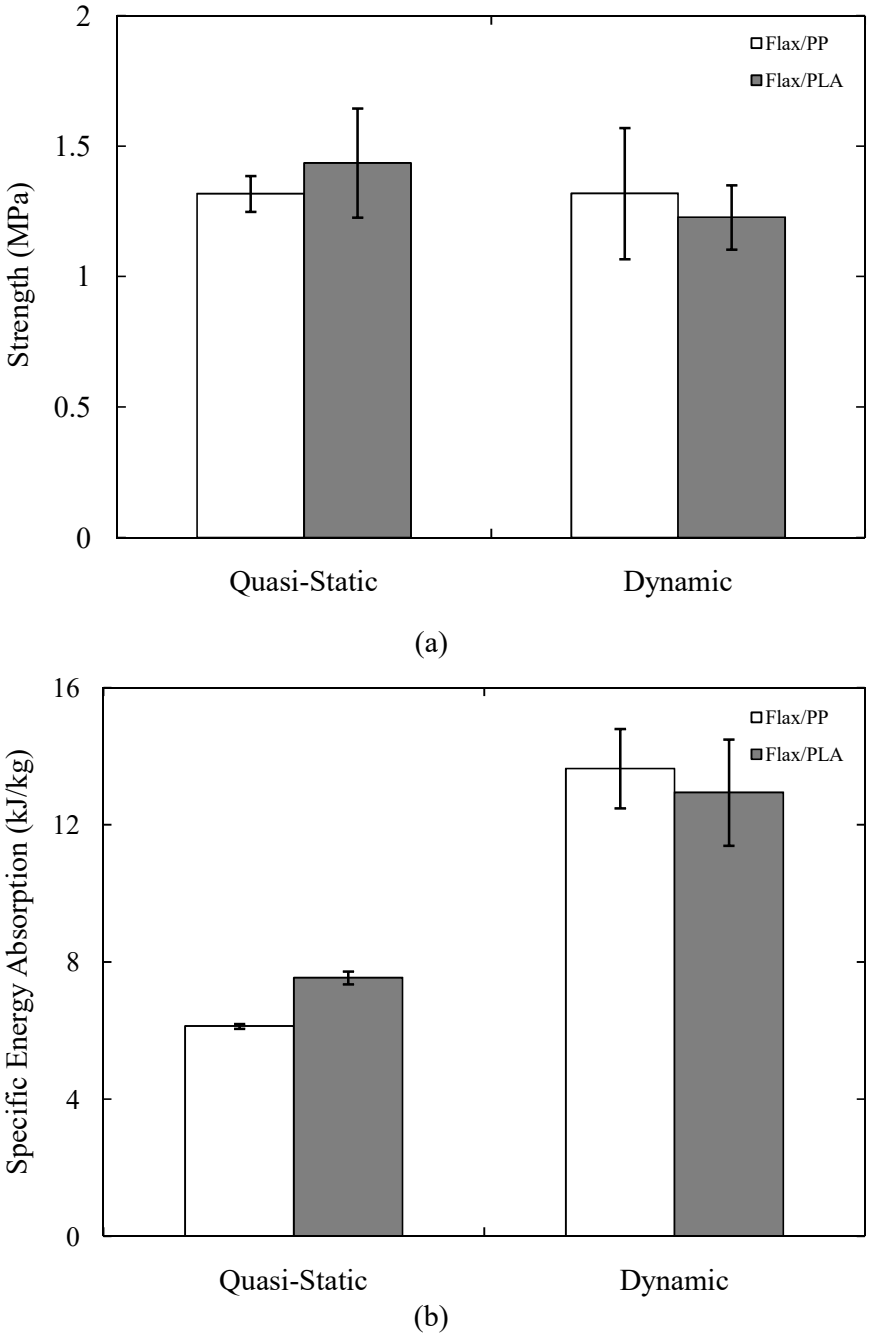

Figure 4.53. Comparison of the quasi-static and dynamic (a) strength and (b) specific energy absorption characteristics of the flax-based composites.

4.8 Interim Conclusions

This section investigates the quasi-static and dynamic response of various designs of sandwich structure based on natural fibres. The study has shown that the collapse mechanisms, for a particular geometry, remain unchanged with increasing strain-rate. It has been shown that the bamboo-based structures offer a great potential in energy-absorbing capacity. In most structures, the flax/PP composite offers greater mechanical properties, compared to the flax/PLA composite, particularly when in the form of corrugated and interlocking structures. The mechanical properties of interlocking structures have shown that there is no significant difference between the square core and triangular core. Such natural fibre-based structures offer potential for use in load-bearing applications as a result of their attractive specific properties and light weight. It also serves to reduce environmental concerns. The rate-sensitivity study has shown that the dynamic strength of most of these natural fibre-based sandwich structures is higher than the quasi-static strength.

CHAPTER 5 : FINITE ELEMENT MODELLING

5.1 Introduction

Finite element analysis (FEA) or the finite element method (FEM) is known as a numerical method used to solve problems relating to engineering and mathematical physics. This method is very useful for problems with complicated geometries, loadings and material properties, which can not be obtained through analytical solutions. In this study, the interlocking structures were simulated using both Abaqus/Standard and Abaqus/Explicit.

Abaqus/Standard: This is a general-purpose analysis product that offers a solution for various linear and nonlinear problems involving the static, dynamic, thermal and electrical response of components. It also solves a system of equations implicitly at each solution 'increment' [151,152].

Abaqus/Explicit: This is a special-purpose analysis package that uses an explicit dynamic finite element formulation. This analysis is convenient to model brief, transient dynamic events, i.e. impact and blast problems, and is likewise extremely proficient for highly nonlinear problems that are associated with changing contact conditions. Abaqus/Explicit marches a solution forward through time in small time increments without solving a coupled system of equation at each increment (or even forming a global stiffness matrix) [151,152].

5.2 Modelling Procedure

5.2.1 Constitutive Models for the Flax-based Composite

This section describes the constitutive models for the flax-based composite (flax/PP and flax/PLA) materials used in the manufacture of the interlocking core structures tested experimentally. Generally, at a microscopic level, a woven type of composite consist of bundles of parallel fibres embedded in a polymer matrix which has a much lower modulus, so that they are commonly treated as homogeneous and isotropic [156]. Therefore, in this study, the flax-based composite has been modelled as an isotropic material. This material model is similar to that studied by Martin *et al*. [153]. The elastic and plastic behaviour, as well as the failure criteria of the flax-based composite, are described herein.

5.2.1.1 Elasticity

The elastic response of the material was generated using an isotropic linear elasticity model. For materials that exhibit a linear elastic behaviour, the total stress is defined from the total elastic strain as:

$$\sigma = D^{el}\varepsilon^{el} \tag{5.1}$$

whereσ = total stress, D^{el}= fourth order elasticity tensor, and ε^{el} = total elastic strain [154].

The stress-strain relationship for isotropic linear elasticity is given as:

$$\begin{bmatrix}\varepsilon_{11}\\ \varepsilon_{22}\\ \varepsilon_{33}\\ \gamma_{12}\\ \gamma_{13}\\ \gamma_{23}\end{bmatrix} = \begin{bmatrix} 1/E & -\nu/E & -\nu/E & 0 & 0 & 0\\ -\nu/E & 1/E & -\nu/E & 0 & 0 & 0\\ -\nu/E & -\nu/E & 1/E & 0 & 0 & 0\\ 0 & 0 & 0 & 1/G & 0 & 0\\ 0 & 0 & 0 & 0 & 1/G & 0\\ 0 & 0 & 0 & 0 & 0 & 1/G \end{bmatrix}\begin{bmatrix}\sigma_{11}\\ \sigma_{22}\\ \sigma_{33}\\ \sigma_{12}\\ \sigma_{13}\\ \sigma_{23}\end{bmatrix} \tag{5.2}$$

The shear modulus, G, can be calculated using $G = E / (2 (1+v))$, where E is the modulus of elasticity and v is the Poisson's ratio. Here, the elastic properties used in the model for the flax-based composite were obtained from the experimental data discussed in Chapter 4.

5.2.1.2 Plasticity

Plastic behaviour occurs after a material has been permanently deformed beyond its yield point. Once the yield surface changes size uniformly in every direction, isotropic hardening occurs. During this stage, the applied load will produce a plastic strain, ε_{pl}, and the yield stress will increase or decrease in all directions of stress. Here, the material was developed using a classical plasticity model, based on a von Mises yield surface. To determine the values of isotropic hardening, the yield stress, σ_y, is given as a tabular function of the plastic strain. The interpolation of the yield stress at any value of plastic strain is generated from the data table until it reaches the last value given in the table (in Abaqus software) [151].

The decomposition of the total increment of strain can be expressed as:

$$\varepsilon_{pl} = \varepsilon_{total} - \frac{\sigma_{total}}{E}, \sigma > \sigma_y \tag{5.3}$$

whereσ_y is the initial yield stress.

5.2.1.3 Failure Criteria

Many theories have been proposed for failure criteria corresponding to the various types of failure that are observed. Generally, failures in structure are caused by material degradation due to the fracture, crack propagation and coalescence micro-cracks/voids in a 'real-life' material element. Here, damage initiation in the flax-based composite interlocking structures was modelled using a ductile damage criterion (for both quasi-static and dynamic loading conditions). The equivalent fracture strain was used as a measure of failure to predict the onset of damage.

The equivalent plastic strain at the beginning of damage, $\bar{\varepsilon}_{\mathrm{D}}^{pl}$, is a function of the stress triaxiality, η , and strain-rate, $\dot{\bar{\varepsilon}}^{pl}$:

$$\eta = -\frac{\mathrm{p}}{\mathrm{q}} \tag{5.4}$$

where q is the von Mises equivalent stress and p is the pressure stress which is defined as:

$$\mathrm{p} = \frac{1}{3}(\sigma_1 + \sigma_2 + \sigma_3) \tag{5.5}$$

Failure associated with this ductile criterion activates once the following condition is fulfilled:

$$\omega_{\mathrm{D}} = \int \frac{\mathrm{d}\bar{\varepsilon}^{pl}}{\bar{\varepsilon}_{\mathrm{D}}^{pl}(\eta, \dot{\bar{\varepsilon}}^{pl})} = 1 \tag{5.6}$$

whereω_{D} is a state variable that increases with plastic deformation. During the analysis, the incremental increase in ω_{D} at each increment is computed as:

$$\Delta\omega_{\mathrm{D}} = \frac{\Delta\bar{\varepsilon}^{pl}}{\bar{\varepsilon}_{\mathrm{D}}^{pl}(\eta, \dot{\bar{\varepsilon}}^{pl})} \geq 0 \tag{5.7}$$

Damage development, associated with ductile deformation, was controlled by the fracture energy, in terms of the energy required for failure development, which is in the form of:

$$\sigma = (1 - D)\bar{\sigma} \tag{5.8}$$

where$D$ is the overall damage variable and $\bar{\sigma}$ is the yield stress at a non-zero plastic strain-rate. A linear softening law was used, specifying a linear relationship between the softening stress and the displacement after the onset of damage for elasto-plastic materials.

5.2.2 Material Properties

The materialsinvestigated in this study were the flax-based composites. Here, the mechanical properties of the flax-based composite were taken from the experimental results presented in Chapter 4. In a finite element analysis, the elastic properties of a material are defined via the Young's Modulus and Poisson's ratio. Here, the Poisson's ratio was set to 0.3 for both flax/PP and flax/PLA composites. The plastic behaviour was taken from the engineering stress – strain relationship, as shown inFigure 5.1 (corresponding to Figure 4.1). Table 5.1 and Table 5.2 summarise the elastic properties and ductile damage behaviour of the flax-based composite used in the FE analysis. Thevalues arecalculated using formula in section 5.2.1.1 to 5.2.1.3, which is taken from the stress – strain relationship (Figure 5.1).

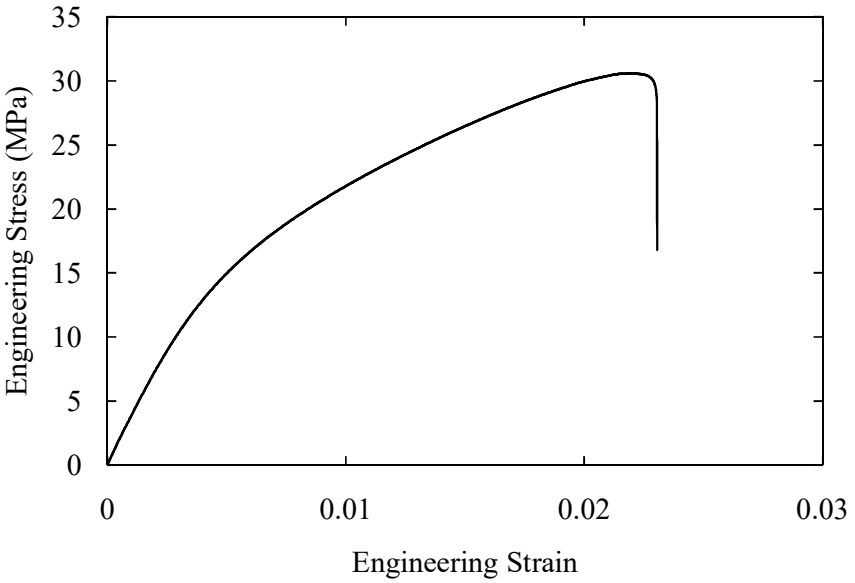

(a)

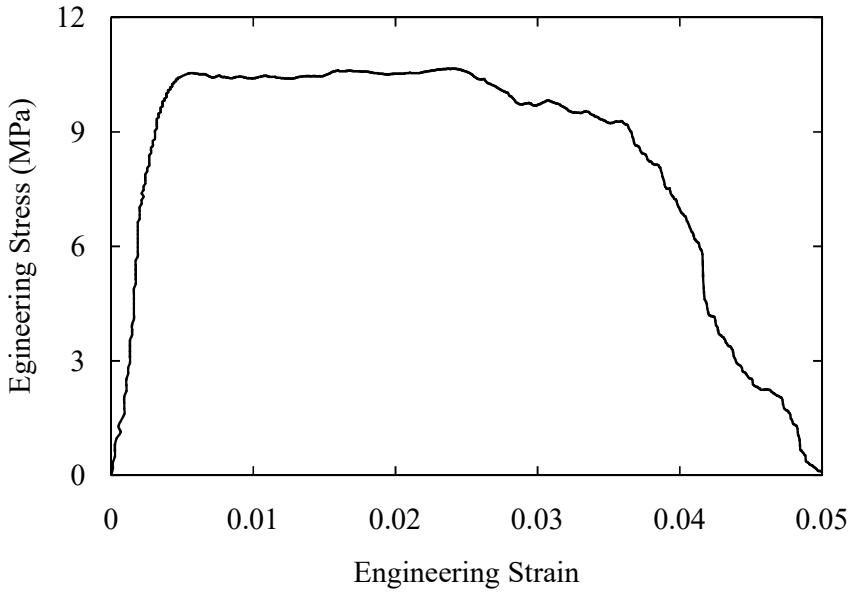

(b)

Figure 5.1. Typical engineering stress vs engineering strain curves for (a) the flax/PP and (b) the flax/PLA composite.

Table 5.1. Summary of the elastic properties of the flax-based composite.

Material	Density (kg/m^3)	Young's Modulus (GPa)	Poisson's Ratio
Flax/PP	800	3.7	0.3
Flax/PLA	1000	2.8	0.3

Table 5.2. Summary of ductile damage behaviour of the flax-based composite.

Flax/PP	Fracture strain	0.022
	Stress triaxiality	2.25
	Quasi-static Strain rate (s^{-1})	0.0001
	Dynamic Strain rate (s^{-1})	190
	Fracture energy (J/m^2)	5000
Flax/PLA	Fracture strain	0.05
	Stress triaxiality	2.25
	Quasi-static Strain rate (s^{-1})	0.0001
	Dynamic Strain rate (s^{-1})	137
	Fracture energy (J/m^2)	9000

5.2.3 Quasi – Static Finite Element Modelling

5.2.3.1 Model Assembly, Loading and Boundary Conditions

Figure 5.2 shows the configuration adopted for the static compression model of a square interlocking sandwich structure. Also included are the boundary conditions applied in the model. In this simulation, the bottom surface of the lower platen was fully constrained. Therefore the displacement, U, and the rotational displacement, UR, were set to zero. In contrast, the top platen was free to move in the y-direction (U_y). This allowed the top platen to move downwards at a constant rate in order to progressively crush the structure. A reference point was placed at the centre of the top platen surface. The reference point was used to record the displacement and the reaction force of the structure through the contact pair between the sandwich top skin and the top platen. A similar method was also adopted to model the triangular interlocking structure. Details of the model dimensions for both types of interlocking core structures are presented inFigure 5.3 and Table 5.3.

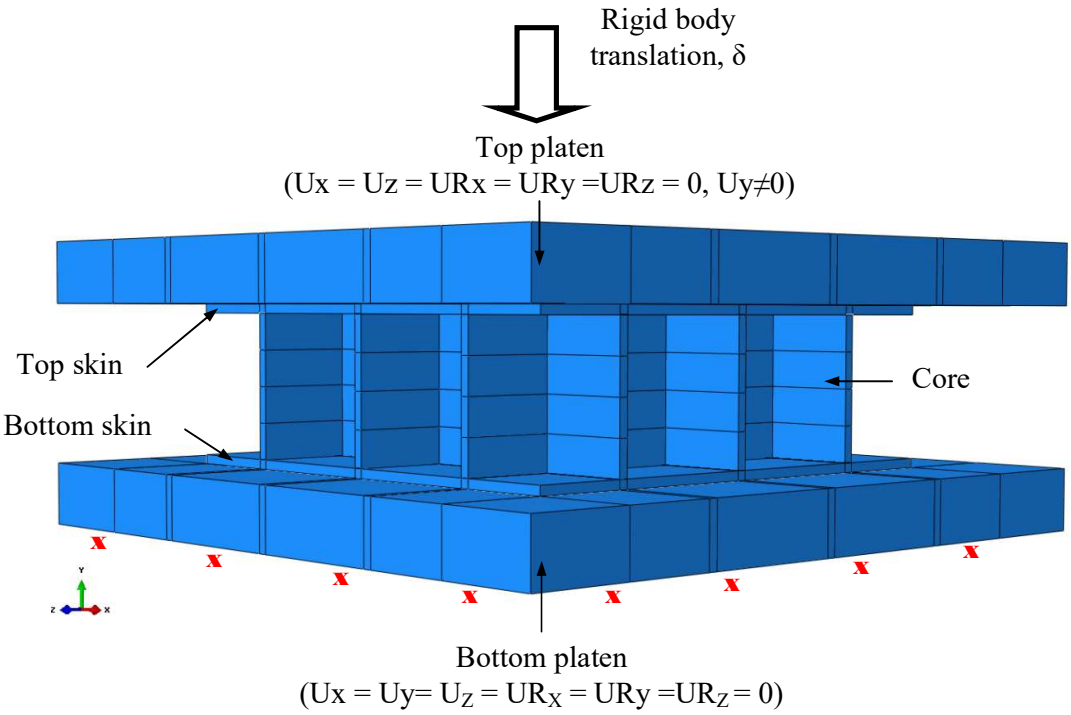

Figure 5.2. The assembly, loading and boundary conditions applied to the square interlocking structure model.

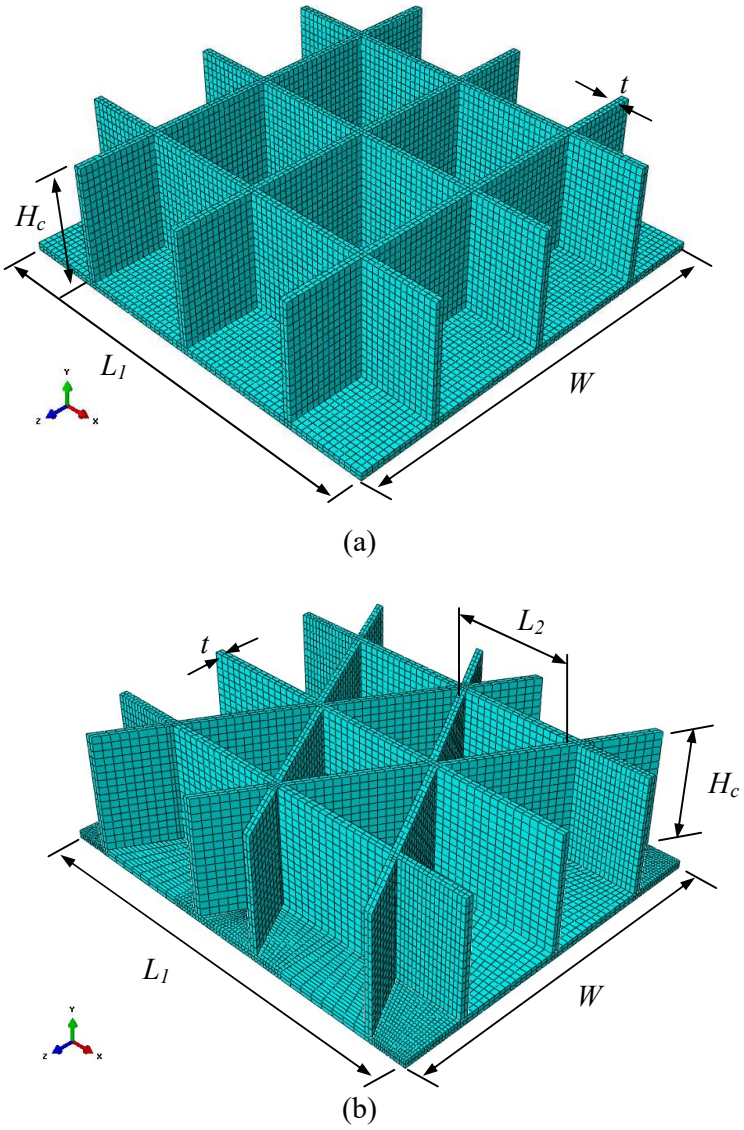

Figure 5.3. FE mesh for the sandwich cores showing the lower skin, (a) square core and (b) triangular core.

Table 5.3. Summary of the dimensions to model the interlocking core structure.

	Core Height (H_c)	Length (L_1)	Length (L_2)	Width (W)	Thickness (t)
Square	20	70	20	70	1.5
Triangular	20	70	20	60	1.3

Unit: mm

5.2.3.2 Element Types

A linear eight-node brick (C3D8R) element was used in modelling the response of the interlocking sandwich structure under quasi-static compression loading. The C3D8R element is a continuum element with reduced integration. Fewer number of Gaussian co-ordinates was used in the reduced integration elements when solving the integral. In general, accurate results can be obtained if using more Gaussion co-ordinates, but this will weighed up the cost of computation time. Reduced integration elements in the first order of 8-node brick element is using only one integration point. Therefore, this could lead to an excessively flexible hourglassing, so, the hourglassing has to be properly controlled.

5.2.3.3 Mesh Generation

The meshing tools in Abaqus/CAE were used to generate the mesh in the interlocking structure (Figure 5.3). Smith *et al*. [96] reported that the element size in every unit cell size should be the same. Ensure that the combination of material property and element size is consistent throughout the study. It is known that the element size will have an effect on the CPU time. Too large elements can leads to a higher stress, whereas a finer mesh can use too much memory and is time consuming. The mesh-sensitivity study was performed by running the analysis with various size of element and stopped until there was no significant change in stress. Here, the element size used for both square and triangular core interlocking models

were sixteen elements along the vertical y-axis and two elements through the thickness.

The total number of elements used in the models were 14076 and 42073 for the square and triangular interlocking sandwich structures, respectively. Both models were simulated usingelements with reduced integration and hourglass control. Hourglass control was selected as a default control, which is available for the C3D8R element.

5.2.3.4 Interaction Properties

Two types of interaction were applied in this interlocking model, these being general contact and surface-to-surface contact. The interlocking model structure used general contact, while a surface-to-surface contact was applied between the platen and the structure. In Abaqus/Explicit, a general contact law allows users to define the contact over multiple or all regions with a single interaction. On the other hand, the surface-to-surface contact is more restrictive and requires more careful selection of the contact condition. Such contact interactions can be defined in the contact properties. A hard contact pressure-overclosure under normal behaviour and a penalty formulation to account for tangential behaviour were set as the contact properties.

The penalty formulation was achieved using the basic Coulomb friction model. This model assumes that no relative sliding occurs if the equivalent frictional stress is less than the criticalstress:

$$\tau_{eq} = \sqrt{\tau_1^2 + \tau_2^2} \tag{5.9}$$

The critical stress is defined as:

$$\tau_{crit} = \mu p \tag{5.10}$$

whereμ is the coefficient of friction and p is the contact pressure between the two surfaces. The penalty formulation is based on the friction coefficient, where it become "frictionless" if the value is zero [151].

The hard contact relationship can minimise the penetration of the slave surface (the structure) into the master surface (the platen) at the constraint locations. It also restrains the transition of the tension stresses across the interface. This contact creates a pressure when the two surfaces become in contact. Conversely, there is no pressure if the clearance is greater than zero. This can be clearly seen in Figure 5.4. Finally, the upper and lower surface of the interlocking core were tied to the skins.

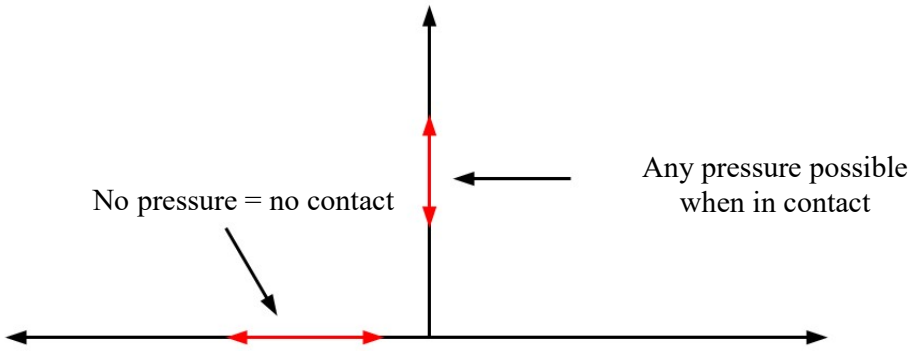

Figure 5.4. The hard contact pressure-overclosure relationship [151].

5.2.3.5 Modelling Data Output

The output from the FE models can be specified by creating the output requests. Large amounts of output data can be requested during a finite element analysis. The results data can be managed by selecting the required data to be interpreted, as Abaqus will calculate the values of many variables at every step. This selected data can be chosen for specific regions, intergration points or reference points and the rate at which it is recorded can also be defined. There are two types of output request, these being field output and history output.

Field outputs are generated from data that is spatially distributed over the whole model or over a portion of it. Here, the output presents images of the specimen at each requested interval. The amount of field output data during analysis is often large and therefore a low rate is recommended for field data to be written to the output database.

History outputs are generated either from the whole model or specific points of the model at a high frequency. An individual component of the variables can also be specified when creating the history output request. In this numerical analysis, the reaction forces and displacement along the relevant directions of the rigid platen and the corresponding interaction force are requested at specific reference points and through the contact pair using the history output.

5.2.3.6 Geometric Imperfection

In most manufacturing processes, it is commonfor the occurrenceof theformation ofsmalldefects or known as imperfection. Such flaws can be associated with many factors, such as an existence of voids during the process of compression moulding, inconsistency of the wall thickness as well as the local variations in the fibre volume fraction. In general, the FE models do not include these structural imperfections in the simulation. Hence, an over-estimation of the peak load and stiffness of the whole structure can occur. A study on imperfections in numerical models has been successfully carried out in previous work. Côté*et al*. [36] and Kazemahvazi and Zenkert [38] introduced an imperfection into their model in order to accurately predict the load-displacement traces of a structure.

In this study, due to the thin nature of the interlocking cells, the composite exhibits buckling before the core finally collapses. Therefore, the geometrical imperfection pattern was included into the model to accurately predict the collapse behaviour of the interlocking core structure. The geometric imperfection pattern is defined as a linear superposition of buckling eigenmodes obtained from a previous eigenvalue buckling prediction performed with Abaqus/Standard [151]. This was conducted using the *IMPERFECTION function in a linear perturbation step in

Abaqus/Standard. The buckling modes were predicted and used to introduce a small imperfection in the straightness of the vertical cell members. The interlocking structure core could then be loaded in the same manner as in the test.

Here, the imperfection takes the form:

$$\Delta x_i = \sum_{i=1}^{M} w_i \phi_i \tag{5.11}$$

whereϕ_i is the *i*th mode shape and w_i is the associated scale factor.

The simplest buckling mode (Mode I) was used to perturb the mesh and the scale factor used was 5% of the web thickness. The geometric imperfection, in terms of the buckling modes, was then imported into the Abaqus/Explicit analysis. The reason for using such an analysis is to make the ductile failure more effective, which is associated with postbuckling of the core cells. The appropriate time duration in the explicit analysis was determined through a series of numerical runs with different durations, until there was no significant dynamic effect. Using this approach, the time duration was set to 0.1 second.

5.2.4 Dynamic Finite Element Modelling

5.2.4.1 Model Assembly and Element Types

The impact response of the flax-based interlocking structure was modelled by considering a square core section. This is due to there being little difference in the strength properties of the square and triangular structures in the compression tests presented in Chapter 4. The geometry of the unit cells in the dynamic models was similar to the quasi-static analysis (Figure 5.2). Here, a dynamic analysis was conducted using eight-noded linear continuum elements with reduced intergration and hourglass control (C3D8R), similar to that used in the quasi-static analysis. Hence, the element size was also the same. The geometrical imperfection also applied in the dynamic modelling structure.

5.2.4.2 Loading, Boundary Conditions and Interaction Properties

In the dynamic FE model, the bottom platen remained fully constrained, while the top platen was subjected to an instantaneous velocity. The top rigid platen with a mass of 10.5 kg, located above the interlocking structure with a 3 mm offset, was used to represent the drop-weight carriage. Here, a small gap was used to avoid any unnecessary over-closure between the top platen and structure at the beginning of the simulation.

The translation of the rigid top platen, U_y, was changed to an initial velocity and a mass was specified at the reference point located on the top platen. The reference point was also used to record the displacement, whereas the contact pair between the top platen and the structure was used to record the interaction force. A general contact algorithm was used for the interlocking structure model. Contact between the platen and the structure model was defined as surface-to-surface contact. The interaction properties were set to 'hard' in the normal direction and a friction coefficient of 0.1 was assumed in the tangential direction. The upper and lower surfaces of the interlocking core were tied to the skins. The bottom surface of the platen was fixed to restrain the lower platen from any movement.

5.2.4.3 Material Properties

Here, the material model used in the dynamic analysis is isotropic elasto-plasticity with rate-dependant hardening. The input data for the material properties of the flax-based composite model are described in Sections 5.2.1 and 5.2.2.

A rate-dependent plasticity model was applied in this dynamic analysis, based on a scaling function. The rate-dependent hardening curve in terms of the static relation can be expressed as [151,152]:

$$\sigma_D(\bar{\varepsilon}^{pl}, \dot{\bar{\varepsilon}}^{pl}) = \sigma_S(\bar{\varepsilon}^{pl})R(\dot{\bar{\varepsilon}}^{pl}) \tag{5.12}$$

where R is a yield stress ratio between the dynamic and static strengths.

The equivalent plastic, $\bar{\varepsilon}^{pl}$, calculated from:

$$\bar{\varepsilon}^{pl} = \int_0^t \frac{2}{3}\dot{\varepsilon}^{pl} : \dot{\varepsilon}^{pl} dt \tag{5.13}$$

$$R = \frac{\sigma_D}{\sigma_S} \tag{5.14}$$

Rate-dependent yield in the dynamic models was used to define the material yield behaviour when the yield strength depends on the applied strain-rate. The yield stress ratios for the flax-based composites used in dynamic modelling are shown in Table 5.4.

Table 5.4. Summary of rate-dependent of hardening yield ratio for the flax-based composite used in dynamic compression modelling.

Flax/PP	Yield stress ratio (R)	1	1.01	1.09	1.1
	Equivalent strain (1/s)	0	90	150	190
Flax/PLA	Yield stress ratio (R)	1	1.001	1.003	1.005
	Equivalent strain (1/s)	0	40	65	137

5.3 Results from the Finite Element Simulations

5.3.1 Quasi – Static Compression

Figure 5.5 shows comparisons of experimental and numerical load-displacement traces for the square and triangular cores based on the flax/PP and flax/PLA composite. In general, correlation between the experimental and numerical data is very good, with all of the main features being captured, including the initial stiffness, peak load, initial failure, plateau and densification stages. The predicted peak loads for both cores are similar, with a very good agreement in the softening and subsequent plateau stages. The finite element model predicts the onset of densification at a slightly later stage in the loading regime for the flax/PP triangular core, also such the predictions for both the square and triangular flax/PLA cores are over-estimated at a later stage. This may be due to perfect bonding between the core and skins being assumed in the model. It is observed that there are wavy lines for the flax/PP coresunder the densification stage. This could be due to the underestimated fracture energy in the failed elements. In addition, the stress level related to strain hardening for the material properties in densification stage were not considered. It is suggests that energy absorption up to densification can be reasonably predicted using the FE models.

The progressive failure modes predicted by the finite element models were compared with those observed experimentally. Figure 5.6 compares the predictions offered by the model with the test specimens subjected to various levels of deformation. Clearly, the basic characteristics of the experimental failure modes are captured by the model, in which buckling of the vertical members and their final collapse is evident. The progressive failure modes predicted in the triangular flax/PP core are shown in Figure 5.7. Again, the basic features observed experimentally are reproduced by the finite element simulations.

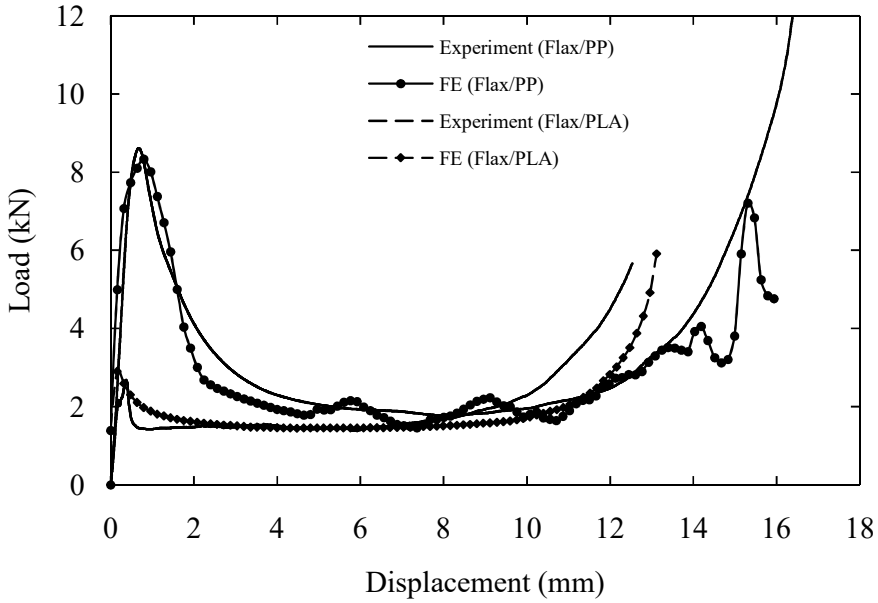

(a) square cores

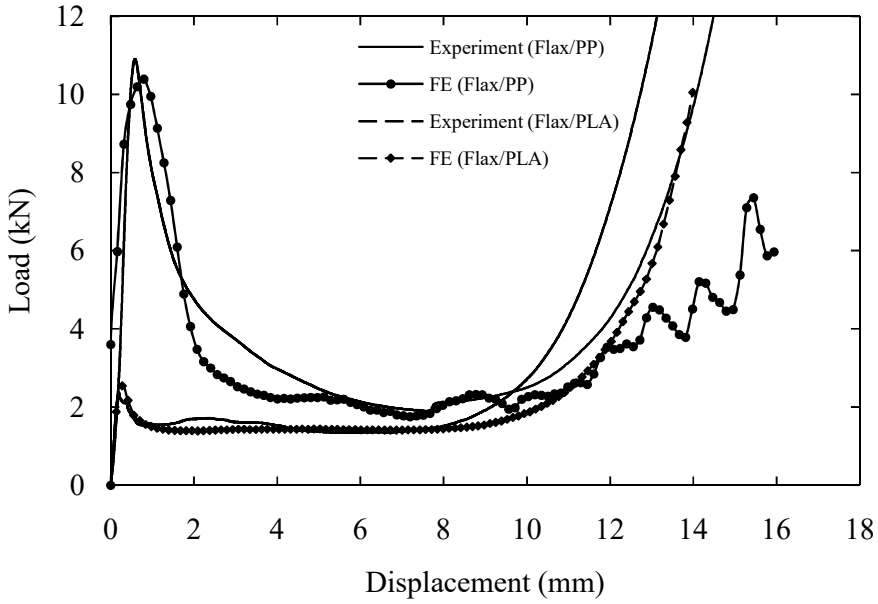

(b) triangular cores

Figure 5.5. Load-displacement traces from the experimental tests and the finite element simulations for (a) the square cores (flax/PP and flax/PLA) and (b) the triangular cores (flax/PP and flax/PLA).

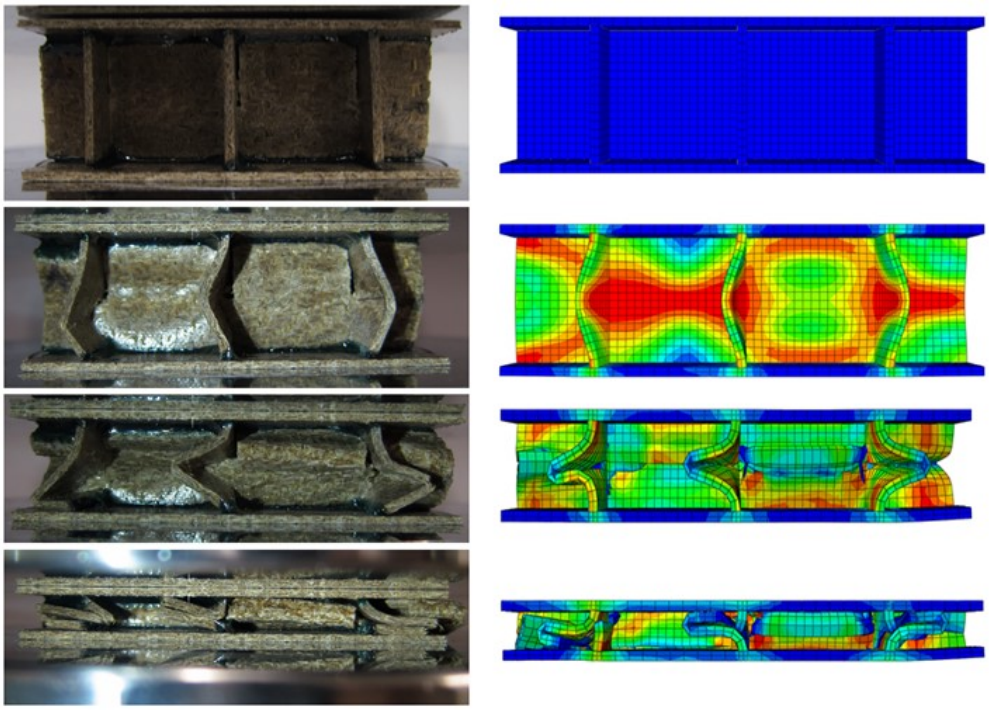

Figure 5.6. Progressive failure modes following testing and modelling for the square interlocking flax/PP with a web thickness = 1.5 mm and a relative density = 0.15.

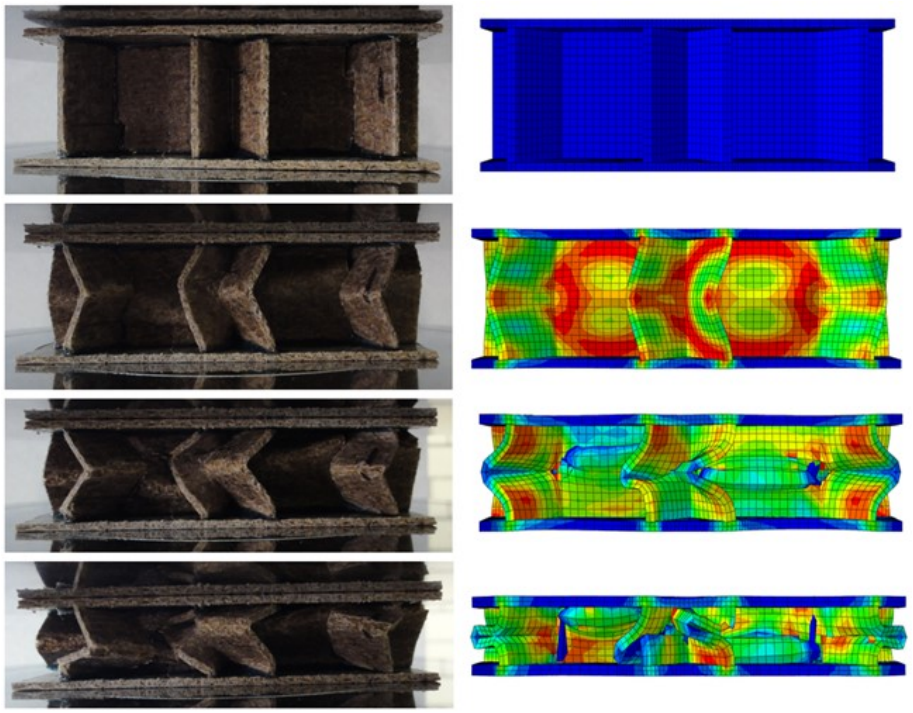

Figure 5.7. Sequencial images showing failure modes in the triangular core flax/PP with a web thickness = 1.5 mm and a relative density = 0.26.

The buckling modes occurring during the early stages of failure were also investigated. Figure 5.8 highlights the modes in both the square and triangular flax/PP cores for the case where the vertical displacement is approximately 2 mm. The FE images provide an insight into the buckling characteristics during the initial loading process, highlighting the onset of core buckling in these structures. In order to obtain a better understanding of the failure modes inside the core, the top skin was removed from the finite element models. Figure 5.9 shows the final crush state in the cores for both the square and triangular designs. It can be clearly seen that all of the vertical members have completely buckled and in some cases fully fractured.

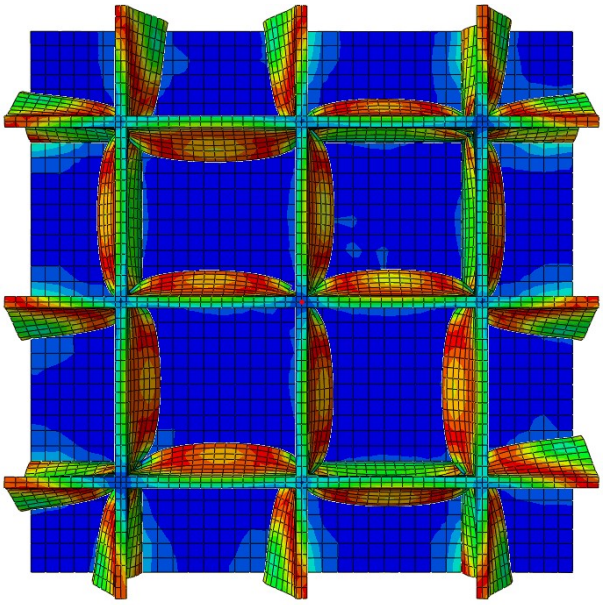

(a) square,

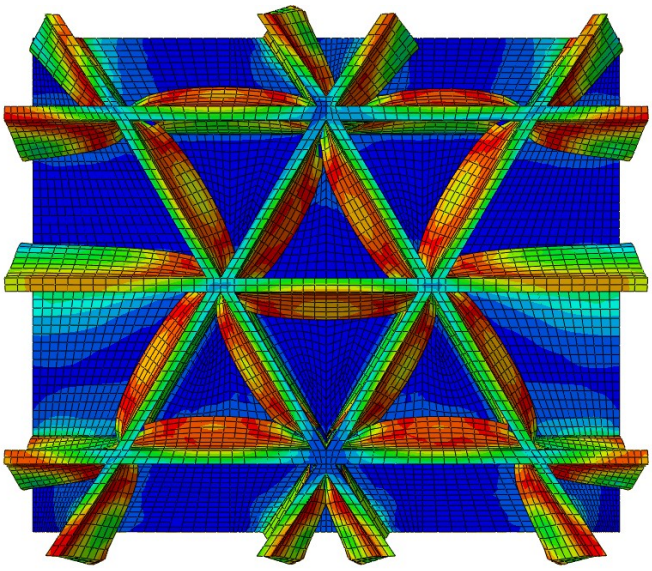

(b) triangular

Figure 5.8. Buckling modes for the flax/PP cores corresponding to a vertical displacement of 2 mm, (a) square core and (b) triangular core.

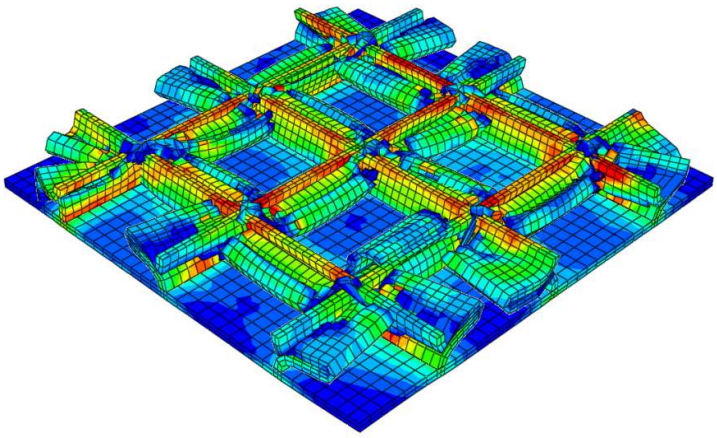

(a) square,

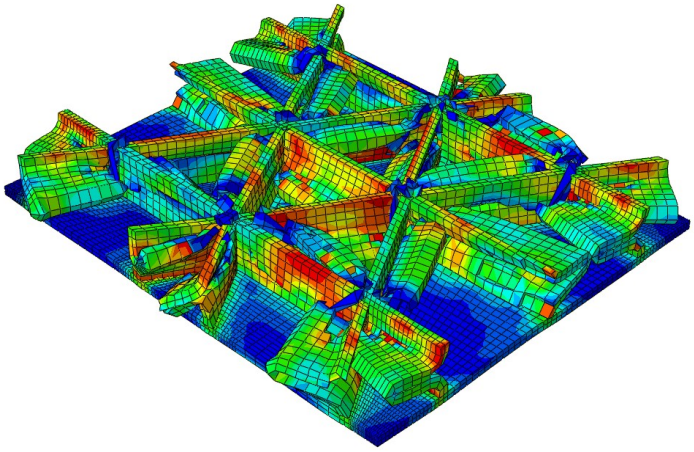

(b) triangular

Figure 5.9. The predicted profiles of the crushed flax/PP cores, (a) square and (b) triangular.

5.3.2 Dynamic Compression

The FE model tested under dynamic loading was simulated on the square interlocking cores. In the impact simulations, the striker mass, M,and the initial velocity assigned to the top platen were based on the experimental work.

In general, an examination of the predicted responses for the flax/PP and flax/PLA cores in Figure 5.10 indicates reasonable agreement with the corresponding experimental measurements. This level of agreement includes the initial stiffness, the peak load and the subsequent buckling behaviour. Beyond the peak load, the predicted load-displacement traces show similar trends to the experimental data. It is observed that the FE models give a prediction of a smoother response, due to the assumption of perfect contact between the platens and the structure. In contrast, the experimental response exhibits an oscillatory response, due to ringing effects in the load cell. The assumption of perfect contact also has an effect on the stiffness of the structure, where the FE has slightly over-estimate the measured stiffness. The predicted peak load is higher than the experimental peak load by about 15%.

The FE model for the flax/PLA core exhibits a reasonable load-displacement response compared with the experimental results. However, it is observed that the peak load and the onset of densification are slightly over-estimated, as for the quasi-static model. It should be noted that delamination between the vertical webs that might occur due to the loss of matrix during the manufacturing process was not taken into consideration. In this study, the model was assumed to fail in a buckling mode and this might cause the peak load and onset densification to be over-estimated.In addition, the perfect bonding also plays some role in the model. Therefore, the onset of densification has been over-estimated, which also affected the value for the energy-absorbing capability. Here, the predicted load is about 25% higher than the experimental peak load.

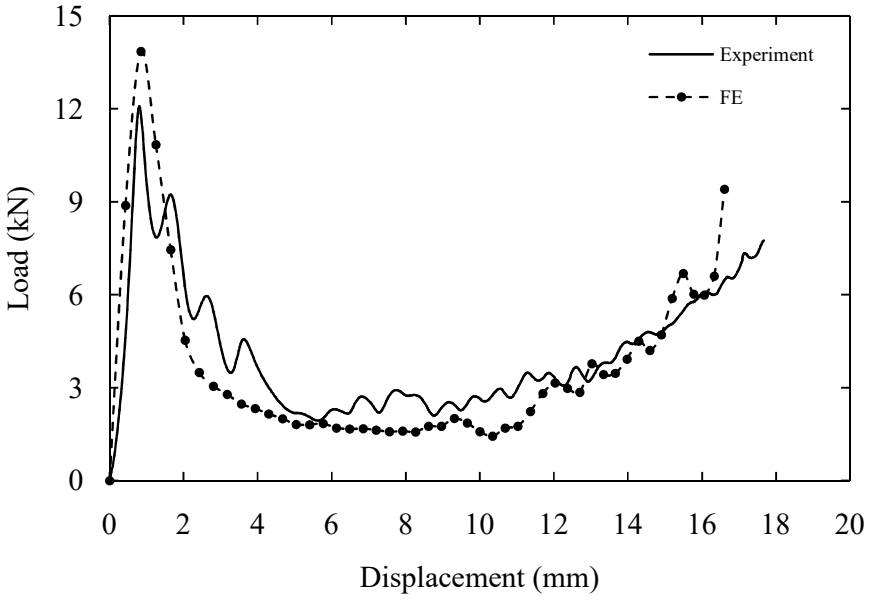

(a)

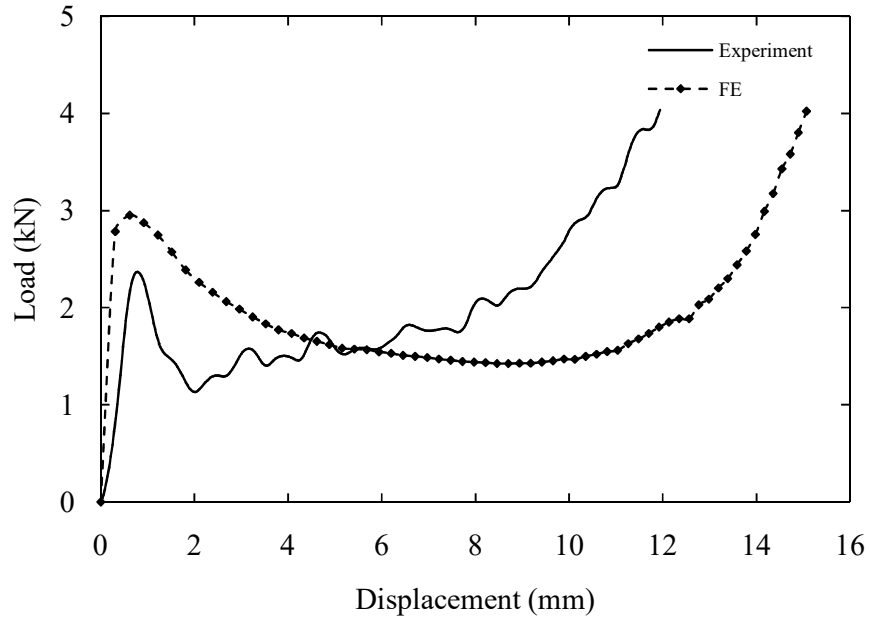

(b)

Figure 5.10. Comparison of the experimental and FE load-displacement traces for (a) flax/PP and (b) flax/PLA structures.

It is known that a finite element analysis (FEA) is dependent on the accuracy of the input parameters, such as the mechanical properties, constraints and loading condition. It is difficult to obtain accurate mechanical properties of natural fibre due to its complexity and variety in nature. Given that both the PP and PLA based composites were manufactured using a similar pressure and pressing time, but with different temperatures, this could also affect the matrix properties of both composites. Gamstedt and Almgren [155] stated that the mechanical properties of natural fibres could be affected by temperature, moisture content, strain-rate, etc. It also should be noted that due to manufacturing defects, the mechanical properties in the experimental work for each strip in the interlocking core could be different and may affect the properties of the structure. Based on the dynamic response, the specific energy absorption results for FE simulation were 4.46 kJ/kg for the flax/PP and 2.22 kJ/kg for the flax/PLA. A close examination of the flax/PP structure shows that the predicted SEA value is lower than the experimental value by approximately 14%, but higher for the flax/PLA structure by over 40%. Figure 5.11 presents the final crushed flax/PP core with the corresponding FE model. Similar to that observed in quasi-static model, the failure in the dynamic model also shows clear basic features produced experimentally.

(a) experiment,

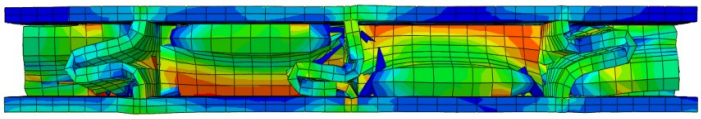

(b) FE model

Figure 5.11. Final crushed failure of flax/PP cores.

5.4 Interim Conclusions

Table 5.5. Comparison of the predicted FE and experimental results following quasi-static tests on the square and triangular interlocking structures.

Material and Core Structure	Experiment, P_{max} (kN)	FE, P_{max} (kN)	Percentage difference (%)	Experiment, SEA(kJ/kg)	FE, SEA(kJ/kg)	Percentage difference (%)
Flax/PP (square)	8.62	8.34	+3.24	3.34	3.26	+2.32
Flax/PP (triangular)	10.90	10.39	+4.72	3.34	3.24	+2.99
Flax/PLA (square)	2.69	2.83	-5.27	1.51	1.88	-24.75
Flax/PLA (triangular)	2.38	2.54	-6.66	1.20	1.30	-8.52

Table 5.6. Comparison of the predicted FE and experimental results following dynamic tests on square interlocking structures.

Material	Experiment, P_{max} (kN)	FE, P_{max} (kN)	Percentage difference (%)	Experiment, SEA(kJ/kg)	FE, SEA(kJ/kg)	Percentage difference (%)
Flax/PP	12.08	13.86	-14.65	5.21	4.46	+14.29
Flax/PLA	2.37	2.95	-24.74	1.50	2.22	-47.62

Finite element models have been developed in order to predict the behaviour of the flax-based composite interlocking structures. The simulations were carried out under quasi-static and dynamic loading conditions. The composite was modelled as an elasto-plastic material witha ductile damage failure criterion. Both the quasi-static and dynamic models were designed in Abaqus/Explicit using C3D8R elements. Due to the thin nature of the vertical web, a geometric imperfection was implemented in the simulation in order to effectively predict the experimental results. This imperfection was simulated in Abaqus/Standard and was later exported to the Abaqus/Explicit. The results for both the quasi-static and dynamic FE predictions were presented and compared with the corresponding experimental results reported previously. In general, the numerical models show good agreement with the essential features of the experimental load-displacement traces. They are listed in Table 5.5 and Table 5.6, where a comparison is given between the FE simulations and experimental data following quasi-static and dynamic tests structures. Considering the results obtained from the experimental and FEA work, this simplified FE model could be used for other types of natural fibre in order to predict their peak force and energy absorption values.

CHAPTER 6 : CONCLUSIONS AND RECOMMENDATIONS

6.1 Conclusions of the Research Work

The aim of this study was to manufacture a range of sandwich structures made from natural fibre composite materials and to investigate their mechanical properties. Two main natural materials were investigated, these being bamboo tubes and flax-based composites. A range of quasi-static and dynamic tests were performed in order to evaluate the mechanical response, energy absorption and the failure modes in the structures. In addition, thefinite element analysis (FEA) has been used to predict the response of the sandwich structures subjected to different loading conditions, which is also validated against the corresponding experimental results. The numerical modelling study focused on interlocking structures, under both quasi-static and dynamic loading regimes. Based on the findings of this study, the following conclusions can be drawn:

- It was shown that the PP-based system was more sensitive to variations in manufacturing temperature. However, this composite did offer tensile properties that were significantly higher than those measured on the PLA-based system.Tests on individual bamboo tubes have shown that decreasing the diameter to thickness ratio (D/t) serves to increase the specific energy absorption (SEA) values of the tubes, under both quasi-static and dynamic loading conditions. Failure in the large diameter tubes was predominantly associated with a bulging and a splitting mode, whereas failure in the smaller diameter tubes involved greater amounts of crushing and splaying, the mechanisms related to absorbing greater levels of energy. Further investigation on the influence of the triggering system used in the larger bamboo tube was also carried out. It has shown that the chamfer profile successfully triggers the tube to exhibit progressive failure during the initial stages. Similar to the tests on the unchamfered large tubes, the failure modes for the chamfered tubes involved a splitting mode under quasi-static loading conditions.

- The compression strength of bamboo honeycomb structures based on flax/PP and flax/PLA skins has shown that the small diameter bamboo cores have out-performed the large diameter cores. The resulting SEA values of both bamboo cores exhibit more than 20 kJ/kg under static and dynamic loading conditions, with a PLA-based system containing large diameter bamboo tubes offering the highest overall value. These energy-absorbing properties compare favourably with those recorded elsewhere on environmentally-friendly energy-absorbing systems. Interestingly, these bamboo-based honeycombs have indicated a great potential for use in engineering applications as energy absorbing structures.

- There is no significant difference in the specific energy absorption properties of the bamboo-foam structures, with all values averaging approximately at 17 kJ/kg. However, an estimation of the energy absorbed by the individual tubes was investigated by removing the contribution of the energy absorbed by the foam from the load-displacement traces of the bamboo-foam combination. As a result, the energy absorbed by the individual bamboo tubes increases as the foam density was increased. Hence, this has shown that higher density foams offer greater support to the tubes, where it has been successful in suppressing longitudinal failure as well as enhancing the specific energy absorption of the tube.

- The compression properties of the flax-based corrugated core increases as the number of cells was increased. Under both static and dynamic loading, the flax/PP corrugated core offers greater properties than its flax/PLA counterpart, in all cases. The specific energy absorption of the flax/PP core is greater than the flax/PLA core. Damage in the flax/PP core was predominantly associated with buckling and fibre fracture, whereas the flax/PLA core exhibited fibre micro-buckling and delamination.

- The compression characteristics of the PP-based interlocking honeycomb core were found to offer strength and energy-absorbing characteristics well in excess of those offered by the PLA-based cores. It is believed that the poorer mechanical response of the PLA-based structures is associated with the relatively low failure strain of the matrix material. Here, it was also shown that the compression strength and energy-absorbing characteristics of the square honeycomb cores were significantly greater than those of their triangular counterparts. Under dynamic loading, the PP-based structures offered a greater strength and energy-absorbing capability than that under quasi-static loading. In contrast, the PLA-based structures offer similar properties when tested under both quasi-static and dynamic loadings. The PP-based core was observed to fail in a buckling mode followed by the fibre fracture, while the PLA-based core failed in delamination and localised buckling. Both types of flax-based composite show an increase in mechanical properties, as the wall thickness of the core is increased, thus, offering greater energy-absorbing capability than the thin wall thicknesses.

- The results for the corrugated paperboard with flax-based composite skins indicate no significant difference in the strength properties, even though the flax/PLA value is slightly higher than the flax/PP. An approximate 20% difference in energy-absorbing capacity in both skins was observed, which is associated with the onset of densification and due to the inconsistency of a number of corrugated cells in the core, following the cutting processes. The higher value of specific energy absorption observed under dynamic loading is associated with the time required to generate the folded cell walls. These environmentally-friendly structures are found to have potential to be used in low-end engineering applications, such as in the packaging industry.

- The compression response of the square and triangular honeycomb structures have been successfully modelled using the finite element analysis (FEA) techniques. The simulation was carried out under both quasi-static and dynamic loading conditions. Due to there being little difference in the compression strengths of the square and triangular cores, the dynamic compression response was simulated only on square cores. In general, the numerical models exhibit reasonably good correlation, in terms of the essential features of the experimental load-displacement responses. Other types of natural fibre based composite can be simulated using this simplified model to predict their peak load and energy-absorbing characteristics.

Finally, it is believed that this study can help increase the use of natural fibres in sandwich structures. Some of these environmentally-friendly structures can offer good mechanical properties and potential for use in engineering applications as energy-absorbing structures. In addition, the use of natural materials gives some added-value to this environmentally-friendly sandwich structure.

6.2 Recommendations for Future Work

The growing awareness of environmental issues has led to a large number of studies on the use of natural fibre composites in green engineering applications. The mechanical properties offered by natural fibres is no longer debatable and these materials offer a great potential. Therefore, in order to transform this so-called "waste" material into a useful composite material, some recommendation for future work are given below:

- Further investigations should be carried out to fully characterise the behaviour of these natural fibre-based structures under bending and torsion as well as under fatigue loading conditions.

- Investigations on the mechanical properties of sandwich structure mades from different natural fibre materials and/or a hybrid composite based on natural and synthetic fibres should be carried out. This would help to reduce the use of synthetic fibres in composite structures, but still offer improvements on mechanical properties.

- The FE analysis presented in this study was developed using a simple model. It would be more interesting if a more comprehensive study on this natural fibre-based structure is carried out. This approach would produce better and more comprehensive simulations to help design these kinds of structures.

REFERENCES

[1] Crupi V., Epasto G. and Guglielmino E. Low–velocity impact strength of sandwich materials, Journal of Sandwich Structures and Materials, 2010; 13: 409 – 426.

[2] Khan M.K. Compressive and lamination strength of honeycomb sandwich panels with strain energy calculation from ASTM standards, Proceedings of The Institution of Mechanical Engineers Part G-Journal of Aerospace Engineering, 2006;220: 375 – 386.

[3] Deshpande V.S. and Fleck N.A. Collapse of truss core sandwich beams in 3–point bending, International Journal of Solids and Structures, 2001; 38: 6275 – 6305.

[4] http://www.compositesworld.com/news/bayer-introduces-sandwich-structure-technology-for-automotive-body-panels.

[5] Herrmann A.S., Zahlen P.C. and Zuardy I. Sandwich structures technology in commercial aviation, Sandwich Structures 7: Advancing with Sandwich Structures and Materials, Springer, 2005: 13 – 16.

[6] Holbery J. and Houston D. Natural-fiber-reinforced polymer composites in automotive applications, Journal of the Minerals, Metals & Materials Society, 2006; 58: 80–6.

[7] Weager B. High-performance biocomposites: novel aligned natural fibrereinforcements, JEC Composites Magazine, 2010; 55: 36–7.

[8] http://greencorenfc.com/news.htm#20120801.

[9] Brouwer W.D. Natural fibre composites in structural components: Alternative applications for sisal?, Proceedings of a seminar held by the Food and Agriculture Organization of the UN (FAO) and the Common Fund for Commodities (CFC), 2000; Technical paper no. 14.

[10] Balakrishna A., Rao D.N. and Rakesh A.S. Characterization and modelling of process parameters on tensile strength of short and randomly oriented Borassus Flabellifer (Asian Palmyra) fiber reinforced composite, Composites: Part B, 2013; 55: 479 – 485.

[11] Saheb D.N. and Jog J.P. Natural fiber polymer composites: A review, Advance in Polymer Technology, 1999; 18: 351 – 363.

[12] http://www.cms.daimler.com/Projects/c2c/channel/documents/2091419_Environmental_Certificate_Mercedes_Benz_M_Class.pdf.

[13] http://www.cms.daimler.com/Projects/c2c/channel/documents/2003704_Environmental_Certificate_Mercedes_Benz_A_Class.pdf.

[14] Corradi S., Isidori T., Soleri F., Olivari L. and Corradi M. Composite boat hulls with bamboo natural fibers, International Journal of Materials and Product Technology, 2009; 36: 73 – 89.

[15] http://www.flaxland.co.uk/fabric%20boats.html.

[16] http://www.reinforcedplastics.com/view/26369/samsara-eco-surfboard-features-biotex-flax-fibre/.

[17] http://www.coolhunting.com/design/schwinn-flax-vestige.php.

[18] Ashby M.F. The properties of foams and lattices, Philosophical Transaction of the Royal Society A: Mathematical, Physical and Engineering Sciences, 2006; 364: 15 – 30.

[19] Gibson L.J. and Ashby M.F. Cellular Solids: Structure Properties, Cambridge University Press, 2nd Edition, Cambridge, UK; 1999.

[20] Wadley H.N.G. Multifunctional periodic cellular metals, Philosophical Transaction of the Royal Society A: Mathematical, Physical and Engineering Sciences, 2006; 364: 31 – 68.

[21] Liu P.S. and Chen G.F. Porous materials: Processing and applications, Butterworth-Heinemann, Oxford, UK; 2014.

[22] Ashby M.F., Evans A., Fleck N.A., Gibson L.J., Hutchinson J.W. and Wadley H.N.G. Metal foams: A design guide, Butterworth-Heinemann, Oxford, UK; 2000.

[23] Gong L., Kyriakides S. and Jang W.Y. Compressive response of open-cell foams. Part I: Morphology and elastic properties, International Journal of Solids and Structures, 2005; 42: 1355 – 1379.

[24] Saint-Michel F., Chazeau L. and Cavaillé J.Y. Mechanical properties of high density polyurethane foams: II Effect of the filler size, Composites Science and Technology, 2006; 66: 2709 – 2718.

[25] Ray S.S. Environmentally Friendly Polymer Nanocomposite: Types, Processing and Properties, Woodhead Publishing, Cambridge, UK; 2013.

[26] Banhart J. Manufacture, characterisation and application of cellular metals and metal foams, Progress in Materials Science, 2001; 46: 559 – 632.

[27] Huber O. and Klaus H. Cellular composites in lightweight sandwich applications, Materials Letters, 2009; 63: 1117 – 1120.

[28] Rubino V., Deshpande V.S. and Fleck N.A. The dynamic response of end-clamped sandwich beams with a Y-frame or corrugated core, International Journal of Impact Engineering, 2008; 35: 829 – 844.

[29] Kazemahvazi S. and Zenkert D. The compressive and shear responses of corrugated hierarchical and foam filled sandwich structures, 8th International Conference on Sandwich Structures (ICSS 8), Porto, 2008.

[30] Kazemahvazi S., Tanner D. and Zenkert D. Corrugated all-composite sandwich structures. Part 2: Failure mechanisms and experimental programme, Composites Science and Technology, 2009; 69: 920 – 925.

[31] Thill C., Etches J.A., Bond I.P., Potter K.D., Weaver P.M. and Wisnom M.R. Investigation of trapezoidal corrugated aramid/epoxy laminates under large tensile displacements transverse to the corrugation direction, Composites: Part A, 2010; 41: 168 – 176.

[32] Dharmasena K.P., Wadley H.N.G., Xue Z. and Hutchinson J.W. Mechanical response of metallic honeycomb sandwich panel structures to high-intensity dynamic loading, International Journal of Impact Engineering, 2008; 35: 1063 – 1074.

[33] Dharmasena K.P., Queheillalt D.T., Wadley H.N.G., Dudt P., Chen Y., Knight D., Evans A.G. and Deshpande V.S. Dynamic compression of metallic sandwich structures during planar impulsive loading in water, European Journal of Mechanics A/Solids, 2010; 29: 56 – 67.

[34] Russell B.P., Deshpande V.S. and Wadley H.N.G. Quasistatic deformation and failure modes of composite square honeycombs, Journal of Mechanics of Materials and Structures, 2008; 3: 1315 – 1340.

[35] Zhu F., Lu G., Ruan D. and Wang Z. Plastic deformation, failure and energy absorption of sandwich structures with metallic cellular cores, International Journal of Protective Structures, 2010; 1: 507 – 541.

[36] Côté F., Deshpande V.S., Fleck N.A. and Evans A.G. The compressive and shear responses of corrugated and diamond lattice materials, International Journal of Solids and Structures, 2006; 43: 6220 – 6242.

[37] Yan-Chang Z., Shi-lian Z. and Zi-li W. Crush behaviour of corrugated cores sandwich panels, Advanced Materials Research, 2011; 217–218: 1584 – 1589.

[38] Kazemahvazi S. and Zenkert D. Corrugated all-composite sandwich structures. Part 1: Modelling, Composites Science and Technology, 2009; 69: 913 – 919.

[39] Zhang J., Supernak P., Mueller-Alander S. and Wang C.H. Improving the bending strength and energy absorption of corrugated sandwich composite structure, Materials and Design, 2013; 52: 767 – 773.

[40] Petras A. and Sutcliffe M.P.F. Failure mode maps for honeycomb sandwich panels, Composite Structures, 1999; 44: 237 – 252.

[41] Abbadi A., Koutsawa Y., Carmasol A., Belouettar S. and Azari Z. Experimental and numerical characterization of honeycomb sandwich composite panels, Simulation Modelling Practice and Theory, 2009; 17: 1533 – 1547.

[42] Kaman M.O., Solmaz M.Y. and Turan K. Experimental and numerical analysis of critical buckling load of honeycomb sandwich panels, Journal of Composite Materials, 2010; 44: 2819 – 2831.

[43] Hou B., Zhao H., Pattofatto S., Liu J.G. and Li Y.L. Inertia effects on the progressive crushing of aluminium honeycombs under impact loading, International Journal of Solids and Structures, 2012; 49: 2754 – 2762.

[44] Côté F., Deshpande V.S., Fleck N.A. and Evans A.G. The out-of-plane compressive behaviour of metallic honeycombs, Materials Science and Engineering A, 2004; 380: 272 – 280.

[45] Chen J.C., Chen Y.C., Wu C.M. and Teng Y.A. Compression of honeycomb preform sandwich composites, 17th International Conference on Composite Materials (ICCM 17), Edinburgh, UK, 2009.

[46] Zheng J., Zhao L. and Fan H. Energy absorption mechanisms of hierarchical woven lattice composites, Composites: Part B, 2012; 43: 1516 – 1522.

[47] Hilbeth P.A.D. and Marcelo K.A. An application for polymeric foams, Second International Symposium on Solid Mechanics, Brazil, 2009.

[48] Ouellet S., Cronin D. and Worswick M. Compressive response of polymeric foams under quasi-static, medium and high strain rate conditions, Polymer Testing, 2006; 25: 731 – 743.

[49] Subhash G., Liu Q. and Gao X.L. Quasistatic and high strain rate uniaxial compressive response of polymeric structural foams, International Journal of Impact Engineering, 2006; 32: 1113 – 1126.

[50] Radford D.D., McShane G.J., Deshpande V.S. and Fleck N.A. Dynamic compressive response of stainless-steel square honeycombs, Journal of Applied Mechanics, 2007; 74: 658 – 667.

[51] Kazemahvazi S., Kiele J., Russel B., Deshpande V.S. and Zenkert D. Impact properties of corrugated composite sandwich cores, 9th International Conference on Sandwich Structures (ICSS 9), Pasadena, California, 2010.

[52] Russell B.P., Malcom A., Wadley H.N.G. and Deshpande V.S. Dynamic compressive response of composite corrugated cores, Journal of Mechanics of Materials and Structures, 2010; 5: 477 – 493.

[53] McShane G.J., Radford D.D., Deshpande V.S. and Fleck N.A. The response of clamped sandwich plates with lattice cores subjected to shock loading, European Journal of Mechanics – A/Solids, 2006; 25: 215 – 229.

[54] Li G. and Muthyala V.D. Impact characterization of sandwich structures with an integrated orthogrid stiffened syntactic foam core, Composites Science and Technology, 2008; 68: 2078 – 2084.

[55] Park S., Russell B.P., Deshpande V.S. and Fleck N.A. Dynamic compressive response of composite square honeycombs, Composites: Part A, 2012; 43: 527 – 536.

[56] Rathburn H.J., Radford D.D., Xue Z., He M.Y., Yang J., Deshpande V.S., Fleck N.A., Hutchinson J.W., Zok F.W. and Evans A.G. Performance of metallic honeycomb-core sandwich beams under shock loading, International Journal of Solids and Structures, 2006; 43: 1746 – 1763.

[57] Velmurugan R. and Manikandan V. Mechanical properties of glass/Palmyra fiber waste sandwich composites, Indian Journal of Engineering and Materials Sciences, 2005; 12: 563 – 570.

[58] Wambua P., Vangrimde B., Lomov S. and Verpoest I. The response of natural fibre composites to ballistic impact by fragment simulating projectiles, Composite Structures, 2007; 77: 232 – 240.

[59] Ali M. Natural fibres as construction materials, 11th International Conference on Non-conventional Materials and Technologies (NOCMAT 2009), Bath, UK, 2009.

[60] Akil H.M., De Rosa I.M., Santulli C. and Sarasini F. Flexural behaviour of pultruded jute/glass and kenaf/glass hybrid composites monitored using acoustic emission, Materials Science and Engineering A, 2010; 527: 2942 – 2950.

[61] Cerqueira E.F., Baptista C.A.R.P. and Mulinari D.R. Mechanical behaviour of polypropylene reinforced sugarcane bagasse fibers composites, Procedia Engineering, 2011; 10: 2046 – 2051.

[62] Bledzki A.K. and Gassan J. Composites reinforced with cellulose based fibres, Progress in Polymer Science, 1999; 24: 221 – 274.

[63] Merta I. and Tschegg E.K. Fracture energy of natural fibre reinforced concrete, Construction and Building Matertials, 2013; 40: 991 – 997.

[64] Sui G.X., Yu T.X., Kim J.K. and Zhou B.L. Static mechanical behavior of bamboo/aluminium composites for applications in industrial structures, Key Engineering Materials, 1998; 145–149: 781 – 786.

[65] Sui G.X., Yu T.X., Kim J.K. and Zhou B.L. Mechanical behavior and failure modes of aluminium/bamboo sandwich plates under quasi-static loading, Journal of Materials Science, 2000; 35: 1445 – 1452.

[66] Zhang J.Y., Yu T.X., Kim J.K. and Sui G.X. Static indentation and impact behaviour of reformed bamboo/aluminium laminated composites, Composite Structures, 2000; 50: 207 – 216.

[67] Vasumathi M. and Murali V. Effect of alternate metals for use in natural fibre reinforced fibre metal laminates under bending, impact and axial loadings, Procedia Engineering, 2013; 64: 562 – 570.

[68] Petrucci R., Santulli C., Puglia D., Sarasini F., Torre L. and Kenny J.M. Mechanical characterisation of hybrid composite laminates based on basalt fibres in combination with flax, hemp and glass fibres manufactured by vacuum infusion, Materials and Design, 2013; 49: 728 – 735.

[69] Verma C.S., Sharma N.K., Chariar V.M., Maheshwari S. and Hada M.K. Comparative study of mechanical properties of bamboo laminae and their laminates with woods and wood based composites, Composites: Part B, 2014; 60: 523 – 530.

[70] Meredith J., Ebsworth R., Coles S.R., Wood B.M. and Kirwan K. Natural fibre composite energy absorption structures, Composites Science and Technology, 2012; 72: 211 – 217.

[71] Yan L. and Chouw N. Crashworthiness characteristics of flax fibre reinforced epoxy tubes for energy absorption application, Materials and Design, 2013; 51: 629 – 640.

[72] Węcławski B.T., Fan M. and Hui D. Compressive behaviour of natural fibre composite, Composites: Part B, 2014; 67: 183 – 191.

[73] Amada S., Munekata T., Nagase Y., Ichikawa Y., Kirigai A. and Zhifei Y. The mechanical structures of bamboos in viewpoint of functionally gradient and composite materials, Journal of Composite Materials, 1996; 30: 800 – 819.

[74] Liese W. Anatomy and properties of bamboo, Proceedings of the International Bamboo Workshop, Hangzhou, China, 1985.

[75] Gupta A. and Kumar A. Potential of bamboo in sustainable development, Asia-Pacific Business Review, 2008; 4: 100 – 107.

[76] Yu X. Bamboo: Structure and culture, PhD thesis, University Duisburg-Essen, 2007.

[77] Jiang Z., Chen F., Wang G., Liu X., Shi S.Q. and Cheng H. The circumferential mechanical properties of bamboo with uniaxial and biaxial compression tests, BioResources, 2012; 7: 4806 – 4816.

[78] Gutu T. A study on the mechanical strength properties of bamboo to enhance its diversification on its utilization, International Journal of Innovative Technology and Exploring Engineering, 2013; 2: 314 – 319.

[79] Tan T., Rahbar N., Allameh S.M., Kwofie S., Dissmore D., Ghavami K. and Soboyejo W.O. Mechanical properties of functionally graded hierarchical bamboo structures, Acta Biomaterilia, 2011; 7: 3796 – 3803.

[80] Ude A.U., Ariffin A.K. and Azhari C.H. An experimental investigation on the response of woven natural silk fiber/epoxy sandwich composite panels under low velocity impact, Fibers and Polymers, 2013; 14: 127 – 132.

[81] Petrone G., Rao S., De Rosa S., Mace B.R., Franco F. and Bhattacharyya D. Initial experimental investigations on natural fibre reinforce honeycomb core panels, Composites: Part B, 2013; 55: 400 – 406.

[82] Stocchi A., Colabella L., Cisilino A. and Álvarez V. Manufacturing and testing of a sandwich panel honeycomb core reinforced with natural-fiber fabrics, Materials and Design, 2014; 55: 394 – 403.

[83] Hoto R., Furundarena G., Torres J.P., Muñoz E., Andrés J. and García J.A. Flexural behavior and water absorption of asymmetrical sandwich composites from natural fibers and cork agglomerate core, Materials Letters, 2014; 127: 48 – 52.

[84] Dweib M.A., Hu B., O'Donnell A., Shenton H.W. and Wool R.P. All natural composite sandwich beams for structural applications, Composite Structures, 2004; 63: 147 – 157.

[85] Rao S., Jayaraman K. and Bhattacharyya D. Short fibre reinforced cores and their sandwich panels: Processing and evaluation, Composites: Part A, 2011; 42: 1236 – 1246.

[86] Rao S., Banerjee S., Jayaraman K. and Bhattacharyya D. Compressive behaviour of fibre reinforced honeycomb cores, Proceedings of the IUTAM Symposium on Multi-Functional Material Structures and Systems, Benguluru, India, 2008.

[87] Rao S., Das R. and Bhattacharyya D. Investigation of bond strength and energy absorption capabilities in recyclable sandwich panels, Composites: Part A, 2013; 45: 6 – 13.

[88] Porras A. and Maranon A. Eco friendly core sandwich panel reinforced with manicaria fiber and PLA matrix, 15th European Conference on Composite Materials (ECCM15), Venice, Italy, 2012.

[89] Yang F. and Fei B. The research on bamboo-wood corrugated sandwich panel, 55th International Convention of Society of Wood Science and Technology, Beijing, China, 2012.

[90] Nordin K., Bahari S.A., Zakaria M.N. and Jamaludin M.A. Environmentally-friendly sandwich panel using bamboo skin wastes as core material, Key Engineering Materials, 2007; 334–335: 41 – 44.

[91] Nordin K., Wahab R., Jamaludin M.A., Bahari S.A. and Zakaria M.N. Strength properties of glued-laminated bamboo (*Gigantochloa scortechinnii*) strips for furniture, Proceedings of Scientific Session 90 XXII IUFRO World Congress "Forest in the Balance", Brisbane, Australia, 2005.

[92] Mansur A. Analysis of Calcutta bamboo for structural composite material, PhD thesis, Virginia Polytechnic Institute and State University, 2000.

[93] Petrone G., Rao S., De Rosa S., Mace B.R., Franco F. and Bhattacharyya D. Behaviour of fibre-reinforced honeycomb core under low velocity impact loading, Composite Structures, 2013; 100: 356 – 362.

[94] Ude A.U., Ariffin A.K., Sopian K. and Azhari C.H. Energy attenuation capability of woven natural silk/epoxy composite plates subjected to drop-weight impacts, ARPN Journal of Engineering and Applied Sciences, 2010; 5: 75 – 87.

[95] Ude A.U., Ariffin A.K. and Azhari C.H. Impact behaviour of reinforced natural silk fibre sandwiched honeycomb core, Journal of Applied Sciences Research, 2013; 9: 3281 – 3287.

[96] Smith M., Guan Z.W. and Cantwell W.J. Finite Element modelling of the compressive response of lattice structures manufactured using the selective laser melting technique, International Journal of Mechanical Sciences, 2013; 67: 28 – 41.

[97] Côté F., Russell B.P., Deshpande V.S. and Fleck N.A. The through-thickness compressive strength of a composite sandwich panel with a hierarchical square honeycomb sandwich core, Journal of Applied Mechanics, 2009; 76: 1 – 8.

[98] Russell B.P., Liu T., Fleck N.A. and Deshpande V.S. Quasi-static three-point bending of carbon fiber sandwich beams with square honeycomb cores, Journal of Applied Mechanics, 2011; 78: 1 – 15.

[99] Burlayenko V.N. and Sadowski T. Effective elastic properties of foam-filled honeycomb cores of sandwich panels, Composite Structures, 2010; 92: 2890 – 2900.

[100] Wang A.J. and McDowell D.L. Effects of defects on in-plane properties of periodic metal honeycombs, International Journal of Mechanical Sciences, 2003; 45: 1799 – 1813.

[101] Chen Y., Zhang Z., Wang Y. and Hua H. Crush dynamics of square honeycomb thin rubber wall, Thin-Walled Structures, 2009; 47: 1447 – 1456.

[102] Vaziri A., Xue Z. and Hutchinson J.W. Metal sandwich plates with polymer foam-filled cores, Journal of Mechanics of Materials and Structures, 2006; 1: 95 – 125.

[103] Rao S., Jayaraman K. and Bhattacharyya D. Micro and macro analysis of sisal fibre composites hollow core sandwich panels, Composites: Part B, 2012; 43: 2738 – 2745.

[104] Zeng Q.Y., Li S.H. and Bao X.R. Effect of bamboo nodal on mechanical properties of bamboo wood, Scientia Silvae Sinicae, 1992; 28: 247 – 252.

[105] Li S.H., Fu S.Y. and Zhou B.L. A natural composite material – bamboo, Chinese Journal of Materials Research, 1994; 8: 188 – 192.

[106] Rao S., Yadama V. and Bhattacharyya D. Composite hollow core high-end bio-panels, 18th International Conference on Composite Materials, Jeju, Korea, 2011.

[107] Ho M.P., Wang H., Lee J.H., Ho C.K., Lau K.T., Leng J. and Hui D. Critical factors on manufacturing processes of natural fibre composites, Composites: Part B, 2012; 43: 3549 – 3562.

[108] Lakkad S.C. and Patel J.M. Mechanical properties of bamboo, a natural composite, Fibre Science and Technology, 1981; 14: 319 – 322.

[109] Biagi R. and Bart-Smith H. Imperfection sensitivity of pyramidal core sandwich structures, International Journal of Solids and Structures, 2007; 44: 4690 – 4706.

[110] Amani M., Alinia M.M. and Fadakar M. Imperfection sensitivity of slender/stocky metal plates, Thin-Walled Structures, 2013; 73: 207 – 215.

[111] Kazemahvazi S., Russell B.P. and Zenkert D. Impact of carbon fibre/epoxy corrugated cores, Composite Structures, 2012; 94: 3300 – 3308.

[112] Ude A.U., Ariffin A.K. and Azhari C.H. Impact damage characteristics in reinforced woven natural silk/epoxy composite face-sheet and sandwich foam, coremat and honeycomb materials, International Journal of Impact Engineering, 2013; 58: 31 – 38.

[113] Mallaiah S., Sharma K.V. and Krishna M. Development and comparative studies of bio-based and synthetic fiber based sandwich structures, International Journal of Soft Computing and Engineering, 2012; 2: 332 – 335.

[114] Du Y., Yan N. and Kortschot M.T. An experimental study of creep behaviour of lightweight natural fiber-reinforced polymer composite/honeycomb core sandwich panels, Composite Structures, 2013; 106: 160 – 166.

[115] Wadley H.N.G., Dharmasena K.P., O'Masta M.R. and Wetzel J.J. Impact response of aluminium corrugated core sandwich panels, International Journal of Impact Engineering, 2013; 62: 114 – 128.

[116] D'Mello R.J., Guntupalli S., Hansen L.R. and Waas A.M. Dynamic axial crush response of circular honeycombs, Proceedings of The Royal Society A: Mathematical, Physical and Engineering Sciences, 2012; 468: 2981 – 3005.

[117] D'Mello R.J. and Waas A.M. Synergistic energy absorption in the axial crush response of filled circular cell honeycombs, Composites Structures, 2012; 94: 1669 – 1676.

[118] Lim G.T., Ramsteiner F. and Altstädt V. Understanding the compressive behaviour of linear and cross-linked polyvinyl-chloride foams, Journal of Cellular Plastics, 2009; 45: 419 – 439.

[119] Kendall M.J. and Siviour C.R. Strain rate and temperature dependence in PVC, Dynamic Behavior of Materials, Volume 1: Proceedings of the 2013 Annual Conference on Experimental and Applied Mechanics, Illinois, 2013.

[120] Tagarielli V.L., Deshpande V.S. and Fleck N.A. The dynamic response of composite sandwich beams to transverse impact, International Journal of Solids and Structures, 2007; 44: 2442 – 2457.

[121] Vaidya U.K., Pillay S., Magrini M. and Mantena P.R. Ballistic impact testing of balsa, PVC foam, glass reinforced polyurethane core sandwich structures, 17th International Conference on Composite Materials (ICCM 17), Edinburgh, UK, 2009.

[122] Saha M.C., Mahfuz H., Chakravarty U.K., Uddin M., Kabir M.E. and Jeelani S. Effect of density, microstructure, and strain rate on compression behavior of polymeric foams, Materials Science and Engineering A, 2005; 406: 328 – 336.

[123] www.gardman.co.uk.

[124] www.corematerials.3AComposites.com.

[125] www.xanita.com.

[126] Reyes G. and CantwellW.J. The mechanical properties of fibre-metal laminates based on glass fibre reinforced polypropylene, Composites Science and Technology, 2000; 60: 1085 – 1094.

[127] Wu H.F. and Wu L.L. A study of tension test specimens of laminated hybrid composites. Part II: Size and alignment effect, Journal of Materials Science, 1994; 29: 5847 – 5851.

[128] Chung K.F. andYu W.K. Mechanical properties of structural bamboo for bamboo scaffoldings, Engineering Structures, 2002; 24: 429 – 442.

[129] El-GebeilyM. and YushauB. Mathematics numerical methods with MS Excel, The Montana Mathematics Enthusiast, 2007; 4: 84 – 92.

[130] www.kistler.com.

[131] www.intertechnology.com/Kistler/pdfs/ACC_5011B_Charge_Amplifier.pdf.

[132] www.jablite.co.uk.

[133] Van de Velde K. and Kiekens P. Biopolymers: Overview of several properties and consequences on their applications, Polymer Testing, 2002; 21: 433 – 442.

[134] Garrett K.W. and Bailey J.E. The effect of resin failure strain on the tensile properties of glass fibre-reinforced polyester cross-ply laminates, Journal of Materials Science, 1997;1 2: 2189 – 94.

[135] Dong-Joo L., Ick-Jae S. and Seung-Wook L. Effects of mold temperature and cooling rate on mechanical properties of press consolidated thermoplastic composite, 13th International Conference on Composite Materials (ICCM-13), Beijing, China, 2001.

[136] Le Duigo A., Davies P. and Baley C. Interfacial bonding of flax fibre/Poly(l-lactide) biocomposites, Composites Science and Technology, 2010; 70: 231 – 239.

[137] Zhang H., Luo H. and Lu X. Reliability of compression strength of hennon bamboo-reinforced extruded tubular particleboard, BioResources, 2014; 9: 2696 – 2704.

[138] Farley G.L. Effect of specimen geometry on the energy absorption capability of composite materials, Journal of Composite Materials, 1986; 20: 390 – 400.

[139] Jones N. Structural Impact, Cambridge University Press, 2nd Edition, Cambridge, UK; 2012.

[140] Farley G.L. Energy absorption of composite materials, Journal of Composite Materials, 1983; 17: 267 – 279.

[141] Thornton P.H. Energy absorption in composite structures, Journal of Composite Materials, 1979; 13: 247 – 262.

[142] Song H.W., Du X.W. and Zhao G.F. Energy absorption behaviour of double–chamfer triggered glass/epoxy circular tubes, Journal of Composite Materials, 2002; 36: 2183 – 2198.

[143] Yan L., Chouw N. and Jayaraman K. Effect of triggering and polyurethane foam-filler on axial crushing of natural flax/epoxy composite tubes, Materials and Design, 2014; 56: 528 – 541.

[144] Ataollahi S., Taher S.T., Eshkoor R.A., Ariffin A.K. and Azhari C.H. Energy absorption and failure response of silk/epoxy composite square tubes: Experimental, Composites: Part B, 2012; 43: 542 – 548.

[145] Aljibori H.S.S. Energy systems and crushing behavior of fiber reinforced composite materials, World Academy of Science, Engineering and Technology, 2011; 50: 248 – 254.

[146] Wang D. Impact behavior and energy absorption of paper honeycomb sandwich panels, International Journal of Impact Engineering, 2009; 36: 110 – 114.

[147] Hamada H., Coppola J.C., Hull D., Maekawa Z. and Sato H. Comparison of energy absorption of carbon/epoxy and carbon/PEEK composite tubes, Composites, 1992; 23: 245 – 252.

[148] Jacob G.C., Fellers J.F., Simunovic S. and Starbuck J.M. Energy absorption in polymer composites for automotive crashworthiness, Journal of Composite Materials, 2002; 36: 813 – 850.

[149] Nisha A.S. and Saraswathy B. Dynamic analysis of delaminated sandwich composites, International Journal of Modern Engineering Research, 2013; 3: 172 – 177.

[150] Wang D.M. and Wang Z.W. Experimental investigation into the cushioning properties of honeycomb paperboard, Packaging Technology and Science, 2008; 21: 309 – 316.

[151] Hibbitt, Karlsson and Sorensen. Abaqus/CAE User's Manual (6.12): Dassault Systèmes Simulia Corp., Providence, RI, USA; 2012.

[152] Hibbitt, Karlsson and Sorensen. Abaqus Theory Manual (6.12): Dassault Systèmes Simulia Corp., Providence, RI, USA; 2012.

[153] Martin R.H., Giannis S., Mirza S. and Hansen K. Biocomposites in challenging automotive applications, 17th International Conference on Composite Materials (ICCM 17), Edinburgh, UK, 2009.

[154] Hibbitt, Karlsson and Sorensen. Abaqus Analysis User's Manual (6.12): Dassault Systèmes Simulia Corp., Providence, RI, USA; 2012.

[155] Gamstedt E.K. and Almgren K.M. Natural fibre composites – with special emphasis on effects of the interface between cellulosic fibres and polymers, Proceeding of 28th Risø International Symposium on Materials Science: Interface Design of Polymer Matrix Composites – Mechanics, Chemistry, Modelling and Manufacturing, Roskilde, Denmark, 2007.

[156] Long A.C. Design and manufacture of textile composites. Cambridge: Woodhead Publishing Limited, University of Nottingham, UK; 2005.